AD-A074 044 ARMY MISSILE RESEARCH AND DEVELOPMENT COMMAND REDSTO--ETC F/G 9/2
MODELING FRICTION IN A SPRING-MASS-DAMPER SYSTEM.(U)
JUL 79 D B MERRIMAN

UNCLASSIFIED DRDMI-T-79-72 NL

1 OF 1
AD A074044

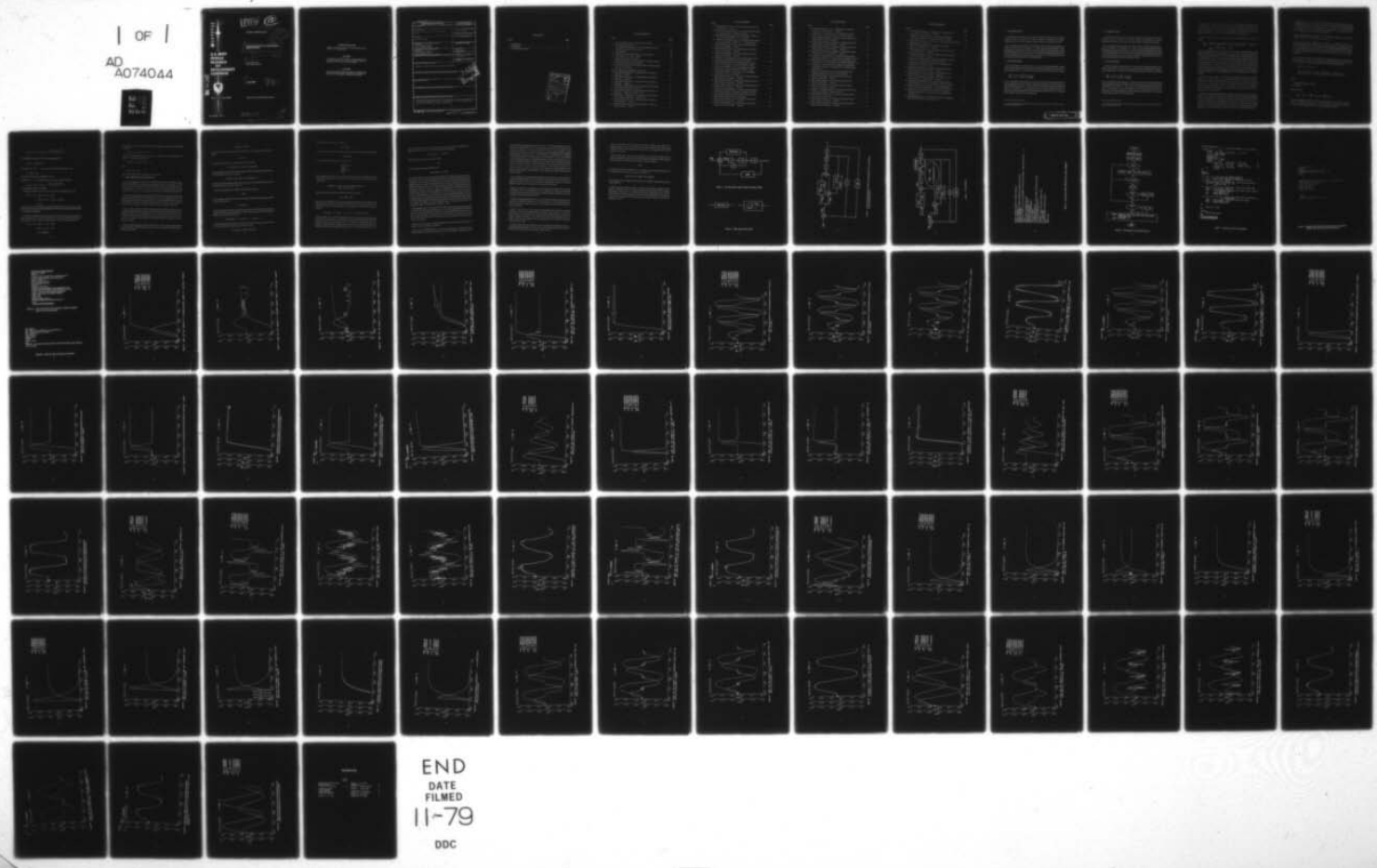

END
DATE FILMED
11-79
DDC

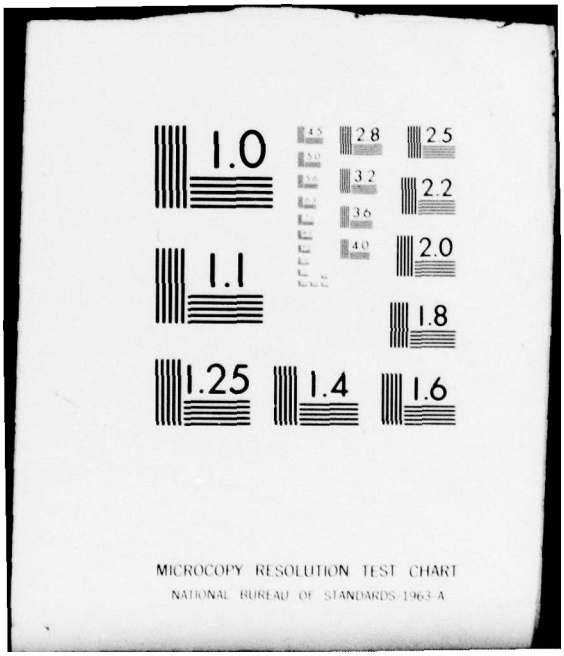
1.0
1.1
1.25
1.4
1.6
1.8
2.0
2.2
2.5
2.8
3.2
3.6
4.0
4.5
5.0
5.6
MICROCOPY RESOLUTION TEST CHART
NATIONAL BUREAU OF STANDARDS-1963-A

AD A074044

LEVEL II

12

DRDMI-

TECHNICAL REPORT T-79-72

6

MODELING FRICTION IN A SPRING-MASS-DAMPER SYSTEM

9 Technical rept.

10

David B. Merriman
Technology Laboratory

U.S. ARMY MISSILE RESEARCH AND DEVELOPMENT COMMAND

11

3 JULY 1979

12 87 p.

Redstone Arsenal, Alabama 35809

DMI FORM 1000, 1 APR 77

393427

DISPOSITION INSTRUCTIONS

DESTROY THIS REPORT WHEN IT IS NO LONGER NEEDED. DO NOT RETURN IT TO THE ORIGINATOR.

DISCLAIMER

THE FINDINGS IN THIS REPORT ARE NOT TO BE CONSTRUED AS AN OFFICIAL DEPARTMENT OF THE ARMY POSITION UNLESS SO DESIGNATED BY OTHER AUTHORIZED DOCUMENTS.

TRADE NAMES

USE OF TRADE NAMES OR MANUFACTURERS IN THIS REPORT DOES NOT CONSTITUTE AN OFFICIAL ENDORSEMENT OR APPROVAL OF THE USE OF SUCH COMMERCIAL HARDWARE OR SOFTWARE.

Unclassified
SECURITY CLASSIFICATION OF THIS PAGE (When Data Entered)

REPORT DOCUMENTATION PAGE		READ INSTRUCTIONS BEFORE COMPLETING FORM
1. REPORT NUMBER T-79-72	2. GOVT ACCESSION NO.	3. RECIPIENT'S CATALOG NUMBER
4. TITLE (and Subtitle) Modeling Friction in a Spring-Mass-Damper System		5. TYPE OF REPORT & PERIOD COVERED Technical Report 6. PERFORMING ORG. REPORT NUMBER
7. AUTHOR(s) David B. Merriman		8. CONTRACT OR GRANT NUMBER(s)
9. PERFORMING ORGANIZATION NAME AND ADDRESS Commander US Army Missile Command ATTN: DRSMI-TDD (R&D) Redstone Arsenal, Alabama 35809		10. PROGRAM ELEMENT, PROJECT, TASK AREA & WORK UNIT NUMBERS
11. CONTROLLING OFFICE NAME AND ADDRESS Commander US Army Missile Command ATTN: DRSMI-TI (R&D) Redstone Arsenal, Alabama 35809		12. REPORT DATE 3 July 1979 13. NUMBER OF PAGES 83
14. MONITORING AGENCY NAME & ADDRESS (if different from Controlling Office)		15. SECURITY CLASS. (of this report) Unclassified 15a. DECLASSIFICATION/DOWNGRADING SCHEDULE

16. DISTRIBUTION STATEMENT (of this Report)

Approved for Public Release; Distribution Unlimited.

17. DISTRIBUTION STATEMENT (of the abstract entered in Block 20, if different from Report)

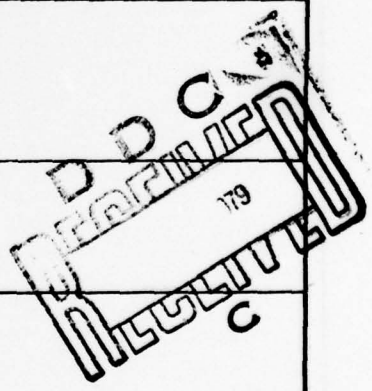

18. SUPPLEMENTARY NOTES

19. KEY WORDS (Continue on reverse side if necessary and identify by block number)

20. ABSTRACT (Continue on reverse side if necessary and identify by block number)

Using simple friction models in digital computer simulations sometimes leads to less than satisfactory results. Consequently two friction models were developed and tested in a second order system.

DD FORM 1 JAN 73 1473 EDITION OF 1 NOV 65 IS OBSOLETE

Unclassified
SECURITY CLASSIFICATION OF THIS PAGE (When Data Entered)

CONTENTS

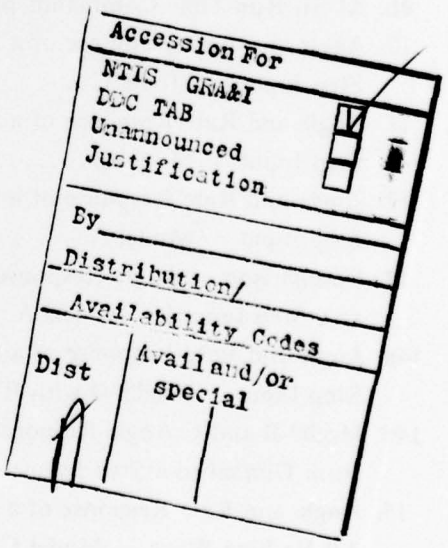

ILLUSTRATIONS

ILLUSTRATIONS

ILLUSTRATIONS

ILLUSTRATIONS

1. INTRODUCTION

Using simple friction models in digital computer simulations sometimes leads to less than satisfactory results. Consequently, two friction models were developed, one being a modification of the other. These models essentially combine two simple friction models.

The two models are compared with a third which is often used for friction modeling. For testing, the models were embedded in a second order spring-mass-damper system. Comparisons are made between the three systems for different system gains, friction values and damping using sine wave and step inputs. Only the RK2 integration algorithm was used because of its predominant usage in the author's simulations. The test program was written in the Advanced Continuous Simulation Language (ACSL).[1]

2. MATH MODELS

The friction models are incorporated into a second order spring-mass-damper system. Similar system models are often used to represent missile seeker platform dynamics. *Figure 1* is a block diagram of the test system. The closed loop equation without the friction nonlinearity is

$$\frac{\psi}{T_{M3}} = \frac{K}{S^2 + B \cdot K \cdot S + K \cdot CMPL}$$

where ψ is the platform angle (radians); T_{M3} is the motor torque into the system (ft-lb); B is the viscous damping (ft-lb/rad/sec); CMPL is the spring constant (ft-lb/rad); and K is the inverse of the platform inertia $(\text{lb-sec}^2\text{-ft})^{-1}$. The values for T_{M3} and CMPL were chosen to keep ψ well below $\pi/2$ rad. Initially, T_{M3} is 5 ft-lb and CMPL is 12 ft-lb/rad. B is made 0.1 ft-lb/rad/sec, which gives a closed loop damping ratio of about 0.08 for a K of 30 $(\text{lb-sec}^2\text{-ft})^{-1}$. For all three friction models a value of 2 ft-lb is initially used.

---

[1] E. E. L. Mitchell and Joseph S. Gauthier, *Advanced Continuous Simulation Language (ACSL) User Guide/ Reference Manual*, Mitchell and Gauthier Associates, 1975.

1. INTRODUCTION

Using simple friction models in digital computer simulations sometimes leads to less than satisfactory results. Consequently, two friction models were developed, one being a modification of the other. These models essentially combine two simple friction models.

The two models are compared with a third which is often used for friction modeling. For testing, the models were embedded in a second order spring-mass-damper system. Comparisons are made between the three systems for different system gains, friction values and damping using sine wave and step inputs. Only the RK2 integration algorithm was used because of its predominant usage in the author's simulations. The test program was written in the Advanced Continuous Simulation Language (ACSL).[1]

2. MATH MODELS

The friction models are incorporated into a second order spring-mass-damper system. Similar system models are often used to represent missile seeker platform dynamics. *Figure 1* is a block diagram of the test system. The closed loop equation without the friction nonlinearity is

$$\frac{\psi}{T_{M3}} = \frac{K}{S^2 + B \cdot K \cdot S + K \cdot CMPL}$$

where ψ is the platform angle (radians); T_{M3} is the motor torque into the system (ft-lb); B is the viscous damping (ft-lb/rad/sec); CMPL is the spring constant (ft-lb/rad); and K is the inverse of the platform inertia $(lb\text{-}sec^2\text{-}ft)^{-1}$. The values for T_{M3} and CMPL were chosen to keep ψ well below $\pi/2$ rad. Initially, T_{M3} is 5 ft-lb and CMPL is 12 ft-lb/rad. B is made 0.1 ft-lb/rad/sec, which gives a closed loop damping ratio of about 0.08 for a K of 30 $(lb\text{-}sec^2\text{-}ft)^{-1}$. For all three friction models a value of 2 ft-lb is initially used.

---

[1] E. E. L. Mitchell and Joseph S. Gauthier, *Advanced Continuous Simulation Language (ACSL) User Guide/ Reference Manual*, Mitchell and Gauthier Associates, 1975.

Often friction is modeled as shown in *Figure 2*. In ACSL code the friction model is T_{FR1}*SGN($-\dot{\psi}$). This model will be referred to as model A. A drawback of this model is that it produces artificial torques when there is no gimbal motion. Model A is used for test comparison purposes. The two friction models designed to improve upon this model are shown in *Figures 3* and *4*. They will be called models B and C, respectively.

In ACSL code, friction model B is incorporated into the expression for net torque as follows:

$$T'_{NET} = RSW(|\dot{\psi}'| < R_{MIN}, DEAD(-T_{FR1}, T_{FR1}, T_{M3} - B*\dot{\psi}' - C_{MPL}*\psi'),$$

$$T_{NET} + SIGN(T_{FR2}, -\dot{\psi}'))$$

When $\dot{\psi}'$, the gimbal angular rate, is less than the value of R_{MIN}, the gimbal friction can be modeled as a dead zone since no gimbal motion will occur until T_{NET} exceeds a value equivalent to the frictional resistance torque, T_{FR1}. Once the gimbal is in motion the gimbal friction will produce an effective torque, T_{FR2}, that always opposes gimbal motion. However, false motion can occur due to at least two things: (1) $\dot{\psi}'$ will not necessarily be smaller than R_{MIN} (the incremental change in $\dot{\psi}'$ over one integration step can be larger than R_{MIN}) so that the dead zone model may not switch back in; (2) If the dead zone model does not switch back in, the frictional torque can not only oppose motion, but can also cause a reversal of gimbal motion, which is not physically correct. So an appropriate value must be chosen for R_{MIN} for model B to operate properly. This is an undesirable feature that was eliminated in the design of model C.

As shown in *Figure 4*, model C is comprised of model B plus logic that zeroes the gimbal angular rate, $\dot{\psi}$, whenever both the net torque minus friction is less than the friction and $\dot{\psi}$ changes sign. It should be noted that the dead zone model uses T_{FR1}, and the sliding friction model uses T_{FR2}. This allows for friction models that have different values for static and sliding friction. The logic for switching $\dot{\psi}$ to zero, as implemented in *Figure 4*, forms an algebraic loop. Thus, model C was implemented as an ACSL macro in which the loop is broken at the desired point in the system model.

The macro code and a flow diagram of the macro are shown in *Figures 5* and *6*, respectively. In the macro, $\dot{\psi}$ (macro local variable YD) is not actually set to zero except when LOTORQ is TRUE (as discussed below). $\dot{\psi}$ is calculated by adding $\dot{\psi}_D$ (YDOT) and $\dot{\psi}'_D$ (YDOTP) as shown in *Figure 5*. Setting $\dot{\psi}$ to zero through biasing $\dot{\psi}_D$ with $\dot{\psi}'_D$ ($\dot{\psi}'_D$ is set to $-\dot{\psi}_D$) keeps $\dot{\psi}$ from having a jump in its value whenever LOTORQ goes from TRUE to FALSE. A jump in $\dot{\psi}$ would otherwise occur since $\dot{\psi}_D$, being a state, cannot be set back to zero. LOTORQ becomes TRUE whenever T_{NET}, the net torque minus friction, is less than T_{FR2} and $\dot{\psi}$ has switched sign.

When the ACSL Executive is in the INITIAL section (ZZICFL is TRUE) the expression for LOTORQ is bypassed since T_{NET} will not yet be defined. When ZZICFL is FALSE, LOTORQ is calculated as discussed above. If LOTORQ is TRUE, $\dot{\psi}$ is set to zero. If this integration step is the first minor step of a multi-step integration method (ZZFST = 1.0), then $\dot{\psi}_D$ is set to $-\dot{\psi}_D$. $\dot{\psi}_D$ is switched only once for each multi-step integration.

When LOTORQ is FALSE or ZZICFL is TRUE, ZZFST is checked for a value of 1.0. If ZZFST is 1.0, then YDL, the old value of $\dot{\psi}$, is set to $\dot{\psi}$.

T'_{NET}, the net torque including friction, and $\dot{\psi}_D$ are calculated outside of the PROCEDURAL block the rest of the code is in. The expressions for T'_{NET} and $\dot{\psi}_D$ are not in the block in order to allow them to be sorted by the ACSL compiler along with the expression for T_{NET}. In the FORTRAN compilation of the test program using the FRICTN macro, the code in the PROCEDURAL block came first followed by the expressions for T_{NET}, T'_{NET} and $\dot{\psi}_D$, respectively.

$\dot{\psi}_D$ and YDL are only reset once per multi-step integration to keep T'_{NET} from having erroneous values. An example of how problems occur when $\dot{\psi}_D$ and YDL are reset more than once is shown below. For RK2 as implemented in ACSL's FORTRAN library,

$$\dot{\psi}_D(t + h) = \dot{\psi}_D(t) +$$

$$\frac{\ddot{\psi}_D\ (t,\ \dot{\psi}_D\ (t)) + 3*\ddot{\psi}_D(t + \frac{2}{3}h, \dot{\psi}_D\ (t) + \frac{2}{3}h\ \ddot{\psi}_D\ (t))}{4}\ h$$

where

h is the major integration step size
$\ddot{\psi}_D = K*T'_{NET}$

Define $\ddot{\psi}_{D1}$ to be

$$\ddot{\psi}_{D1} = \ddot{\psi}_D\ (t + \frac{2}{3}h,\ \dot{\psi}_D\ (t) + \frac{2}{3}h\ \ddot{\psi}_D\ (t)$$

Suppose LOTORQ goes TRUE on the intermediate integration step. Then $\ddot{\psi}_{D1}$ will be zero since T_{NET} and $\dot{\psi}$ are zero. Suppose $\dot{\psi}_D$ is set to $-\dot{\psi}_D$ and YDL is set to $\dot{\psi}$ on this intermediate step. On the final evaluation for $\dot{\psi}_D$ (t + h) the RK2 algorithm reduces to

$$\dot{\psi}_D\ (t + h) = \dot{\psi}_D\ (t) + \frac{\ddot{\psi}_D\ (t,\ \dot{\psi}_D\ (t))}{4}\ h$$

For LOTORQ to have gone TRUE on the intermediate step,

$$\dot{\psi}_D\ (t) + \frac{2}{3}\,h\,\ddot{\psi}_D\ (t),$$

the expression for $\dot{\psi}_D\ (t + {}^2/_3\ h)$, had to be of opposite sign from $\dot{\psi}_D(t)$, since

$$\dot{\psi} = \dot{\psi}_D + \dot{\psi}_D'$$

(Assume $\dot{\psi}_D' = 0.0$ before LOTORQ went TRUE).

Assuming $\dot{\psi}_D\ (t + {}^2/_3\ h)$, is negative and $\dot{\psi}_D(t)$ is positive then the expression

$$\dot{\psi}_D\ (t + h) = \dot{\psi}_D\ (t) + \frac{\ddot{\psi}_D\ (t,\ \dot{\psi}_D\ (t))}{4}\ h$$

can conceivably be positive or negative.

Suppose it is negative. Then, on the next derivative calculation for $\dot{\psi}_D\ (t + h)$,

$$\begin{aligned}\dot{\psi}\ (t + h) &= \dot{\psi}_D\ (t + h) + \dot{\psi}_D' \\ &= \dot{\psi}_D\ (t + h) - \dot{\psi}_D\ (t + \tfrac{2}{3}h) \\ &\neq 0.0\end{aligned}$$

Since YDL is zero when LOTORQ is calculated, LOTORQ will be FALSE. Thus T_{NET} and $\dot{\psi}\,(t + h)$ will have nonzero values and $\dot{\psi}_D\,(t+2h) \neq \dot{\psi}_D\,(t+h)$. So $\dot{\psi}$ is not zero as it should be, and $\dot{\psi}_D$ is continuing to be integrated.

To make the system behave properly, $\dot{\psi}_D'$ and YDL must not be reset on an intermediate step since the value of $\dot{\psi}_D\ (t + h)$ does not depend only on $\ddot{\psi}_{DI}$. It is to be noted that either the resetting of $\dot{\psi}_D'$ or YDL would have caused problems. If $\dot{\psi}_I$ and $\dot{\psi}_D'$ had not been reset

$$\begin{aligned}\dot{\psi}\ (t + h) &= \dot{\psi}_D\ (t + h) + \dot{\psi}_D' \\ &= \dot{\psi}_D\ (t + h) + 0.0 \\ &\neq 0.\ \text{usually}\end{aligned}$$

Since YDL is $\dot{\psi}$ (t) (= $\dot{\psi}_D$ (t) when $\ddot{\psi}_D$(t) = 0.0) when LOTORQ is calculated, then LOTORQ will be TRUE if

$$\dot{\psi}_D \ (t) \ * \ \dot{\psi}_D \ (t + h) \ < \ 0$$

and $\dot{\psi}$ (t + h) will be reset from $\dot{\psi}_D$ (t + h) to zero. T_{NET} and $\ddot{\psi}_D$ (t + h) will consequently be zero, and $\dot{\psi}_D$ (t + h) will remain constant. If

$$\dot{\psi}_D \ (t) \ * \ \dot{\psi}_D \ (t + h) \ > \ 0$$

then

$$\dot{\psi} \ (t + h) \neq 0,$$

and the system will continue to integrate $\dot{\psi}_D$ as it should.

3. TEST PROGRAM AND RESULTS

Figure 7 is a listing of the test program. In the DERIVATIVE section seeker platform angles SI ($\dot{\psi}$), SIP and SIPP are calculated for friction models C, B and A, respectively. T_{M3} is the input motor torque for all three models. If SINSTP is TRUE T_{M3} is a sine wave; otherwise, T_{M3} is a step function. T_{NET} and T_{NET2} are the net torque minus friction for models C and B, respectively. T_{NET} and T_{NET3} are the net torques with friction for models B and A, respectively.

Parameters and initial conditions are defined in the INITIAL section through CONSTANT statements. The CINTERVAL statement specifies the data recording interval. The RK2 integration algorithm is specified by setting IALG to 4 in the ALGORITHM statement. The MAXTERVAL statement overrides the NSTEPS statement to specify a 2.5 msec integration step size. WP is the frequency of the T_{M3} sine wave in rad/sec and W is WP in Hz.

ACSL run time commands are used for altering parameters and initial conditions on states; running the simulation; and specifying the output. The simulation was run interactively on a CYBER 74 using run time commands entered on a Tektronix console. Hard copy plots were generated along with line printer listings. Run time commands that were used every session were put on a temporary mass storage file that could be attached as a local file to the user's interactive terminal.

Figure 8 is a list of interactive session setup and ACSL run time commands. After logging onto the CYBER 74 INTERCOM system via the Tektronix terminal, the following setup statements are entered:

CONNECT, OUTPUT

specifies the system output file default name OUTPUT, will be displayed on the Tektronix screen.

ETL, 170

extends the execution time per statement entered to 170 octal sec.

ATTACH, INPUT, TEK, ID = DDXXXH

attaches the highest cycle (2) of TEK to the Tektronix. INPUT is the default file name for input to local programs executing in the system.

ATTACH, LGOB, TEK, ID = DDXXXH, CY = 1

attaches the simulation absolute binary file which was previously compiled in a batch job via the system control cards listed in *Figure 9a*.

After this initial preparation, LGOB is executed by the statement

LGOB

and the simulation reads the ACSL run time commands on file INPUT, the contents of which are shown in *Figure 9b*:

SET PRN = 9

tells the simulation that the line printer data will be placed on the PRINT file (logical unit number 9) instead of the default file name OUTPUT. After termination of the simulation the PRINT file is batched to a line printer.

SET PRNPLT = .F., CALPLT = .T., TTLCPL = .T.

replaces the default printer plot routines with the special Tektronix plot routines and TTLCPL set TRUE causes titles to be placed on the Tektronix plots.

SET TITLE = 'FRICTN TESTER-'

specifies the first two words of the plot title.

SET DUMP = .1.

causes the last values of all the variables to be written to the file with logical unit number PRN.

SAVE 'BASE'

'saves' the initial parameters and I.C.'s for later use.

```
PROCED GO
START
PRINT 'ALL'
END
```

defines a PROCED that starts execution of the simulation and causes the variables specified in the PREPAR command to be recorded every CINT seconds onto the file with logical unit number PRN.

PREPAR T, SI, SID, SIP, SIPD, SIPP, SIPPD, TM3,
TNET, TNET2, TNET 3

specifies the variables whose values will be output on a line printer.

SET CMD = DIS

indicates to the simulation that run time commands will now be input from the DISPLAY file whose logical unit number is DIS. DIS is by default 6 which is also the number for the OUTPUT file. Thus, run time commands are now expected to come from the Tektronix terminal.

SET TFR1 = 14., TFR2 = 14., G = 20., K = 10., MAXT = 0.015

Although MAXT was set to 0.015 the integration step size was 0.010 sec due to CINT being 0.010. Instead of starting with a typical spring-mass-damper system, the parameters have been changed to reflect how they would be relative to each other for a missile seeker platform. Namely, the frictional torques are higher than torques due to the spring constant and viscous damping; K , the reciprocal of the platform inertia, is the system gain and is arbitrarily set to 10;

and G is made 20. ft-lbs in order for the platform torquer to overcome the friction. MAXT was changed to reflect the lower value of the undamped natural frequency.

SET TITLE(3) = '8 JUNE 79'

fills the third word of the plot title with the date.

GO

starts the simulation through PROCED GO.

PLOT 'XHI' = 2., SI, SID

limits the plot abscissa to 2 sec and causes the plotting of SI and SID (ψ and $\dot{\psi}$) for the system with model C. *Figure 10* is the resulting Tektronix hard copy. SI limits to a steady state value and SID stays at zero. SIP and SIPD (ψ and $\dot{\psi}$) for the system with model B and SIPP and SIPPD (ψ and $\dot{\psi}$) for model A are plotted in *Figures 11* and *12*, respectively. Notice SIP and SIPP do not reach a steady state value and that SIPD and SIPPD are chattering when they physically should not be. *Figure 13* compares SI, SIP and SIPP. SIPP leads SIP and SI primarily due to the initial spurious oscillations in SIPPD before T_{M1} rose above zero. Since RMN for model B is set to 10^{-30} in the INITIAL section of the program, spurious oscillations are to be expected. RMN was reset to 0.015 rad/sec, and the resulting SIP and SIPD are shown in *Figure 14a*. Only an improper step in SIPD shows up. It is due to the jump in TNETP caused by SIPD changing sign and still being greater than RMN in absolute value. Eventually SIPD gets caught in the ±RMN interval and model B reverts to a dead zone model. *Figure 14b* compares the angles of models B and C for RMN = 0.015.

Resetting RMN to 10^{-30} and setting SINSTP to TRUE (the torquer motor input is a 1.0 Hz sine wave) results in the plots shown in *Figures 15-18*. Note that although SIPD and SIPPD do not stay zero when they should, the comparison of SI, SIP and SIPPD in *Figure 18* is not as bad as for the step inputs. The systems with models A and B showed improved sine wave response with a decrease in step size, but their step responses still did not steady out when the step size was lowered.

RMN was set to 0.5 rad/sec and the resulting SIP and SIPD for model B are shown in *Figure 19*. *Figure 20* compares SI and SIP.

With a call to "RESTOR 'BASE'" the original parameter and I.C. specifications in the INITIAL section are restored to the program. That is, G, the platform torquer gain, is 5.0 ft-

lbs; K, the inverse of the platform inertia is 30. (lb-sec^2-ft)$^{-1}$; TFR1 and TFR2 are made 2 ft-lbs; the spring constant CMPL and the viscous damping B remain at 12. ft-lb/rad and 0.1 ft-lb/rad/sec, respectively. The spring-mass-damper system no longer resembles a seeker platform. The second order system has a damping coefficient of about 0.08, and an undamped natural frequency of about 19 rad/sec. This has added to it a healthy but not overwhelming frictional torque of 2 ft-lbs. The RMN parameter for model B is 10^{-30} rad/sec. The simulation is run by invoking GO, and the resulting angles and angular rates are shown in *Figures 21-23*. *Figure 24* compares the angles for models A, B and C. Again one notices models A and B do not reach a steady state value for a step input. However, their values are close due to MAXT being set at 2.5 msec. Model B was looked at with RMN set at 0.0025 and 0.05, and the plots are shown in *Figures 25* and *26*, respectively. The importance of picking RMN for good performance of model B is readily apparent. The response of the system without friction is shown in *Figure 27*.

K is set to 300 to increase the undamped natural frequency to 60 rad/sec. B is made 0.032 to keep the damping coefficient 0.08. Even though the integration step size of 2.5 msec is still adequate for stability, *Figures 28-31* show that the performance of Models A and B has degraded. *Figure 32* shows the response of the system with no friction.

With K = 30 and B = 0.1 a 1.0 Hz sine wave is used as the system forcing function. G remains 5 ft-lb, RMN is 10^{-30} rad/sec and MAXT is 2.5 msec. *Figures 33-35* are the results for models C, B and A, respectively. *Figure 36* shows the good match for all three models. *Figure 37* shows the response for the system without friction.

When K is made 300 and B is 0.032, the accuracy of models A and B deteriorates as shown in *Figures 38-41*. Model B had RMN set at 10^{-30}. Resetting it to 0.1 rad/sec produced the nice match with model C as shown in *Figures 42* and *43*. *Figure 44* shows the system response for the no friction case.

With K = 30., B is set to 2.0 to obtain an overdamped system. This gives a damping coefficient of 1.58, and the undamped natural frequency remains 19 rad/sec. The frictional torque remains at 2 ft-lb. *Figures 45-47* show the results for a step input to the system with models C, B and A, respectively. *Figure 48* shows the good overlays obtained for all three models. This is due to the angular rate never dropping below zero. *Figure 49* is the system response without friction.

Setting K to 300. and B to 0.632 makes the linear undamped natural frequency 60 rad/sec, and the damping ratio remains at 1.58. *Figures 50-53* show the good comparisons for the three models. *Figure 54* shows the system response without friction.

With K = 30. and B = 2.0, the system is driven with a 1.0 Hz sine wave. RMN is 10^{-30}. Although models A and B have angular rates with high oscillations their angle histories compare very well to that of model C as shown in *Figures 55-58*. *Figure 59* is the frictionless response of the system.

With K = 300. and B = 0.632, one sees significant errors in models A and B as shown in *Figures 60-63*. RMN is changed to 0.1, and the resulting improvement in model B is reflected in *Figures 64* and *65*. *Figure 66* shows the system's frictionless response.

STOP

terminates the simulation. The PRINT file, now attached to the interactive terminal as a local file, is batched for line printing to interactive terminal 3D.

BATCH, PRINT, PRINT, 3D, HDMDD

The Tektronix terminal is logged out and terminal 3D is logged in to obtain the line printer listing of PRINT.

Model C is clearly superior in accuracy to models A and B under the conditions tested. However, Model B is much less complex and gives good results when RMN is adjusted appropriately. Angle errors in A and B with a sine wave forcing function were relatively smaller than those in which the input was a step except for the overdamped case. Obviously the greater the relative magnitude of the frictional torque, the greater the accuracy required in the modelling of friction.

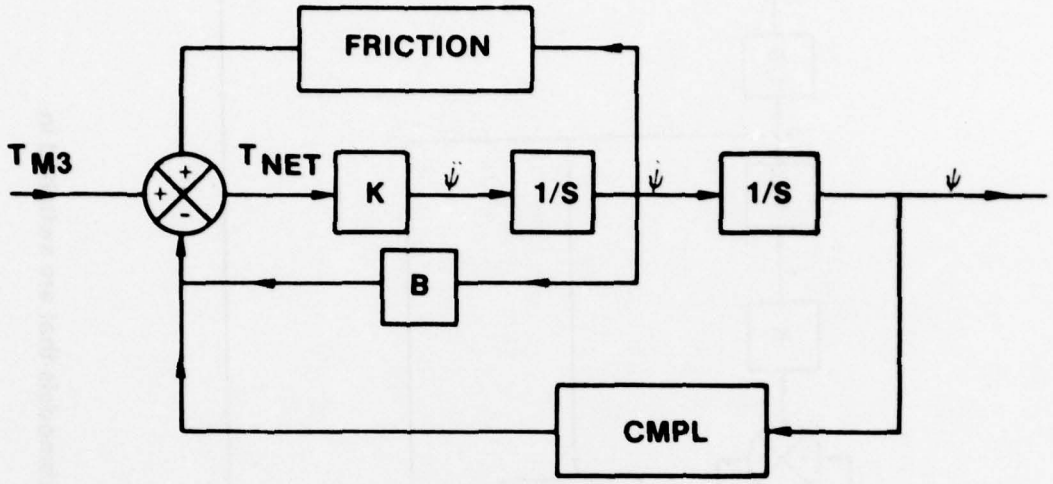

Figure 1. The test problem used to study the friction models.

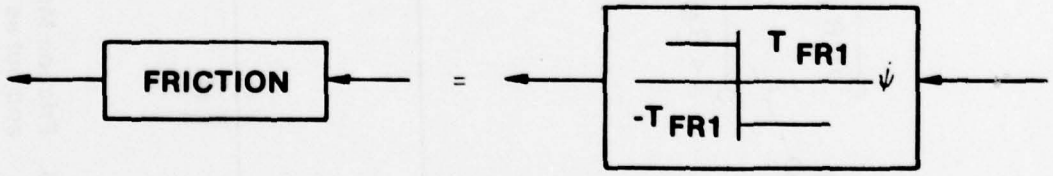

Figure 2. Often used friction model.

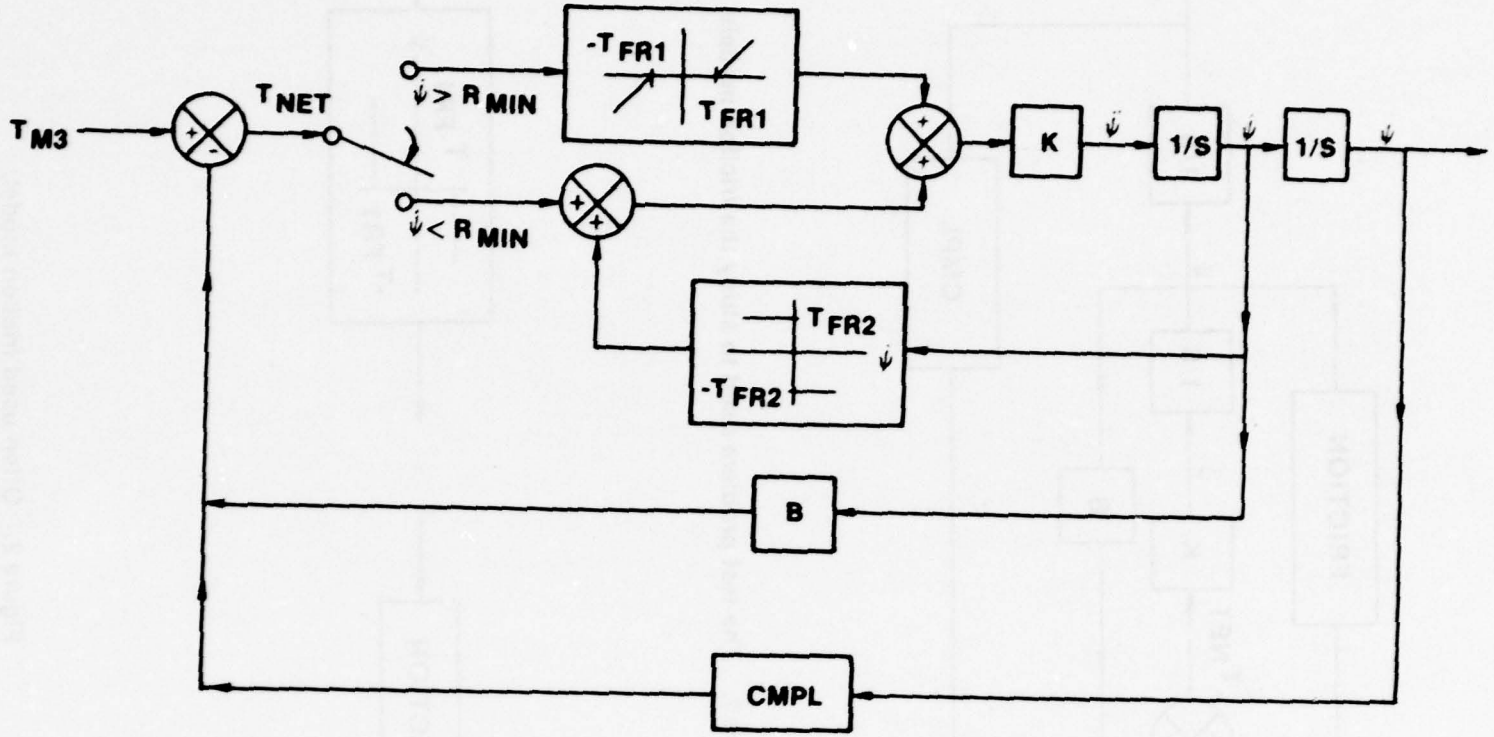

Figure 3. Friction Model B implemented with two submodels that are switched in and out as a function of $\dot{\psi}$.

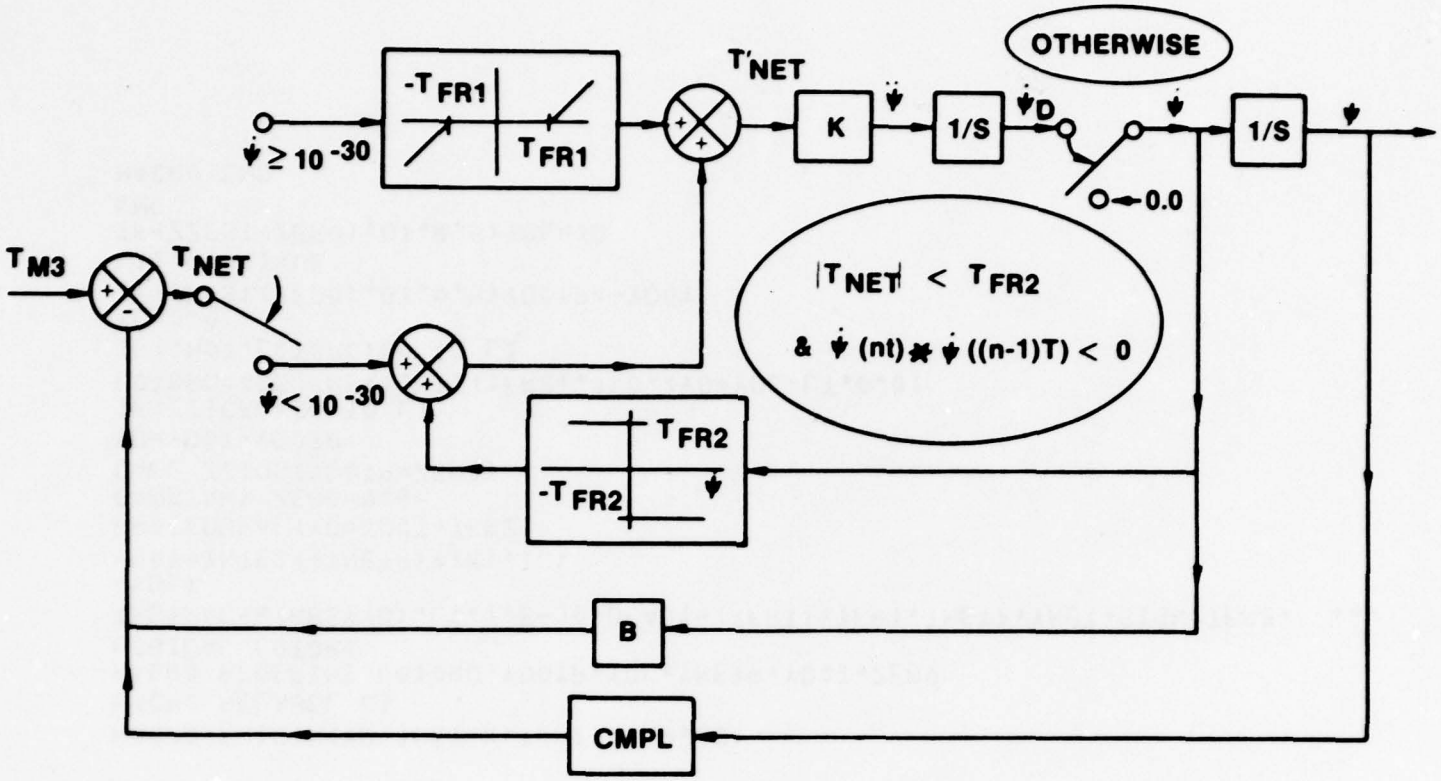

Figure 4. Friction Model C.

```
MACRO FRICTN(YD,TNET,K,TFR1,TFR2,IC)
MACRO RELABEL L1
MACRO REDEFINE LOTORQ,YDOTP,YDL,TNETP,YDOT,ZERO
LOGICAL LOTORC
TNETP=FSW(ABS(YD).LT.1.E-30,DEAD(-(TFR1),TFR1,TNET),TNET+SIGN(TFR2,   ...
-YD))
YDOT=INTEG((TNETP)*(K),IC)
PROCEDURAL(YD=YDOT,TFR2)
CONSTANT ZERO=0.0
CALL ZZICS(YDOTP=ZERO)
YD=YDOT+YDOTP
IF(ZZICFL)GO TO L1
LOTORQ=ABS(TNET).LT.(TFR2).AND.(YD*YDL.LT.0.0)
IF(.NOT.LOTORC)GO TO L1
YD=0.0
IF(ZZFST(ZERO).GT.0.5)YDOTP=-YDOT
L1..CONTINUE
IF(ZZFST(ZERO).GT.0.5)YDL=YD
END
MACRO END
```

Figure 5. Listing of the ACSL FRICTN macro code for Model C.

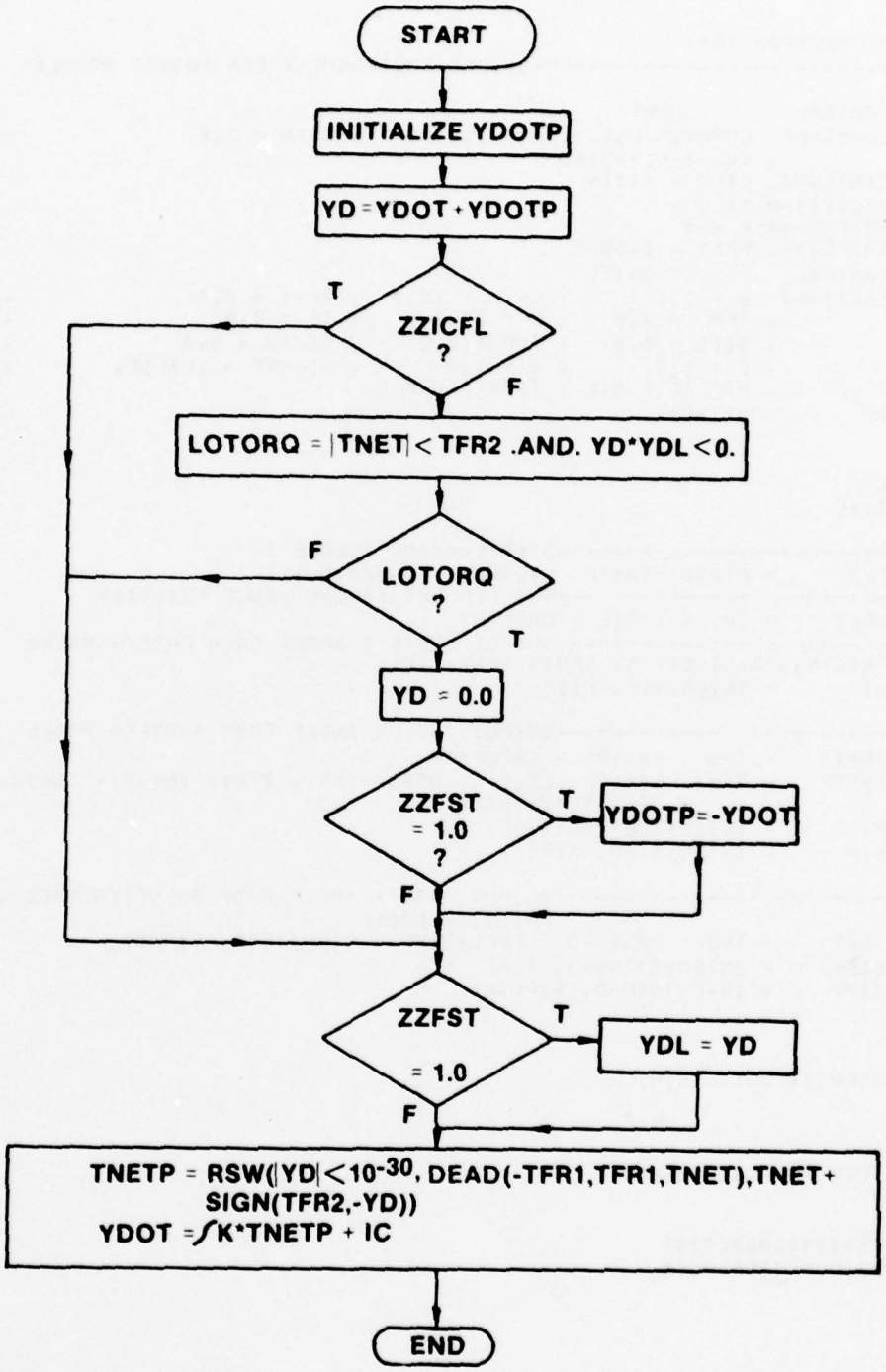

Figure 6. Flow diagram for the FRICTN macro.

```
PROGRAM FRICTION TEST
      "----------------------PROVIDES ENVIRONMENT FOR FRICTN MODULE    "
INITIAL
      LOGICAL         DUMP
      CONSTANT  DUMP=.FALSE. , RMN=1.E-30    , TSTP = 2.0              ...
              , TWOPI=6.283185
      CINTERVAL CINT = 0.010
      ALGORITHM IALG = 4
      NSTEPS NSTP = 1
      MAXTERVAL MAXT = 0.0025
      LOGICAL         SINSTP
      CONSTANT  B = 0.1       , CMPL = 12.0   , TFR1 = 2.0              ...
              , TFR2 = 2.0    , K = 30.0      , IC = 0.0                ...
              , SIIC = 0.0    , ICP = 0.0     , SIPIC = 0.0             ...
              , G = 5.0       , W = 1.0       , SINSTP = .FALSE.        ...
              , SIPPIC = 0.0 , ICPP = 0.0
      WP      = W*TWOPI
END

DYNAMIC
DERIVATIVE

"-----------------------------STEP COMMAND TORQUE IN                    "
      TM3     = G*RSW(SINSTP, SIN(WP*T), STEP(0.1))
"-----------------------------SUM FOR NET TORQUE MINUS FRICTION         "
      TNET    = TM3 - B*SID - CMPL*SI
"-----------------------------OUTPUT  RATE , ANGLE FROM FRICTN MACRO    "
      FRICTN(SID, TNET, K, TFR1, TFR2, IC)
      SI      = INTEG(SID, SIIC)

"-----------------------------OUTPUT RATE , ANGLE FROM ANOTHER MODEL    "
      TNET2   = TM3 - B*SIPD - CMPL*SIP
      TNETP   = RSW(ABS(SIPD).LT.RMN, DEAD(-TFR1, TFR1, TNET2), TNET2...
                  , SIGN(TFR2,-SIPD))
      SIPD    = INTEG(TNETP*K, ICP)
      SIP     = INTEG(SIPD, SIPIC)

"-----------------------------OUTPUT RATE , ANGLE FROM AN OFTEN USED ...
                              FRICTION MODEL                            "
      TNET3   = TM3 - B*SIPPD - CMPL*SIPP , SIGN(TFR2,-SIPPD)
      SIPPD   = INTEG(K*TNET3, ICPP)
      SIPP    = INTEG(SIPPD, SIPPIC)

END

      TERMT(T .GT. TSTP)
END

TERMINAL
      IF(DUMP) CALL DEBUG
END
END
0000000000000000000000
0000000000000000000000
```

Figure 7. Listing of the ACSL test program.

```
CONNECT.OUTPUT
ETL.170
ATTACH.INPUT.TEK.ID=DDXXXH
ATTACH.LGOR.TEK.ID=DDXXXH.CY=1
LGOR
     .
     .
     .
SET TFR1=14..TFR2=14..G=20..K=10..MAXT=0.015
SET TITLE(3)="8 JUNE 79"
PLOT "XPI"=2..SI.SID
PLOT SIP.SIPD
PLOT SIPP.SIPPD
PLOT SIPP.SIP.SI
     .
     .
     .
STOP
BATCH.PRINT.PRINT.HERE.HDMDD
```

Figure 8. Outline of the Tektronix keyboard inputs for interactive session setup and ACSL run time commands.

```
00000000000000000000
HDMDD,CM77000.
ACCT...
ATTACH(MACFIL,DCMACFIL,ID=DCACSLSYS)
ATTACH(ACSL,DCACSL,ID=DCACSLSYS)
ACSL(I=INPUT)
RETURN,ACSL,MACFIL.
FTN(I=COMPILE,R=2)
MAP,OFF.
REQUEST,LGOB,*PF.
ATTACH(ACSLLIB,DCACSLLIB,ID=DCACSLSYS)
ATTACH,PLT,TEKTRONIX4014,ID=WTPLOT,CY=2.
LDSET(LIB=PLT,SUBST=ZZDRAW-TEKPLT)
LDSET(LIB=ACSLLIB,PRESET=INDEF)
LOAD,LGO.
NOGO,LGOB.
RETURN,ACSLLIB,PLT.
CATALOG,LGOB,TEK,ID=DCXXXH,CY=1.
EXIT.
00000000000000000000
```

Figure 9a. Job control stream used to generate LGOB, the absolute binary file of the test program.

```
SET PRN=9
SET PRNPLT=.F.,CALPLT=.T.,TTLCPL=.T.
SET TITLE="FRICTN TESTER -"
SET DUMP=.T.
SAVE "BASE"
PROCED GO
START
PRINT "ALL"
END
PREPAR T,SI,SID,SIP,SIPD,SIPP,SIPPD,TM3,TNET,TNET2,TNET3
SET CMD=DIS
```

Figure 9b. ACSL run time commands on file INPUT.

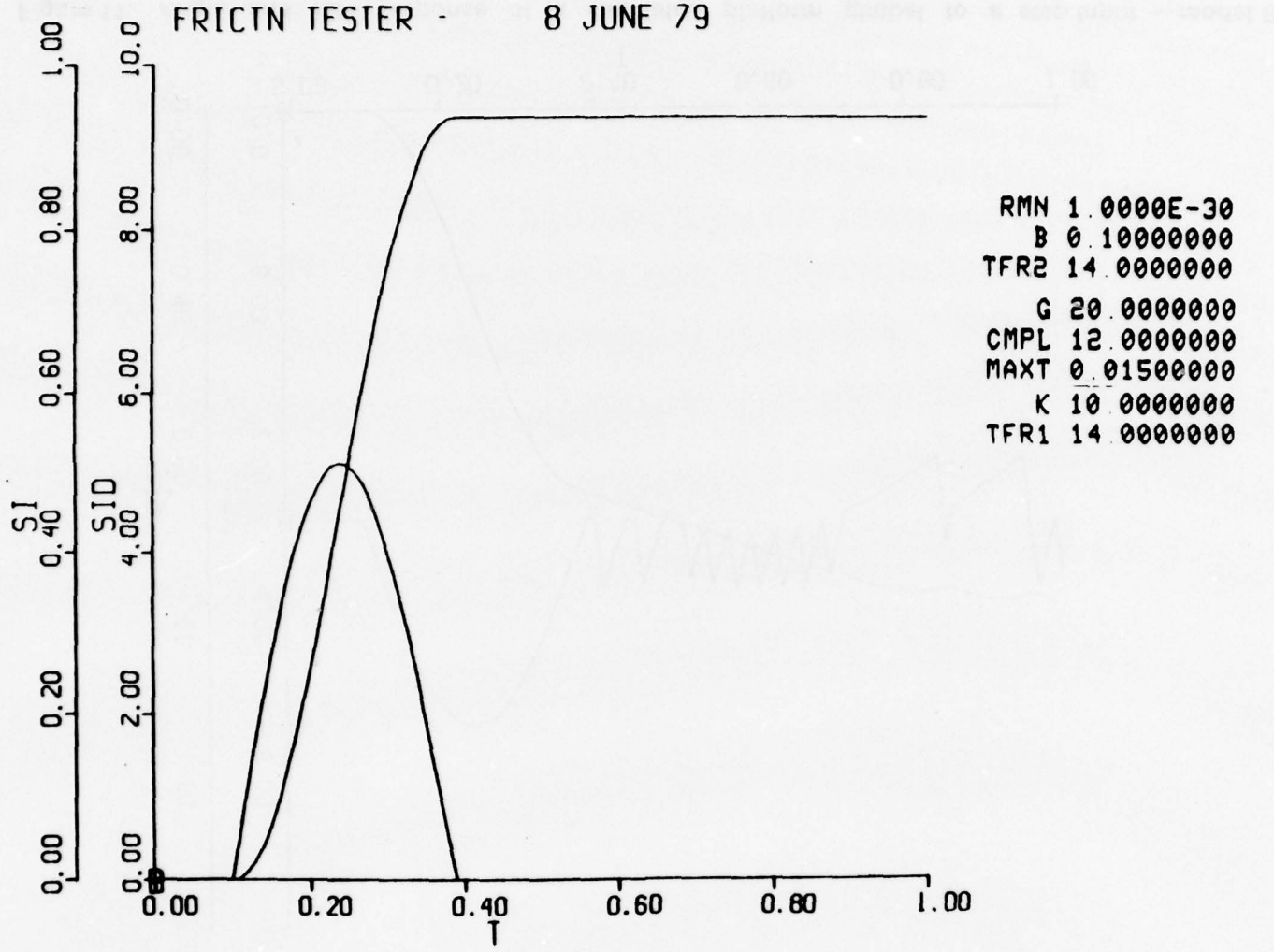

Figure 10. Angle and rate response of a simulated platform gimbal to a step input — model C.

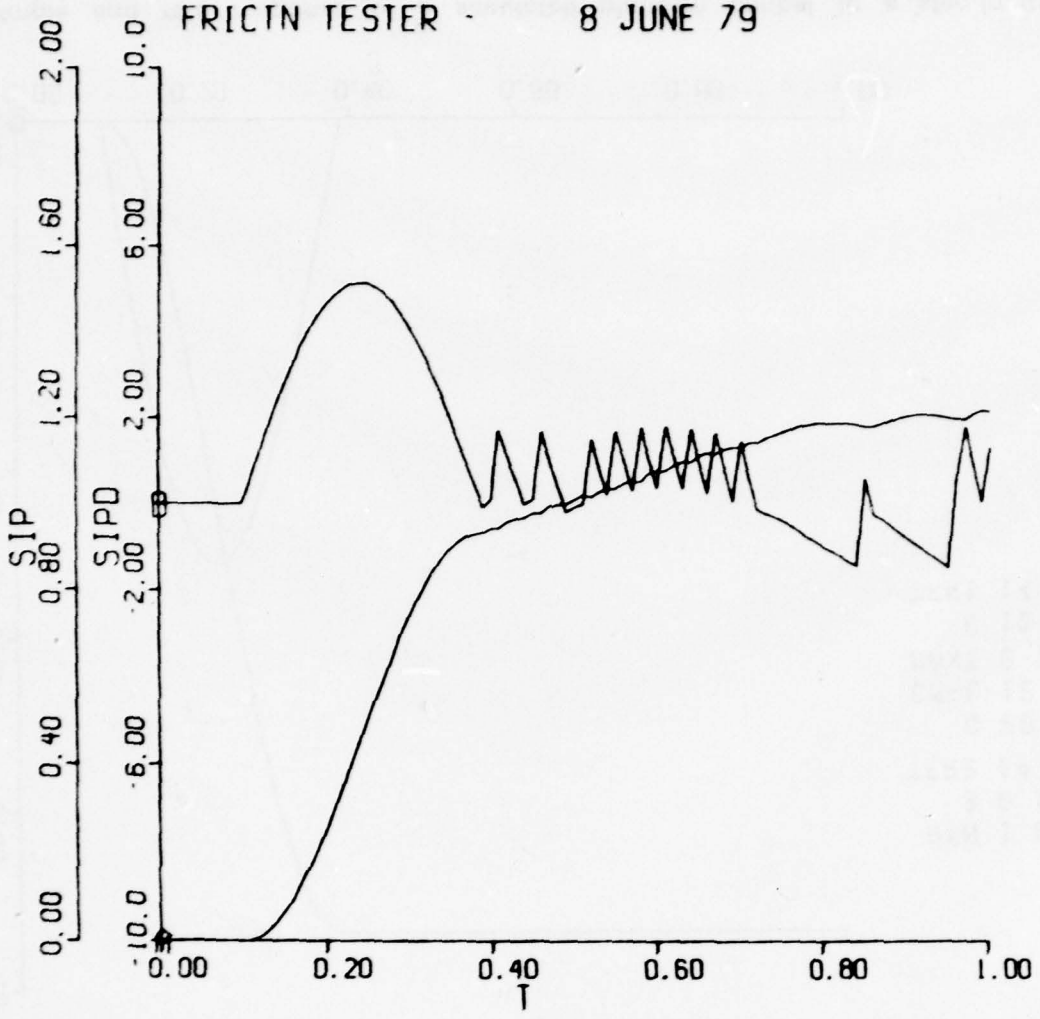

Figure 11. Angle and rate response of a simulated platform gimbal to a step input — model B.

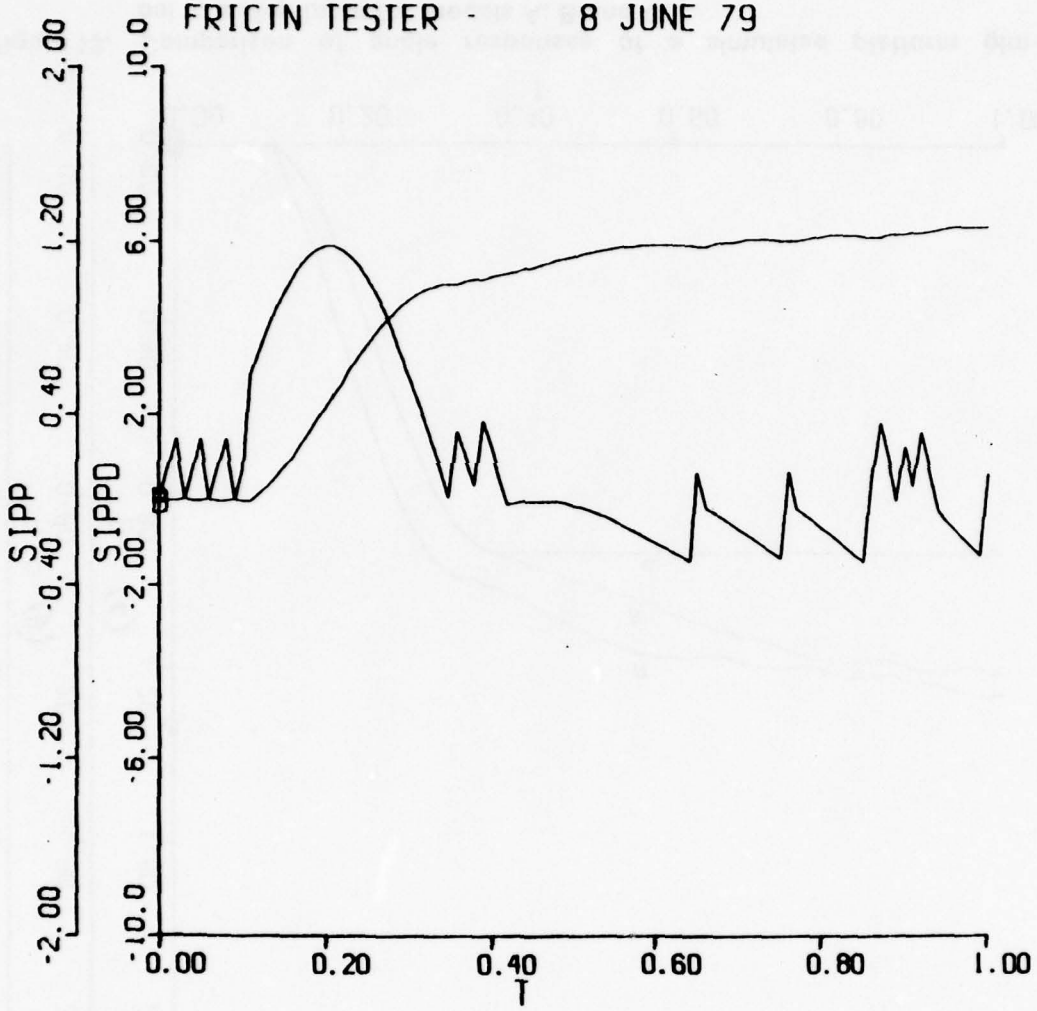

Figure 12. Angle and rate response of a simulated platform gimbal to a step input — model A.

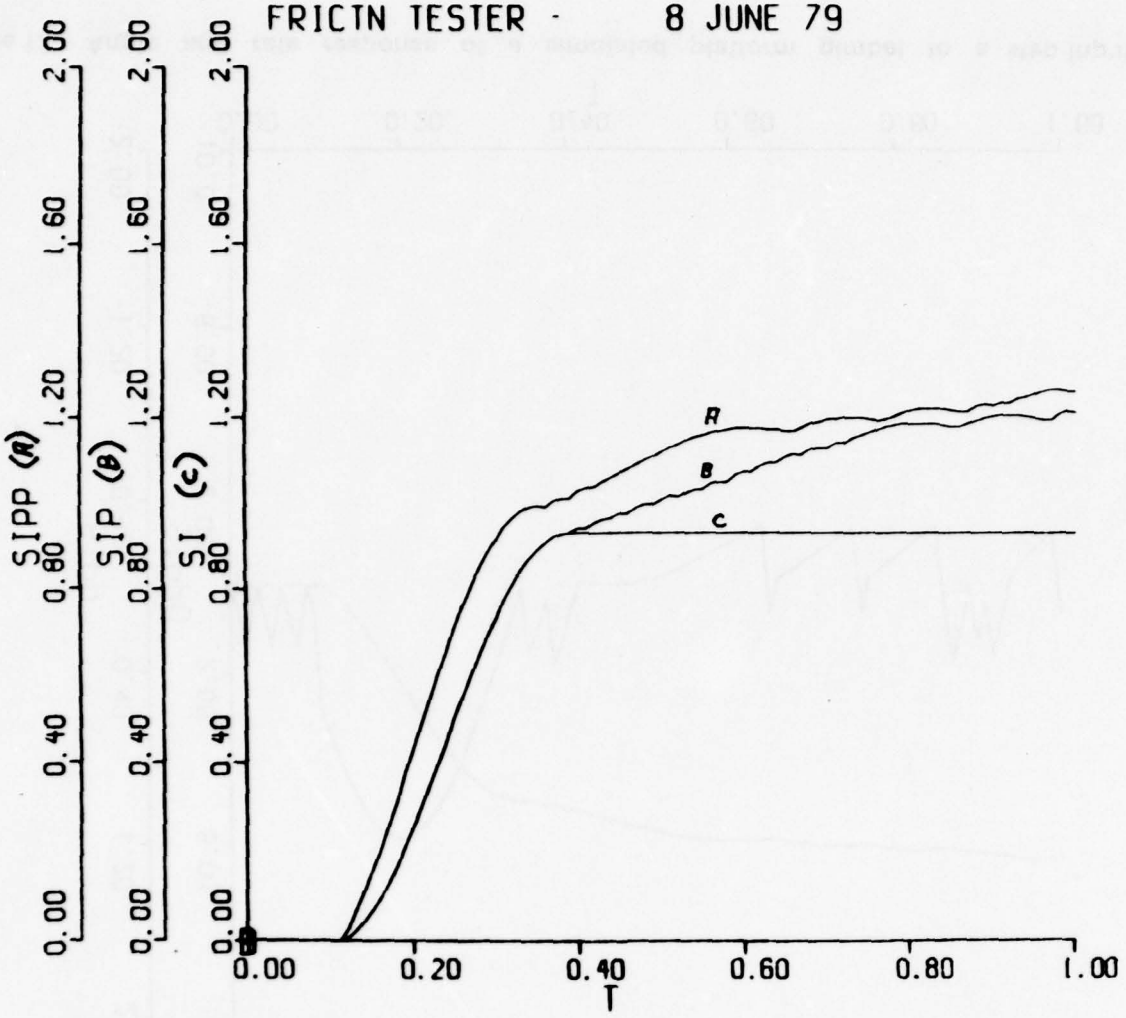

Figure 13. Comparison of angle responses of a simulated platform gimbal to a step input for models A, B and C.

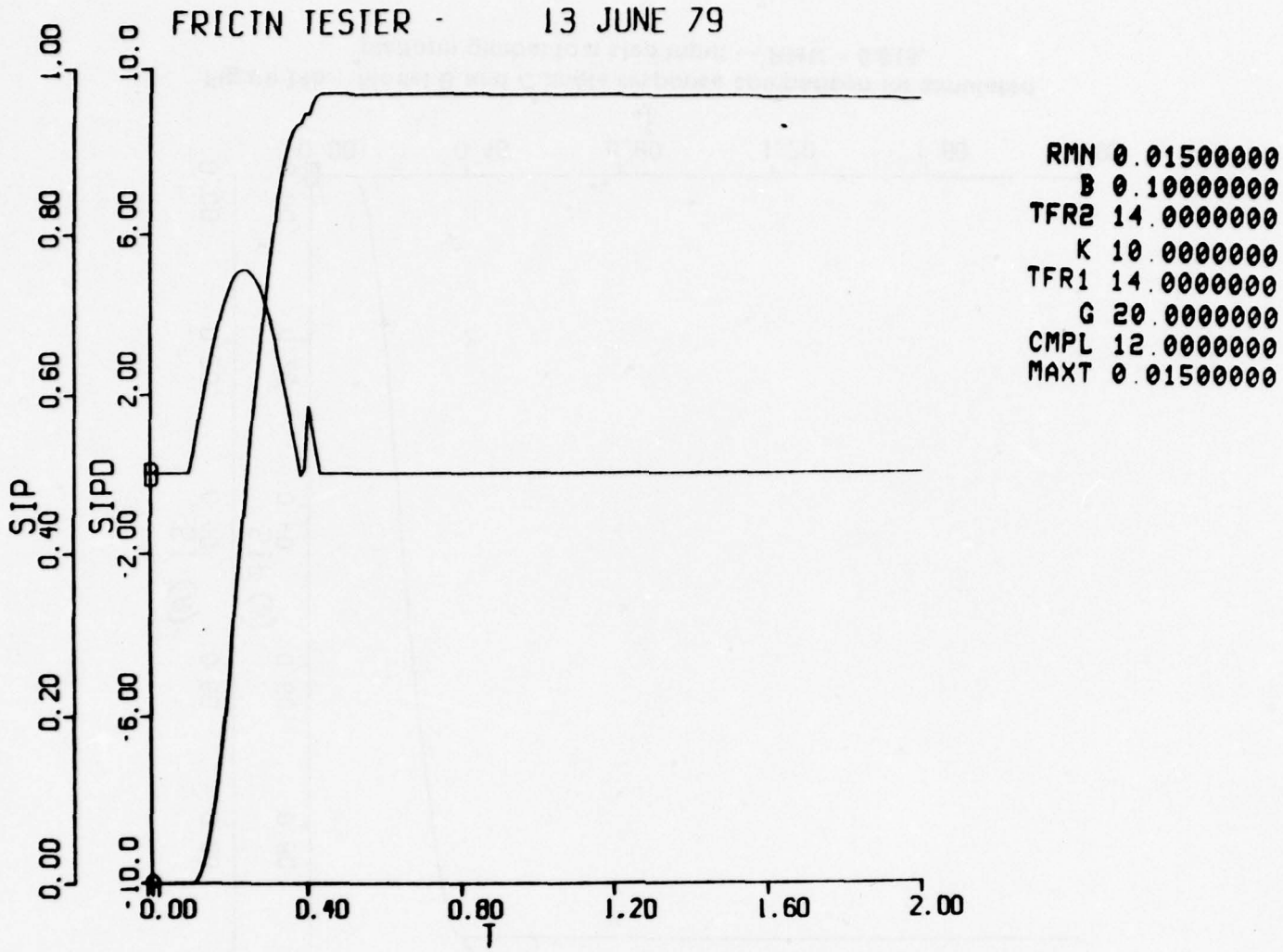

Figure 14a. Angle and rate response of a simulated platform gimbal to a step input — model B with RMN = 0.015.

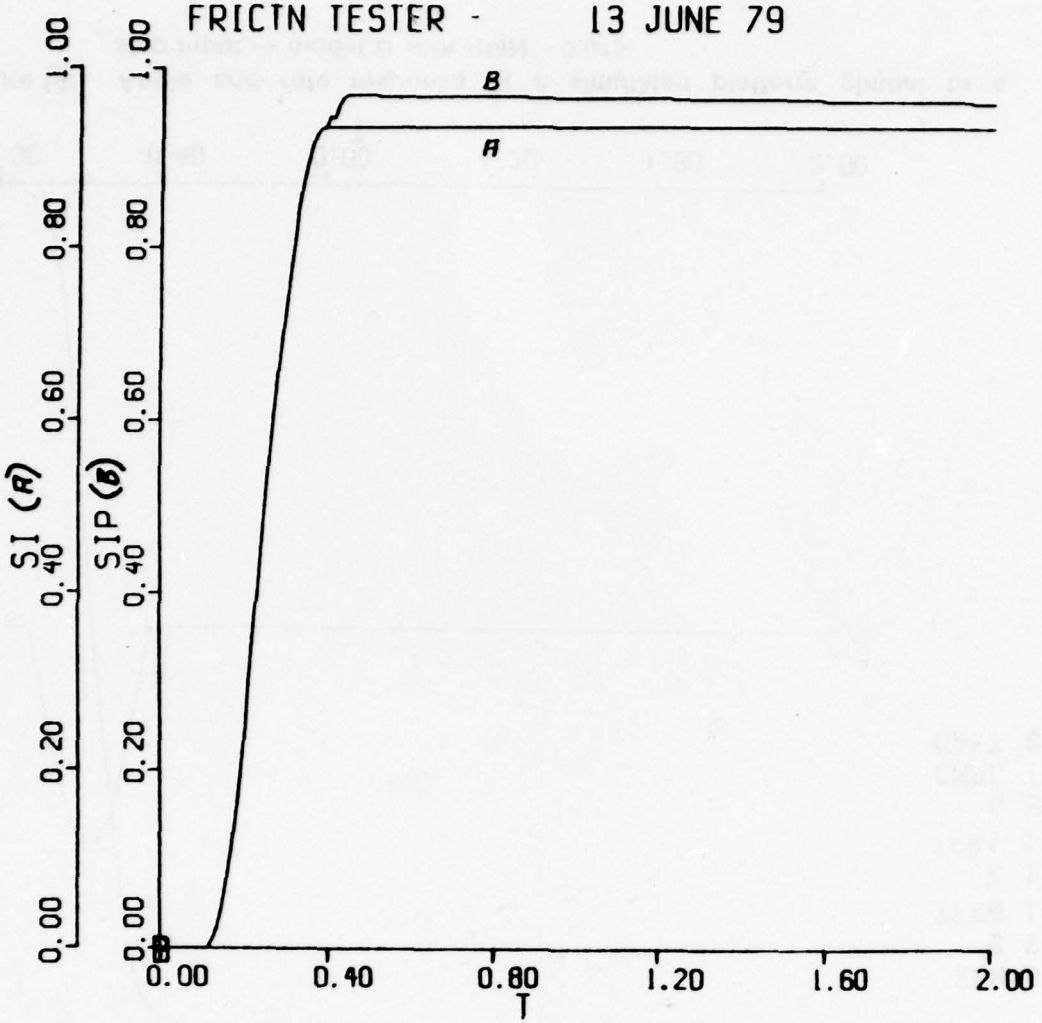

Figure 14b. Model B and C angle response comparison for simulated platform gimbal to a step input — RMN = 0.015.

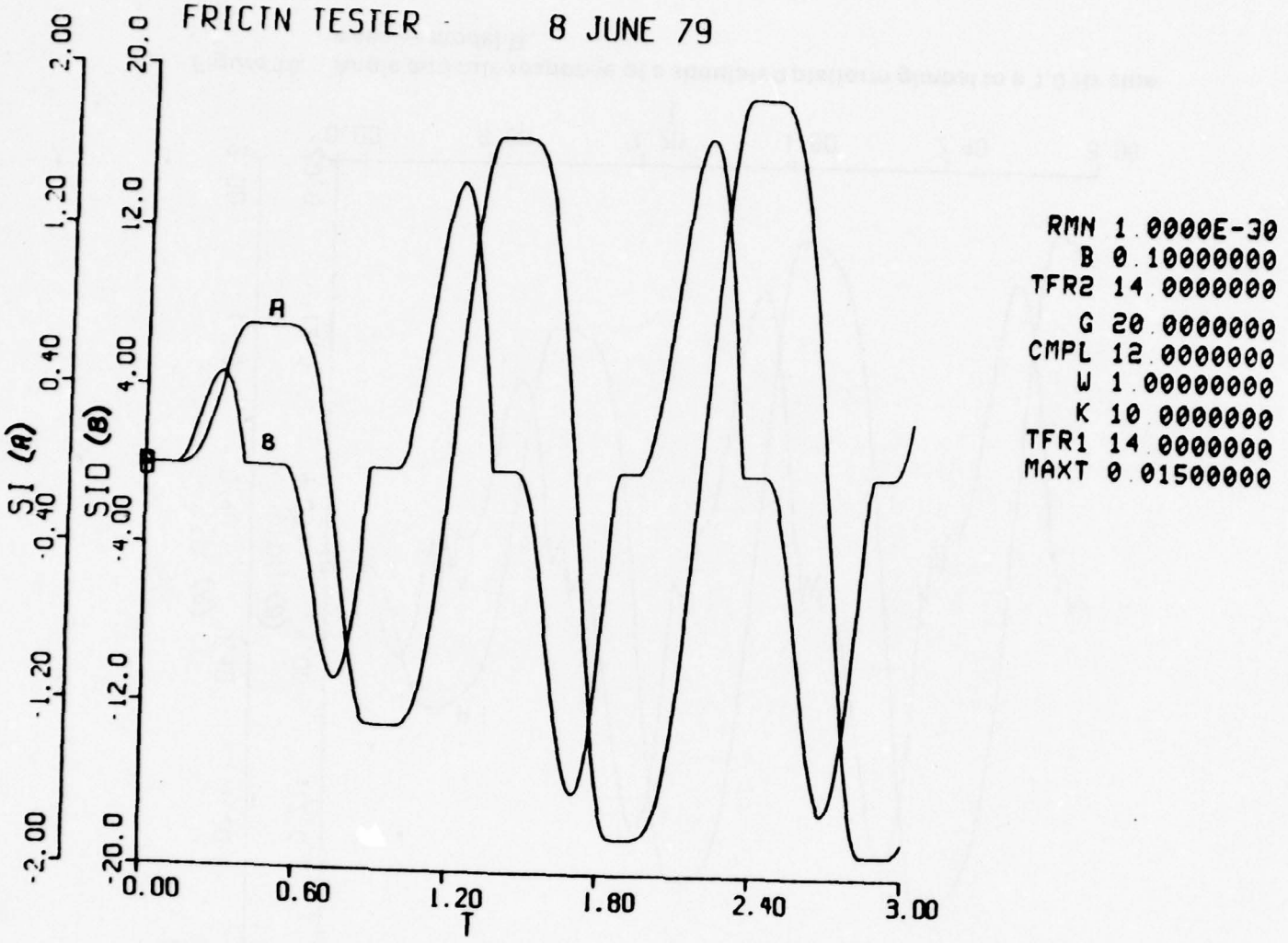

Figure 15. Angle and rate response of a simulated platform gimbal to a 1.0 Hz sine wave — model C.

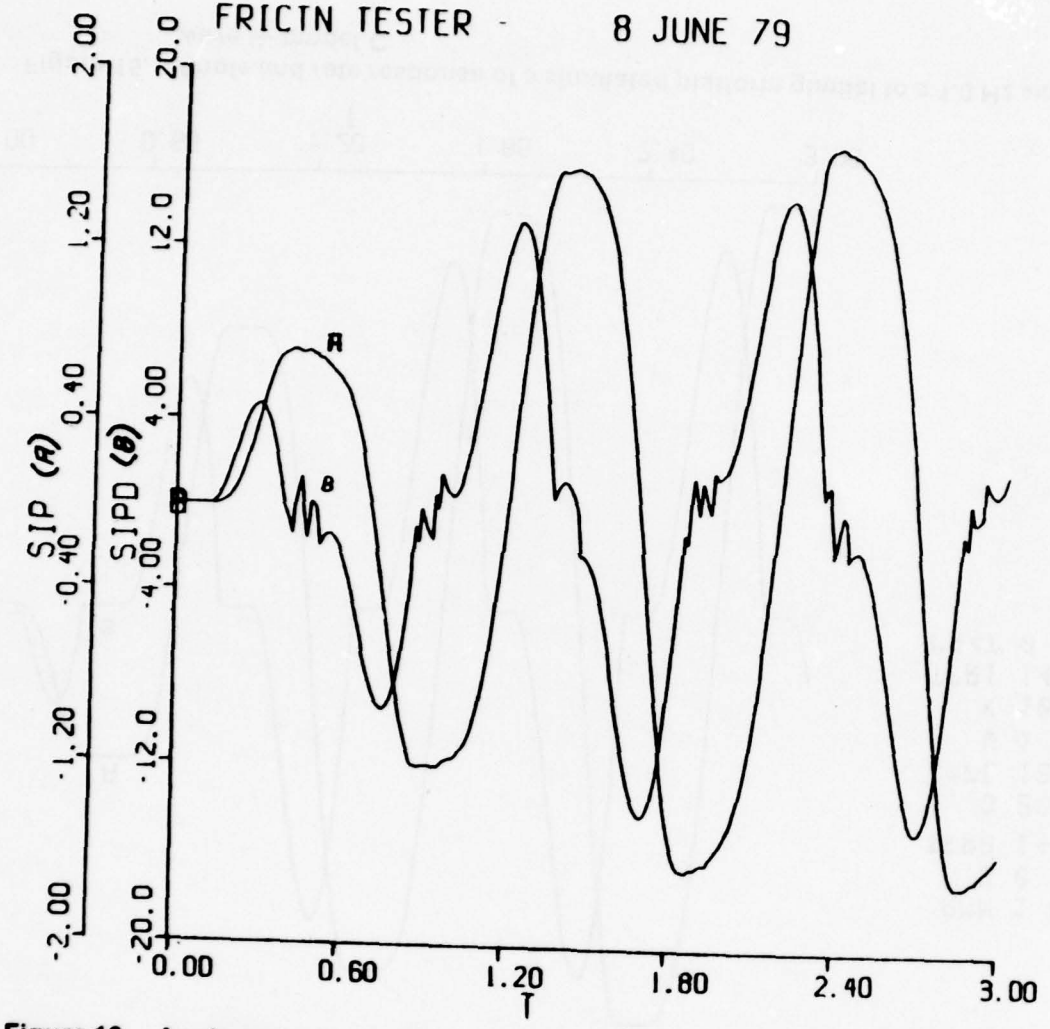

Figure 16. Angle and rate response of a simulated platform gimbal to a 1.0 Hz sine wave — model B.

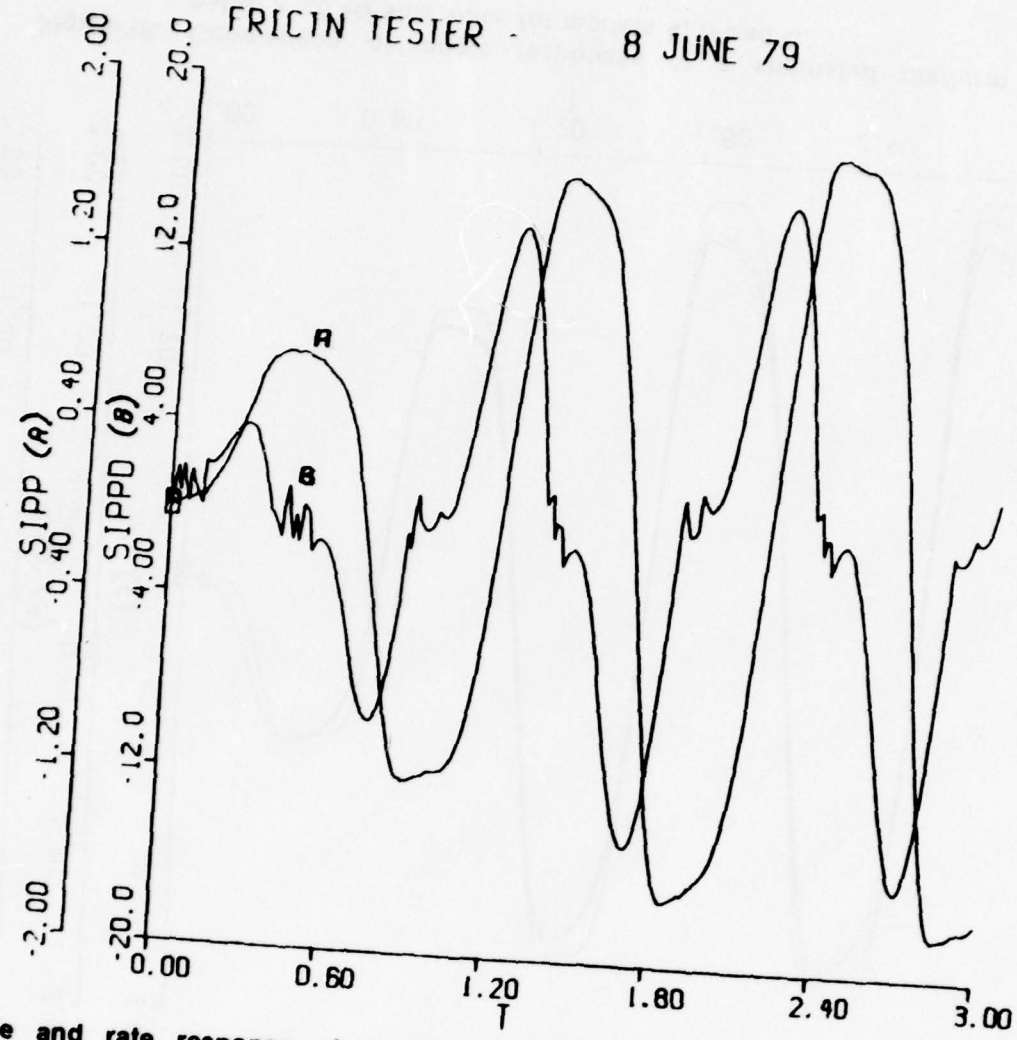

Figure 17. Angle and rate response of a simulated platform gimbal to a 1.0 Hz sine wave — model A.

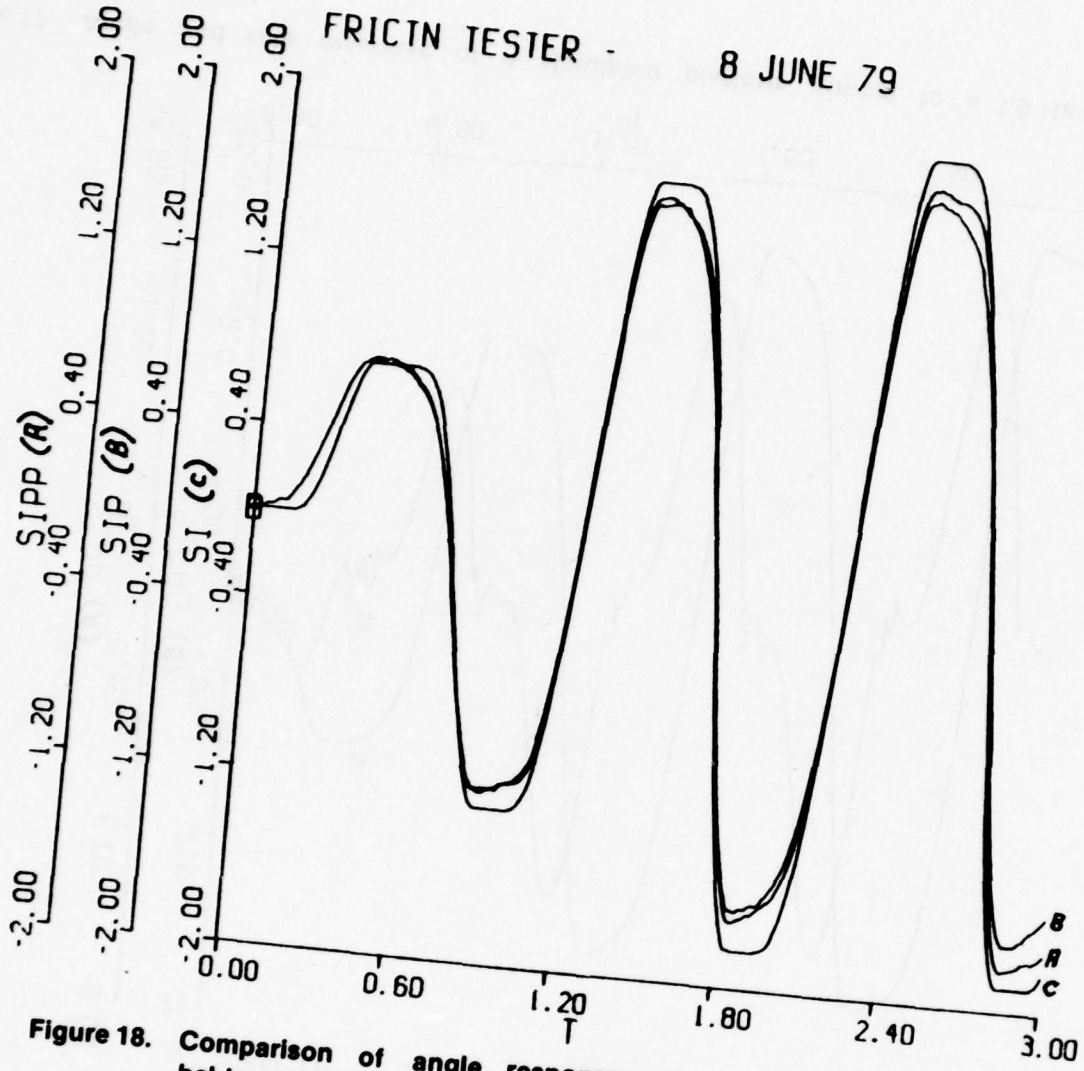

Figure 18. Comparison of angle responses of a simulated platform gimbal to a 1.0 Hz sine wave for models A, B and C.

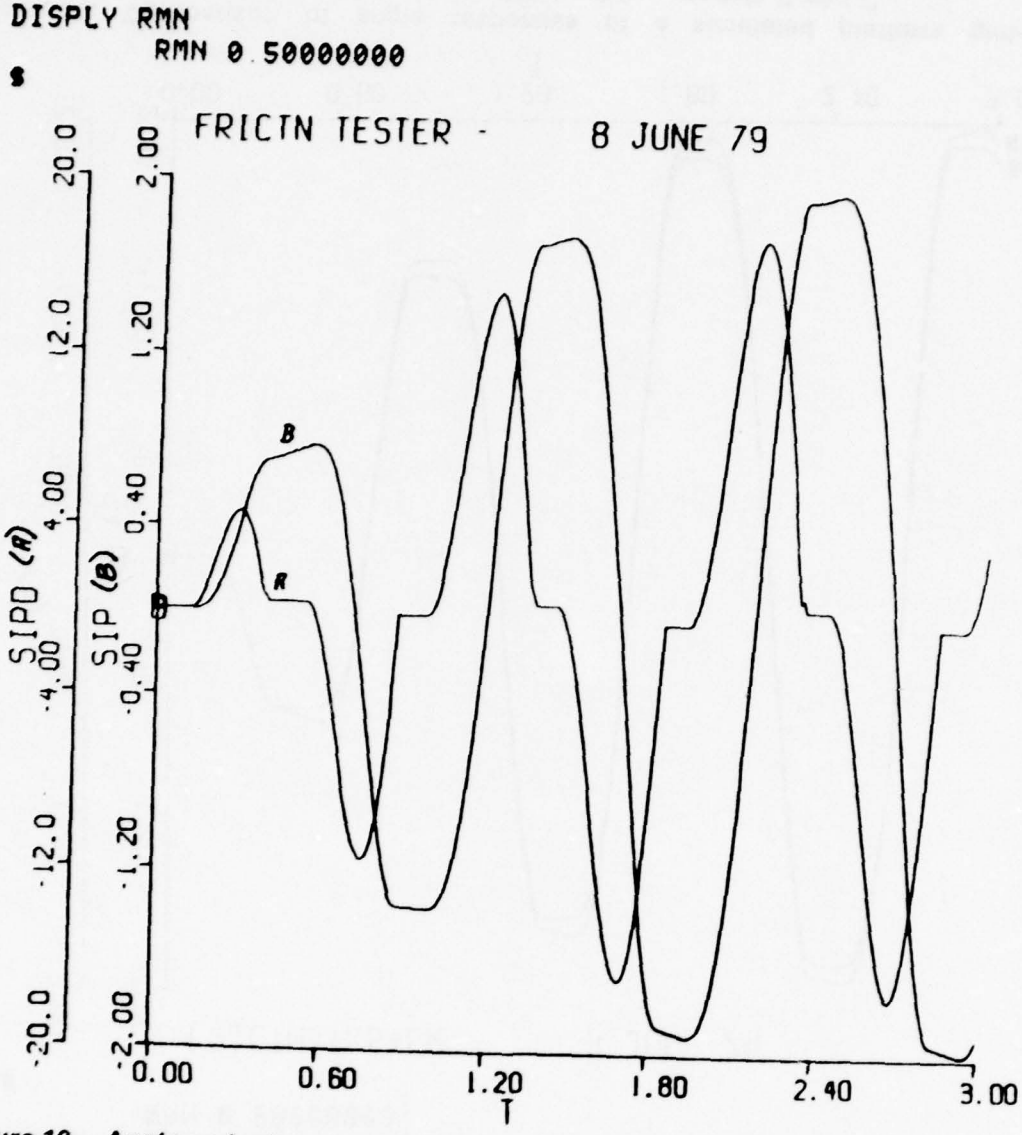

Figure 19. **Angle and rate response of a simulated platform gimbal to a 1.0 Hz sine wave for RMN = 0.5 — model B.**

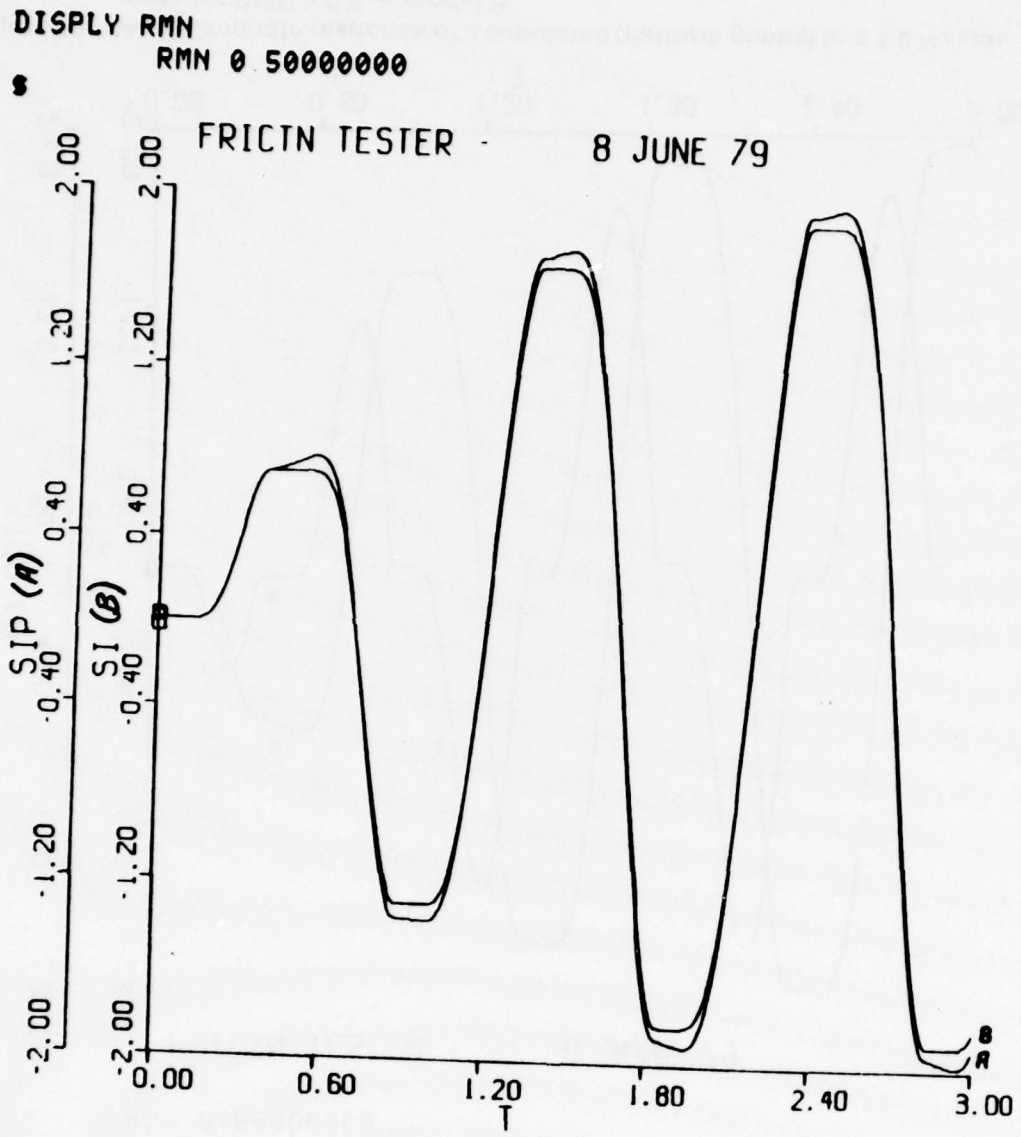

Figure 20. Comparison of angle responses of a simulated platform gimbal to a 1.0 Hz sine wave for RMN = 0.5 — models B and C.

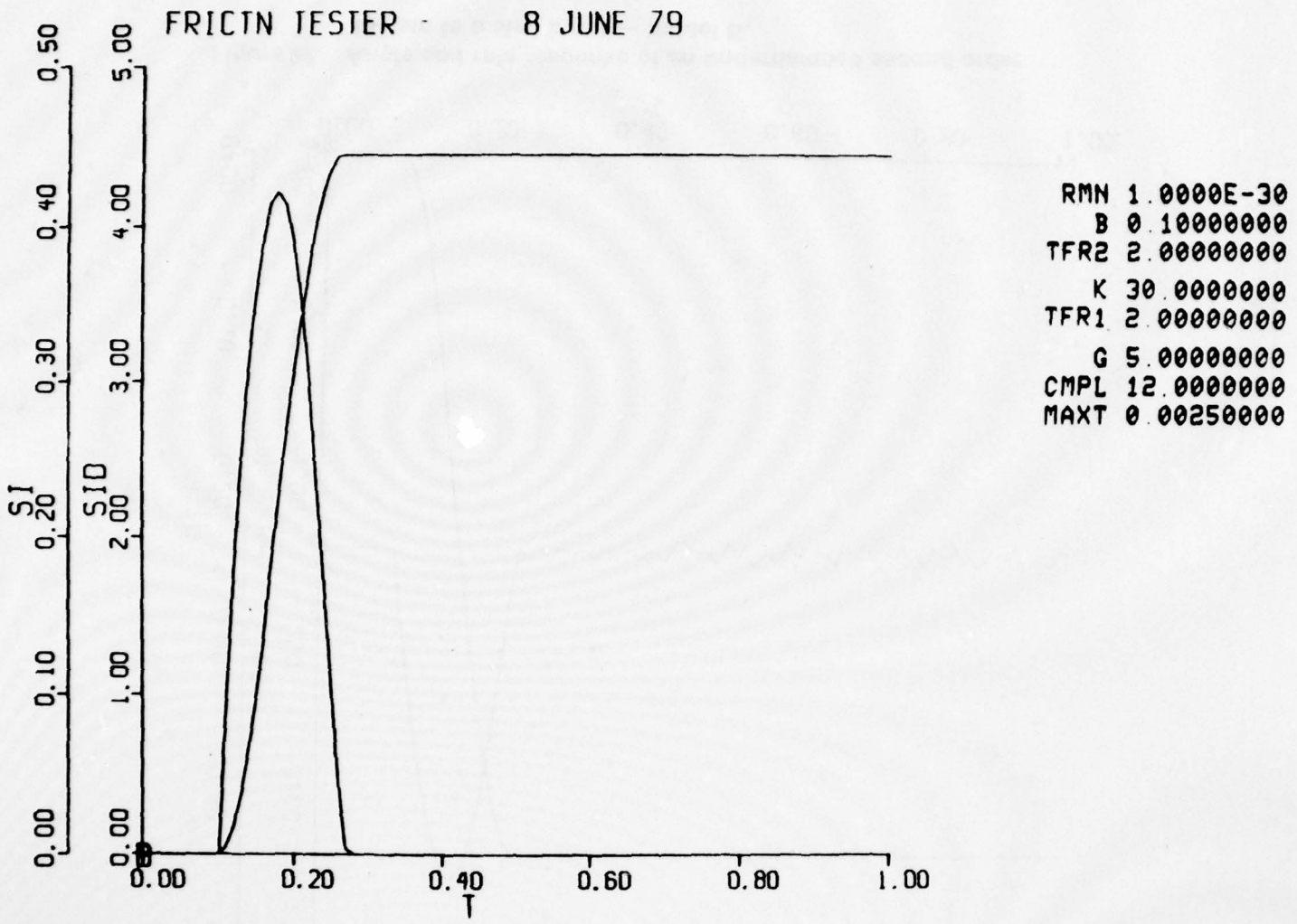

Figure 21. Angle and rate response of an underdamped second order system to a step input — model C.

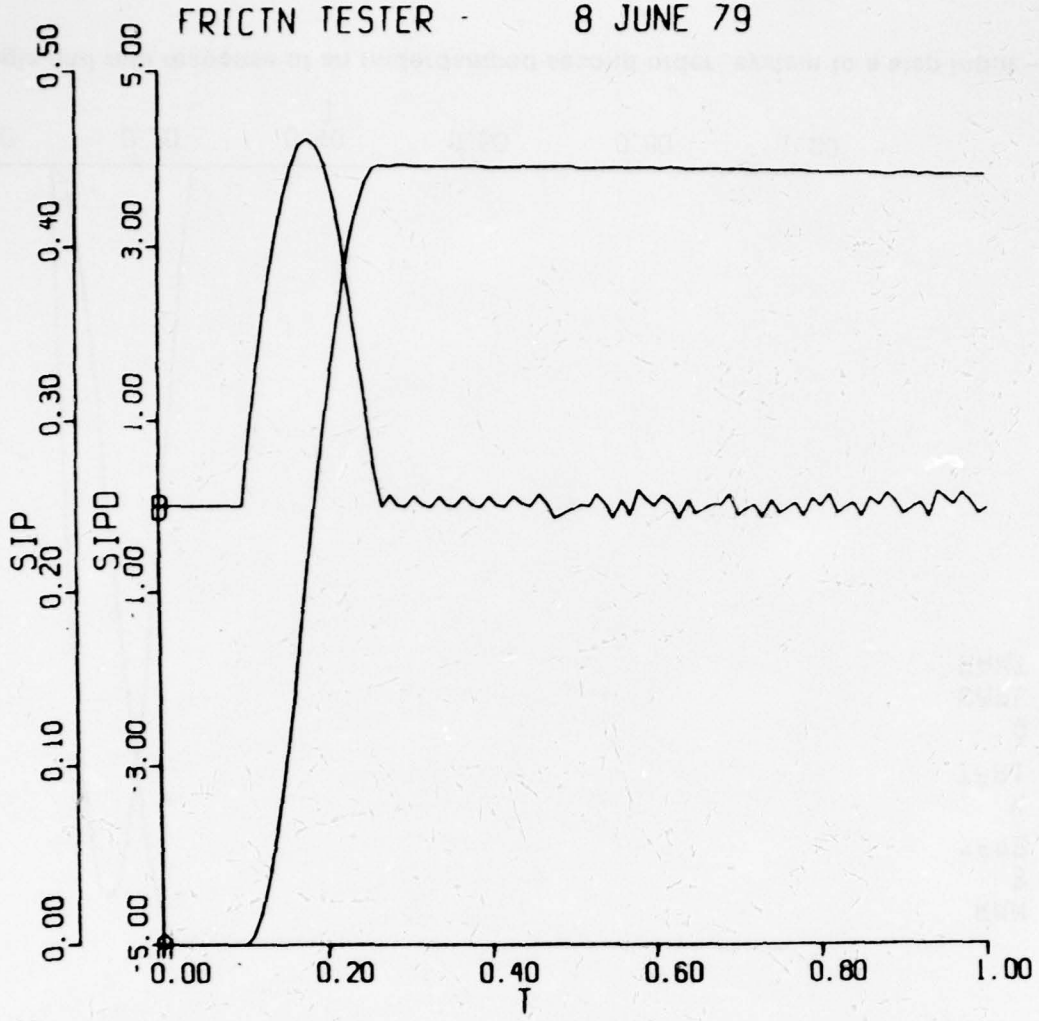

Figure 22. Angle and rate response of an underdamped second order system to a step input — model B.

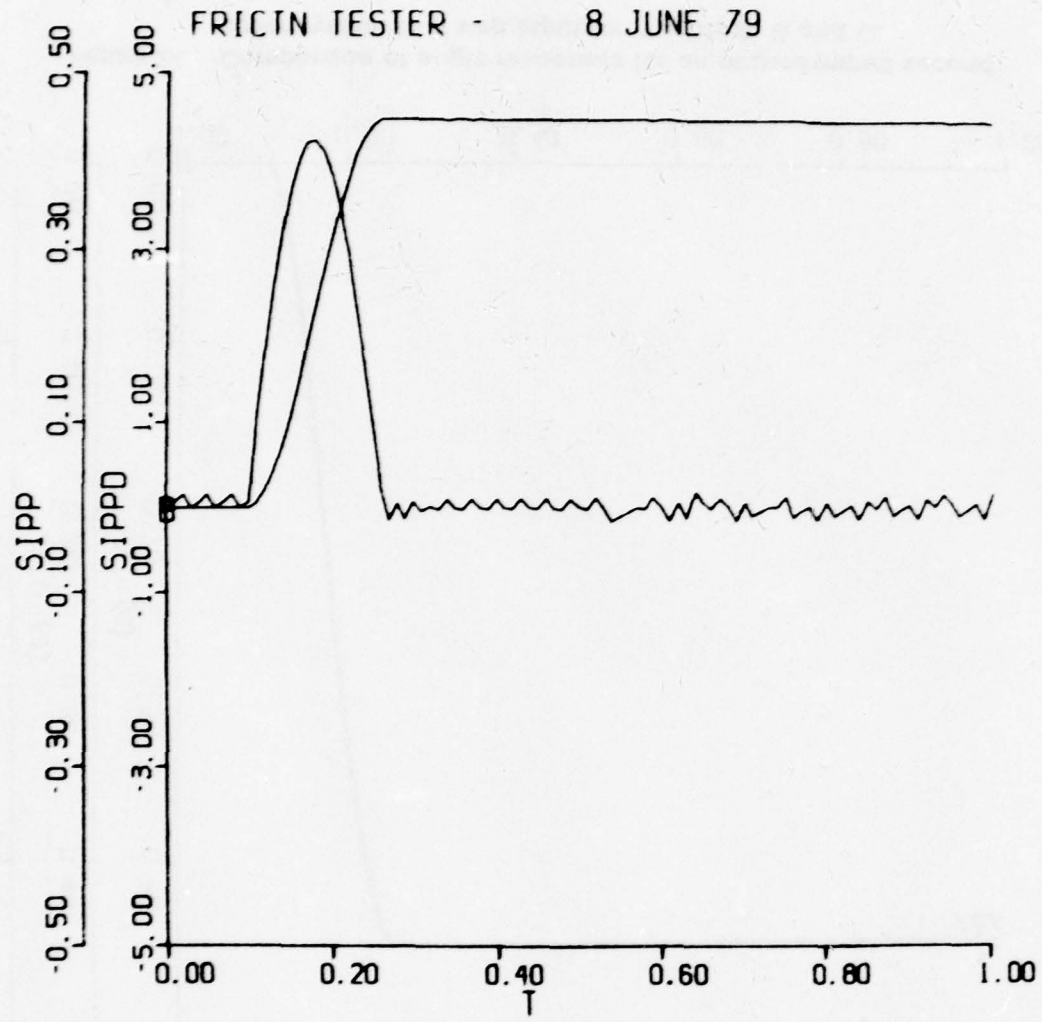

Figure 23. Angle and rate response of an underdamped second order system to a step input — model A.

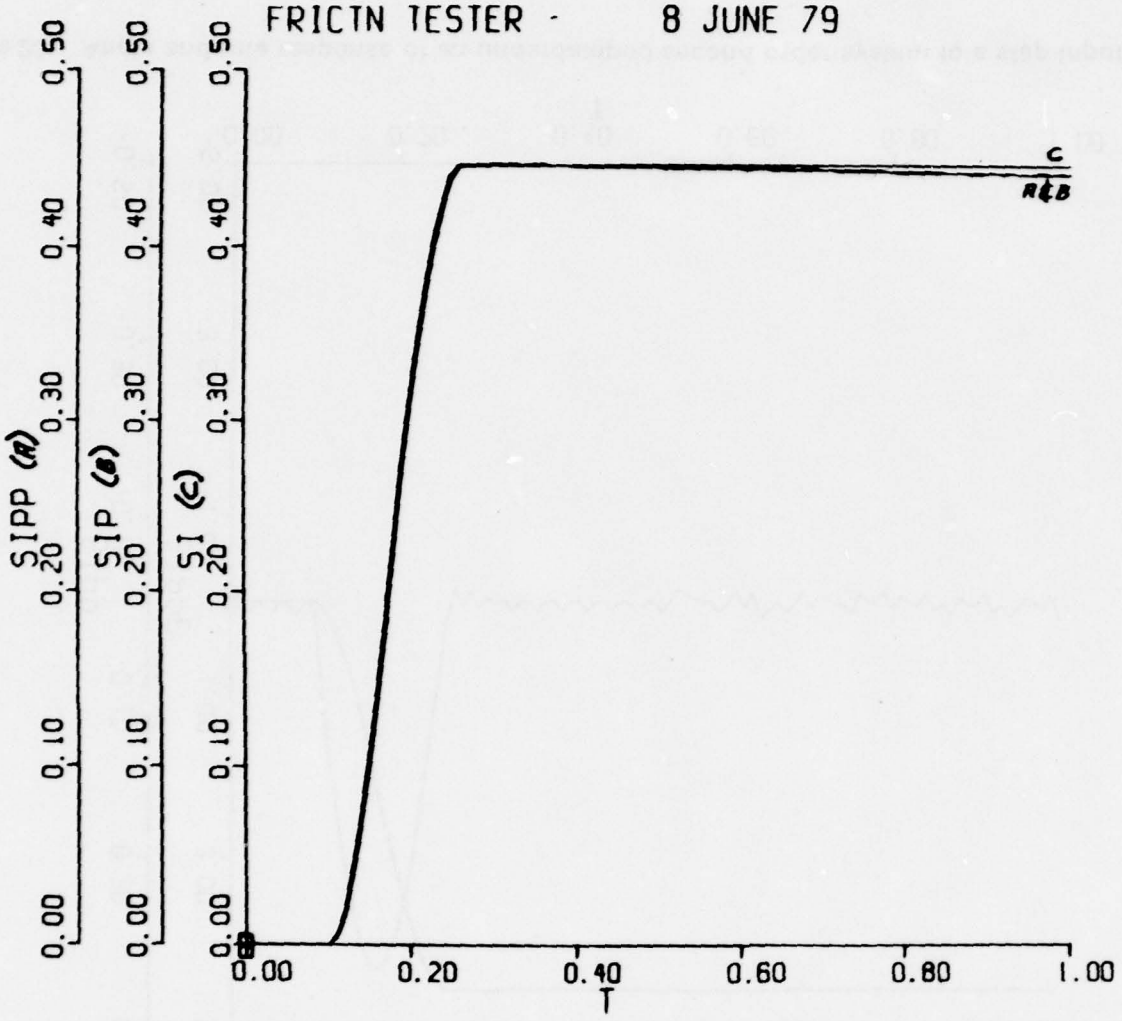

Figure 24. Comparison of angle responses for an underdamped second order system to a step input for models A, B and C.

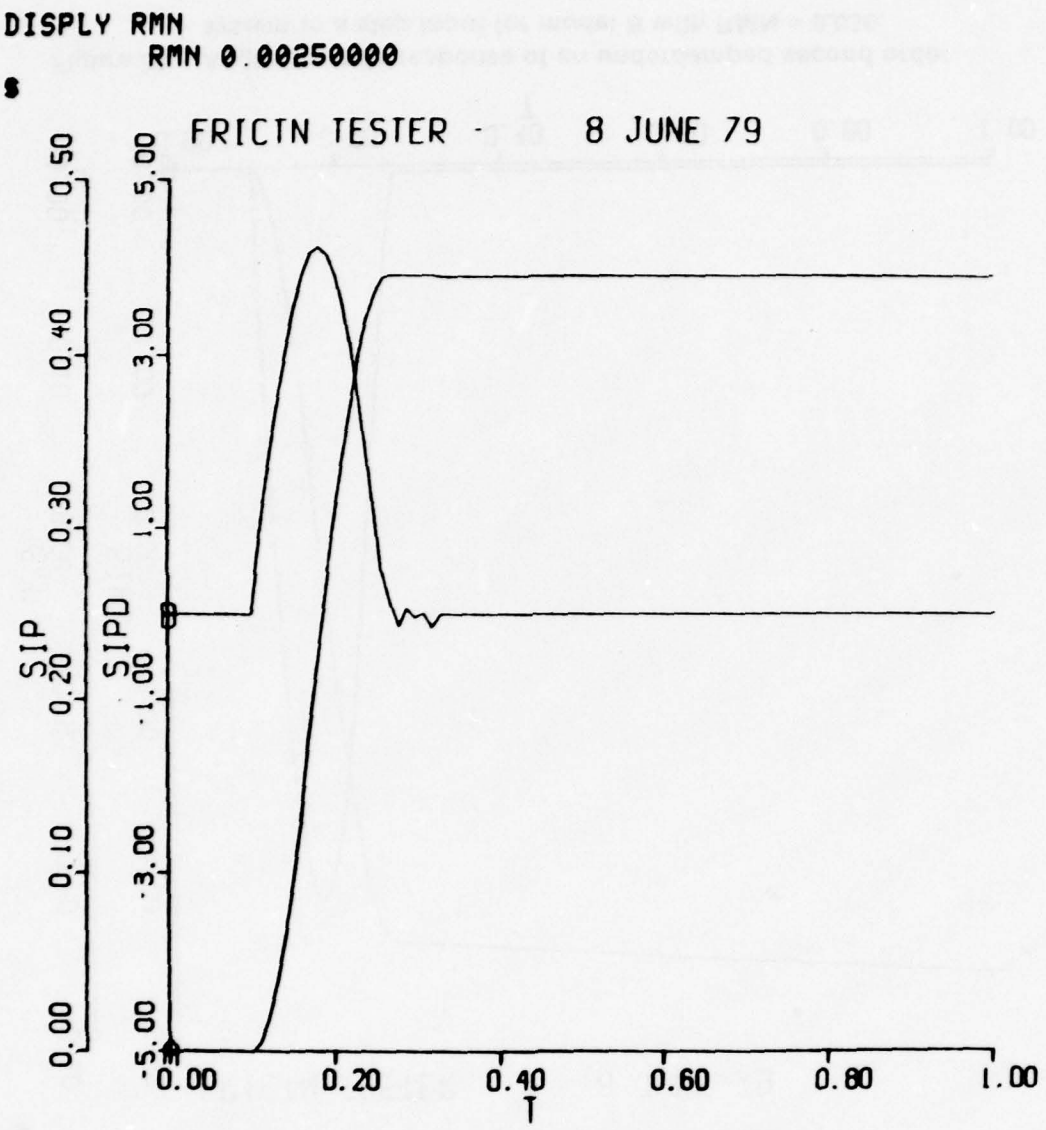

Figure 25. Angle and rate response of an underdamped second order system to a step input for model B with RMN = 0.0025.

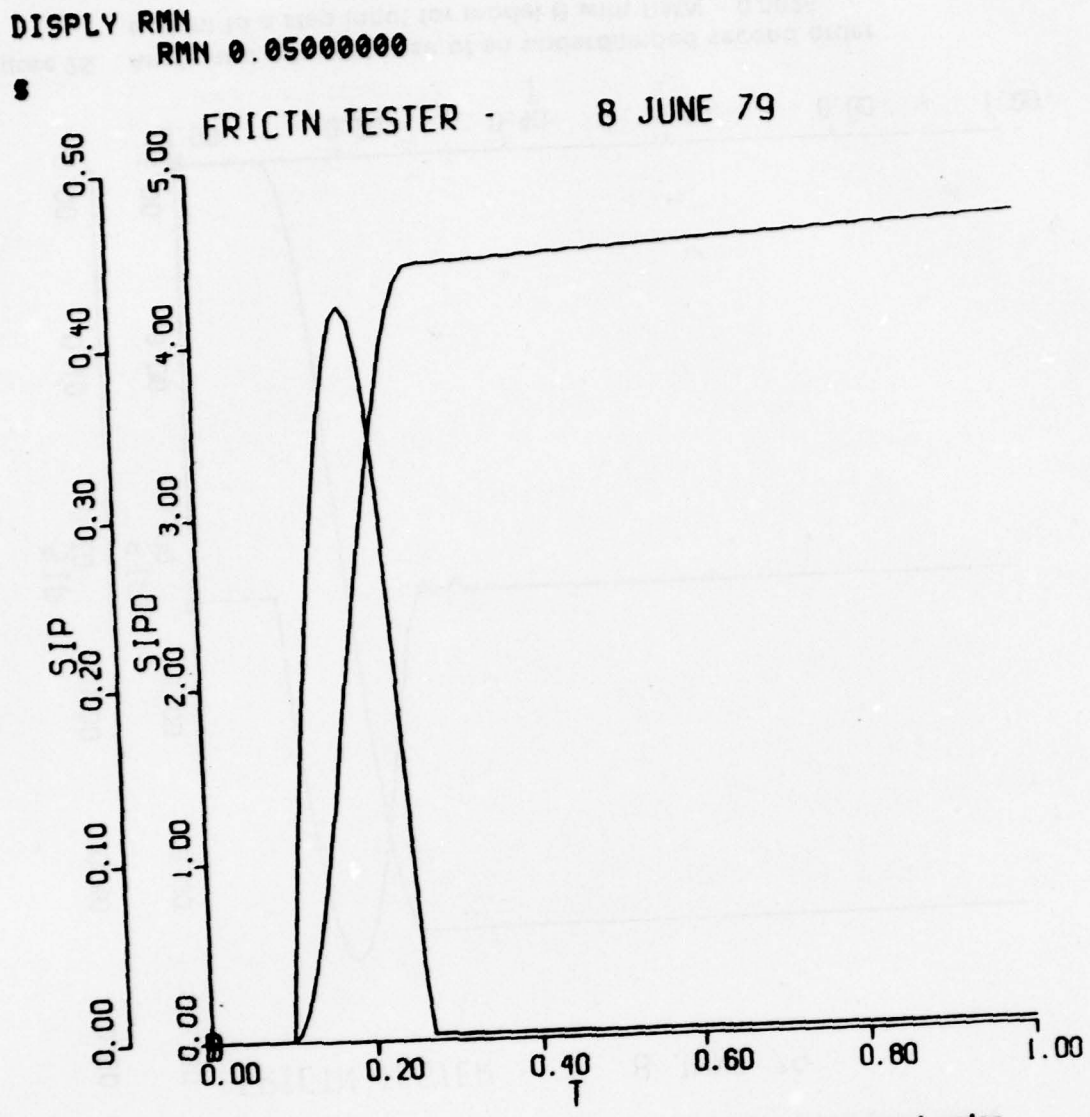

Figure 26. Angle and rate response of an underdamped second order system to a step input for model B with RMN = 0.050.

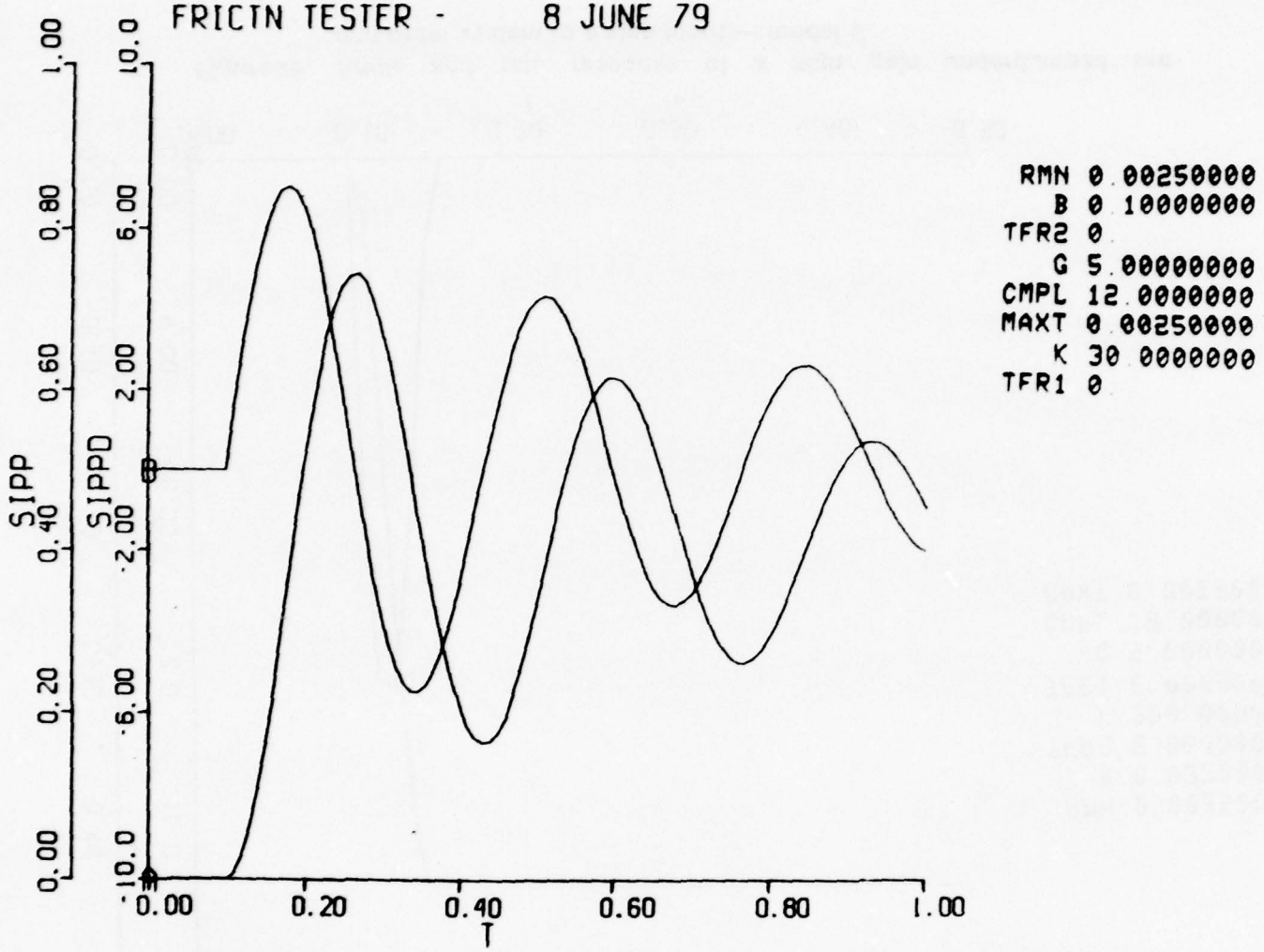

Figure 27. Angle and rate response of the frictionless underdamped second order system to a step input.

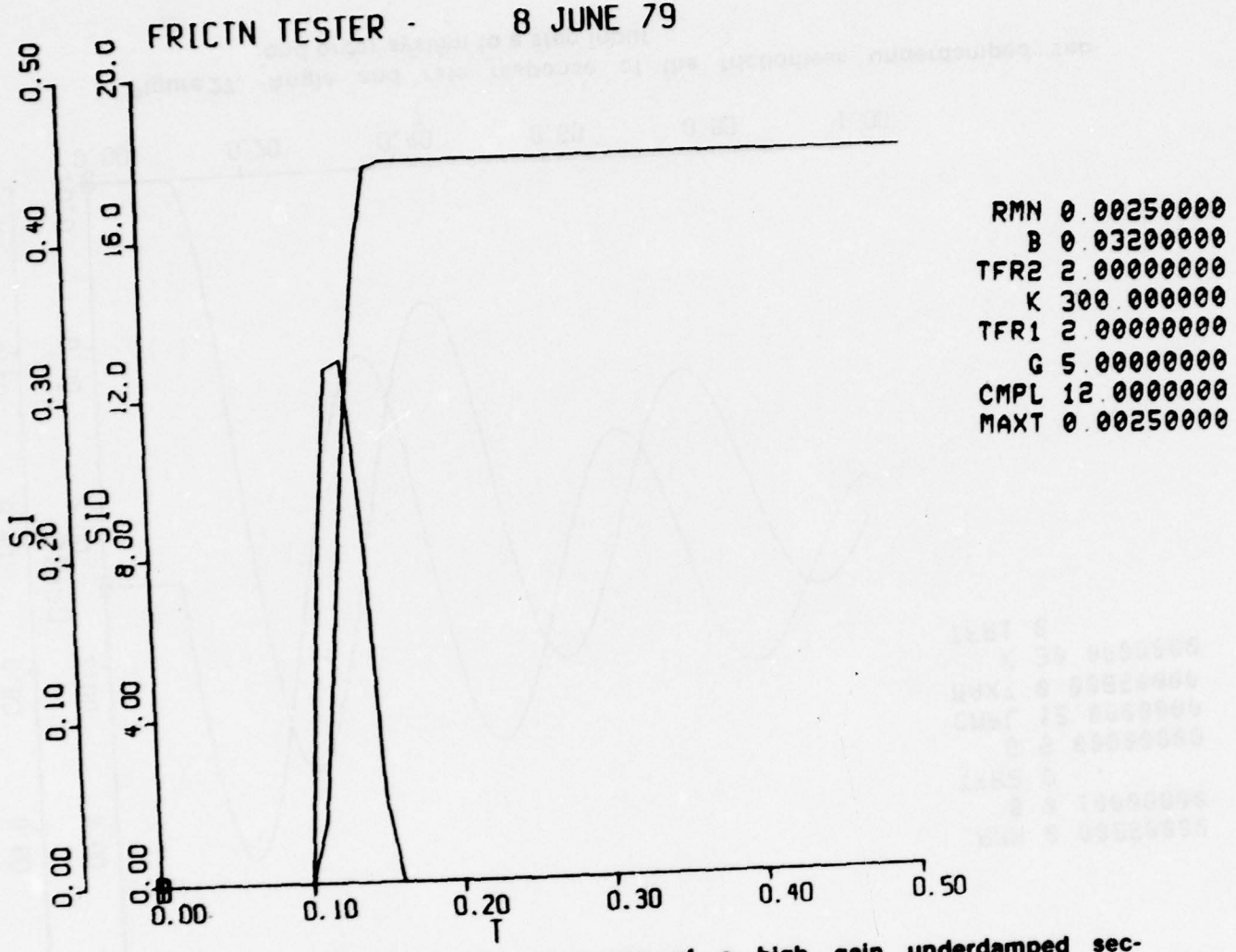

Figure 28. Angle and rate response of a high gain underdamped second order system to a step input — model C.

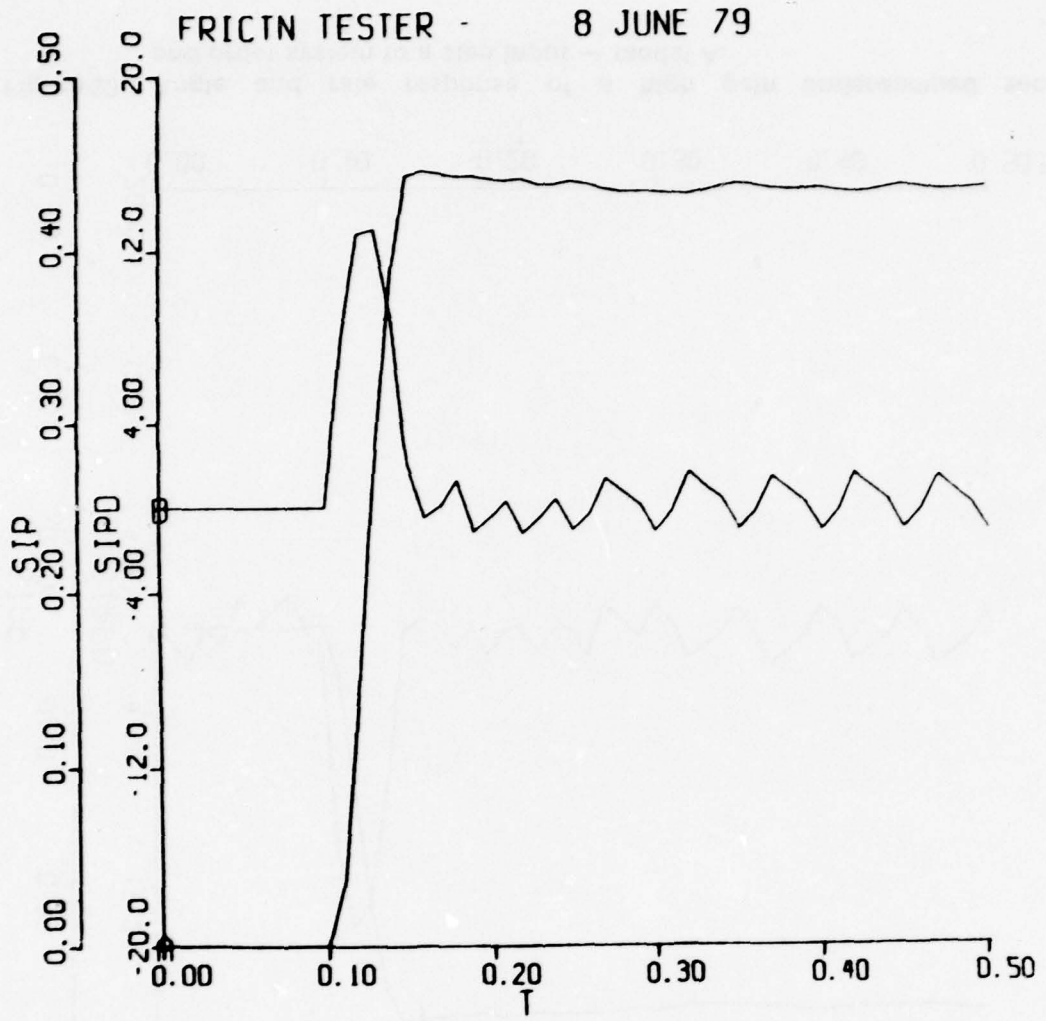

Figure 29. Angle and rate response of a high gain underdamped second order system to a step input — model B.

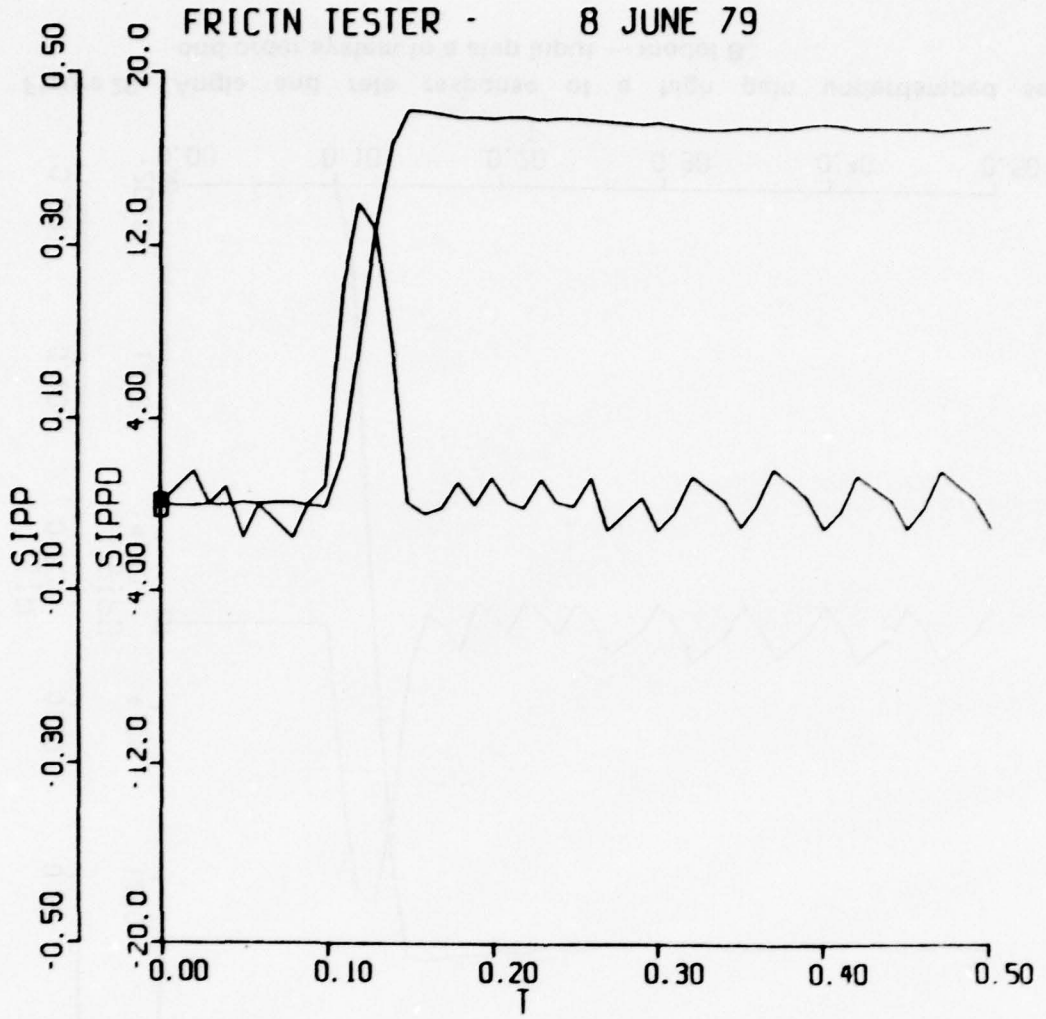

Figure 30. Angle and rate response of a high gain underdamped second order system to a step input — model A.

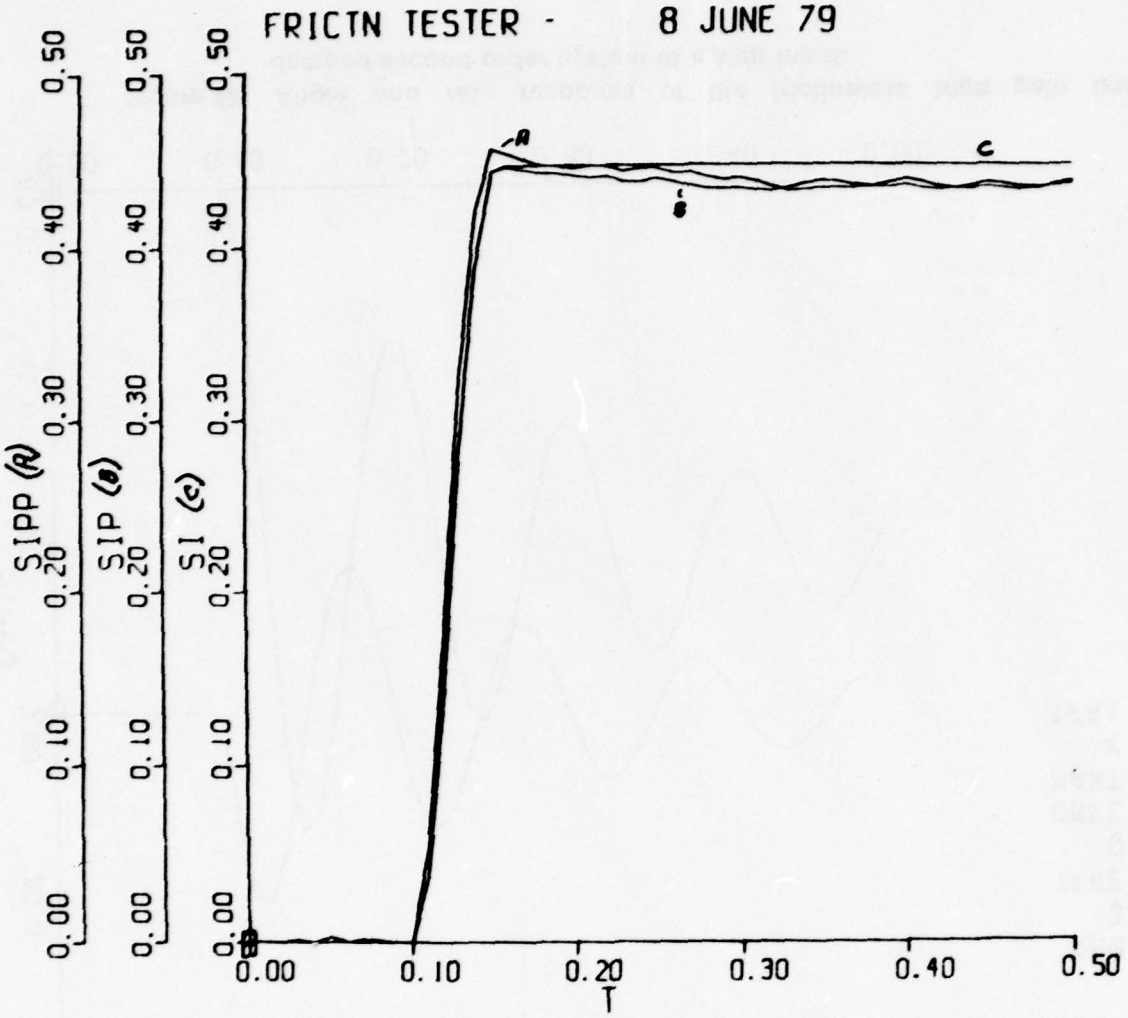

Figure 31. Comparison of angle responses of a high gain underdamped second order system to a step input for models A, B and C.

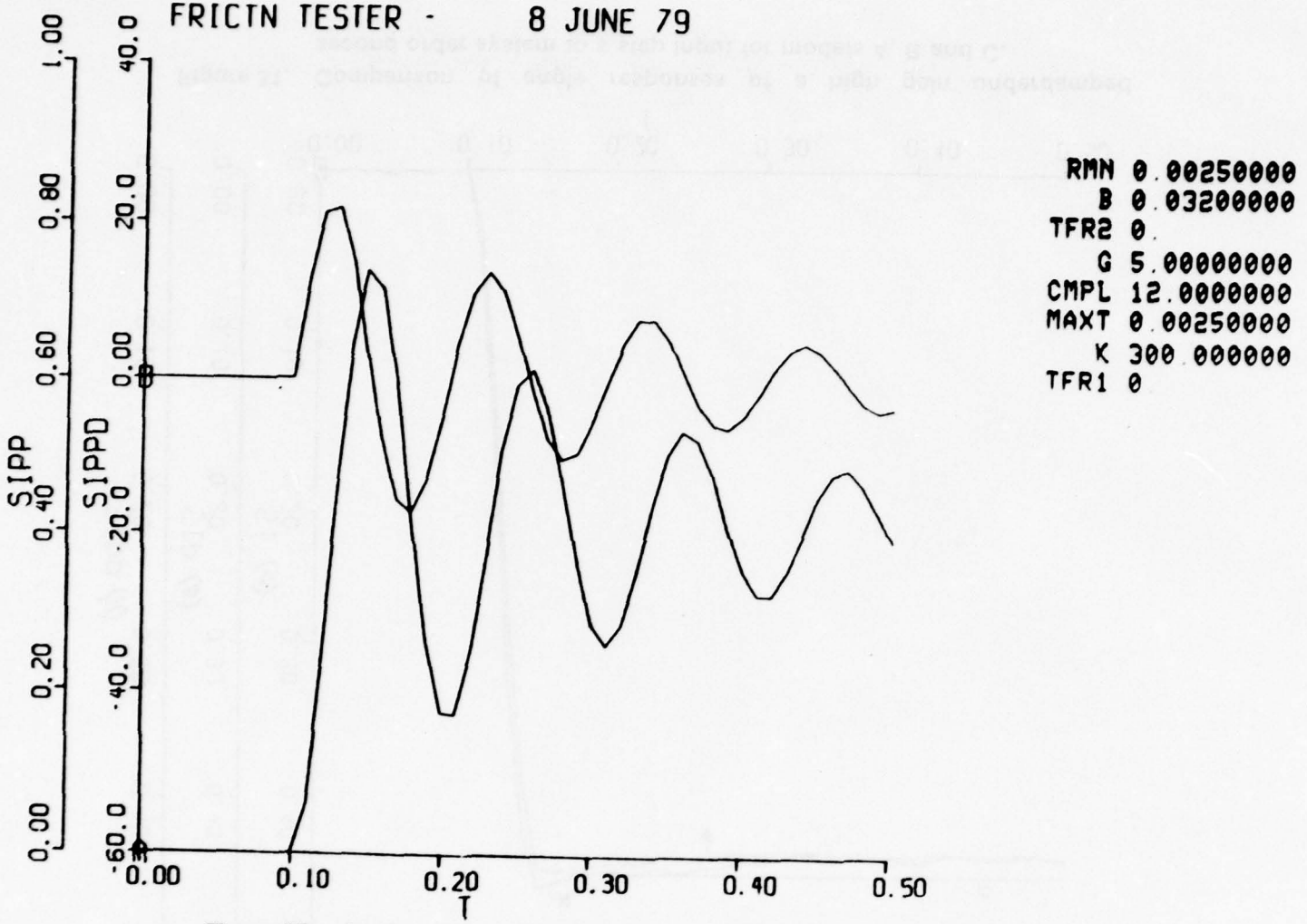

Figure 32. Angle and rate response of the frictionless high gain underdamped second order system to a step input.

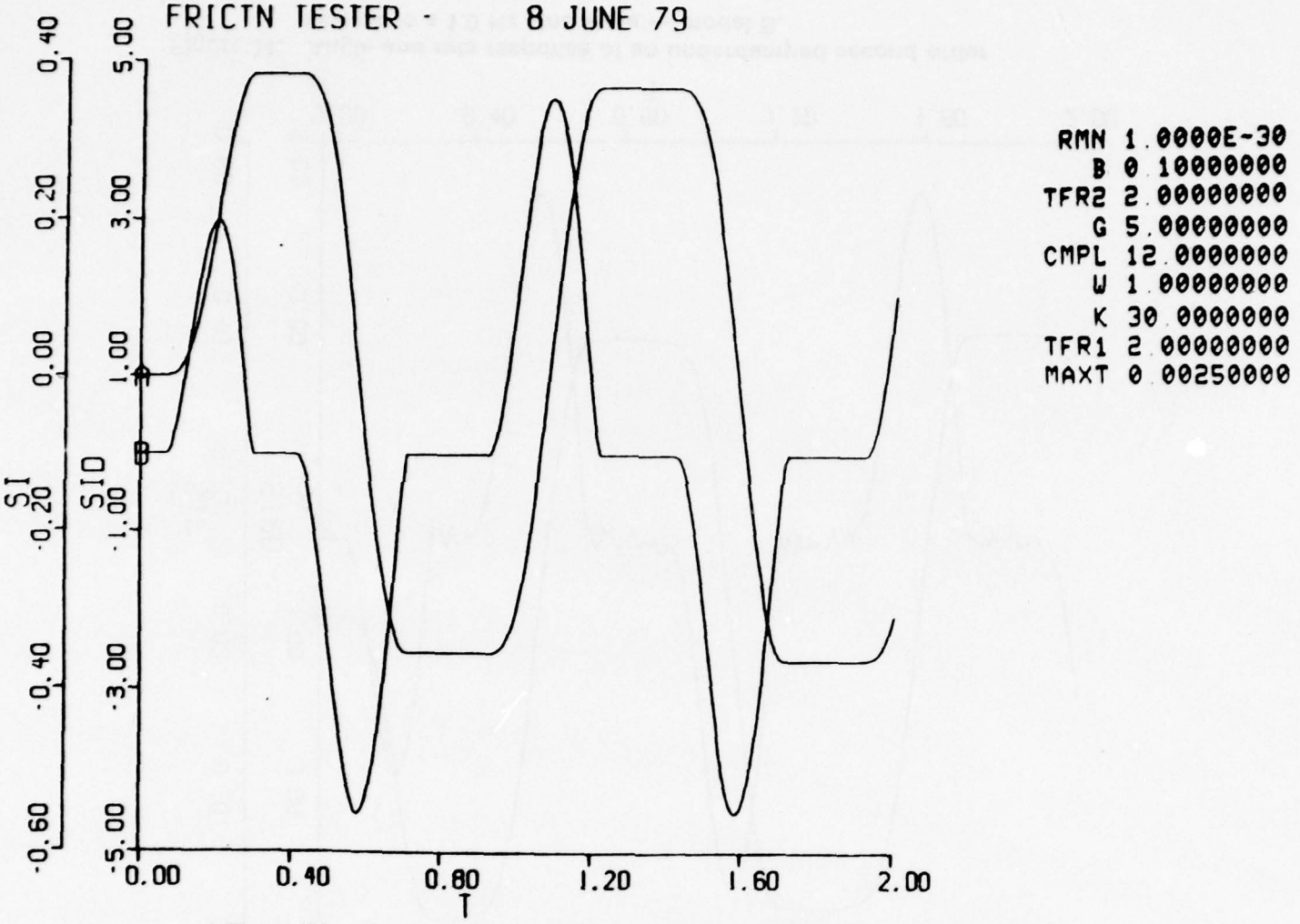

Figure 33. Angle and rate response of an underdamped second order system to a 1.0 Hz sine wave — model C.

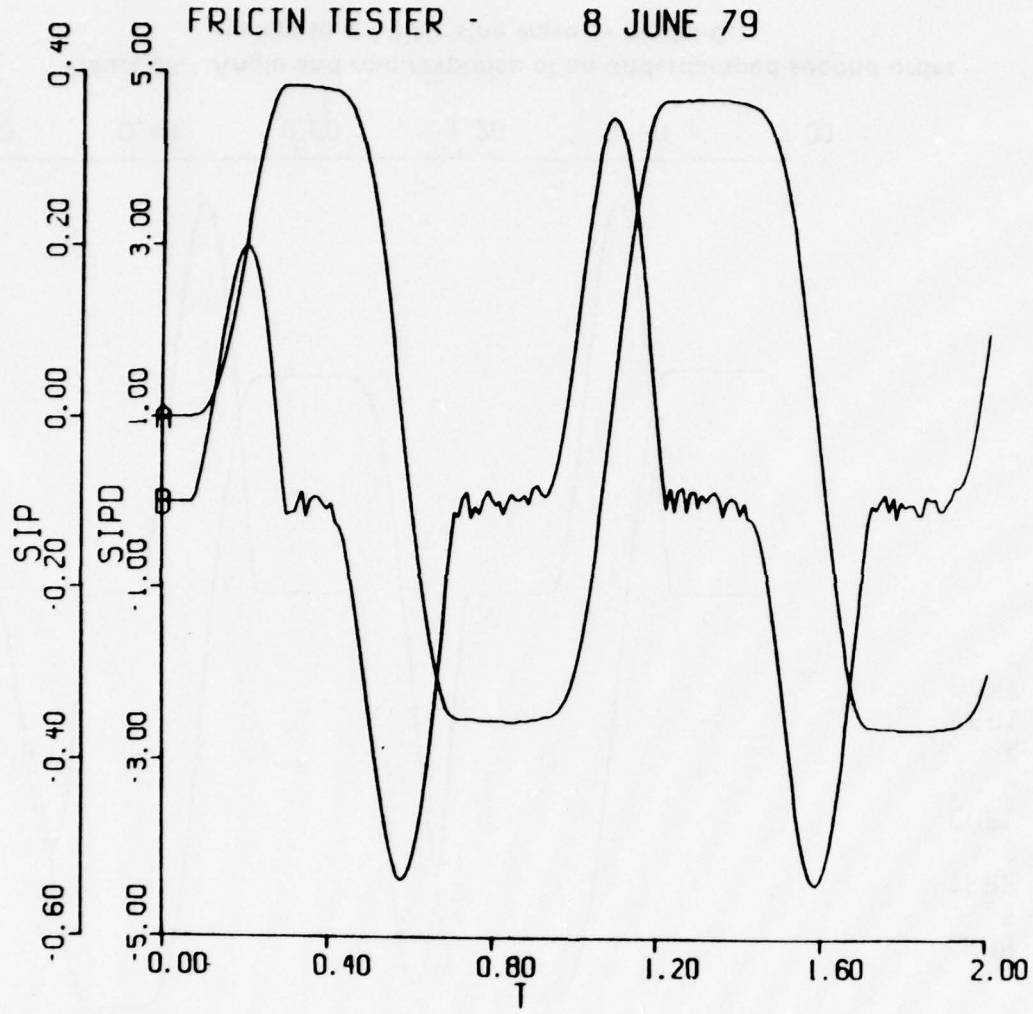

Figure 34. Angle and rate response of an underdamped second order system to a 1.0 Hz sine wave — model B.

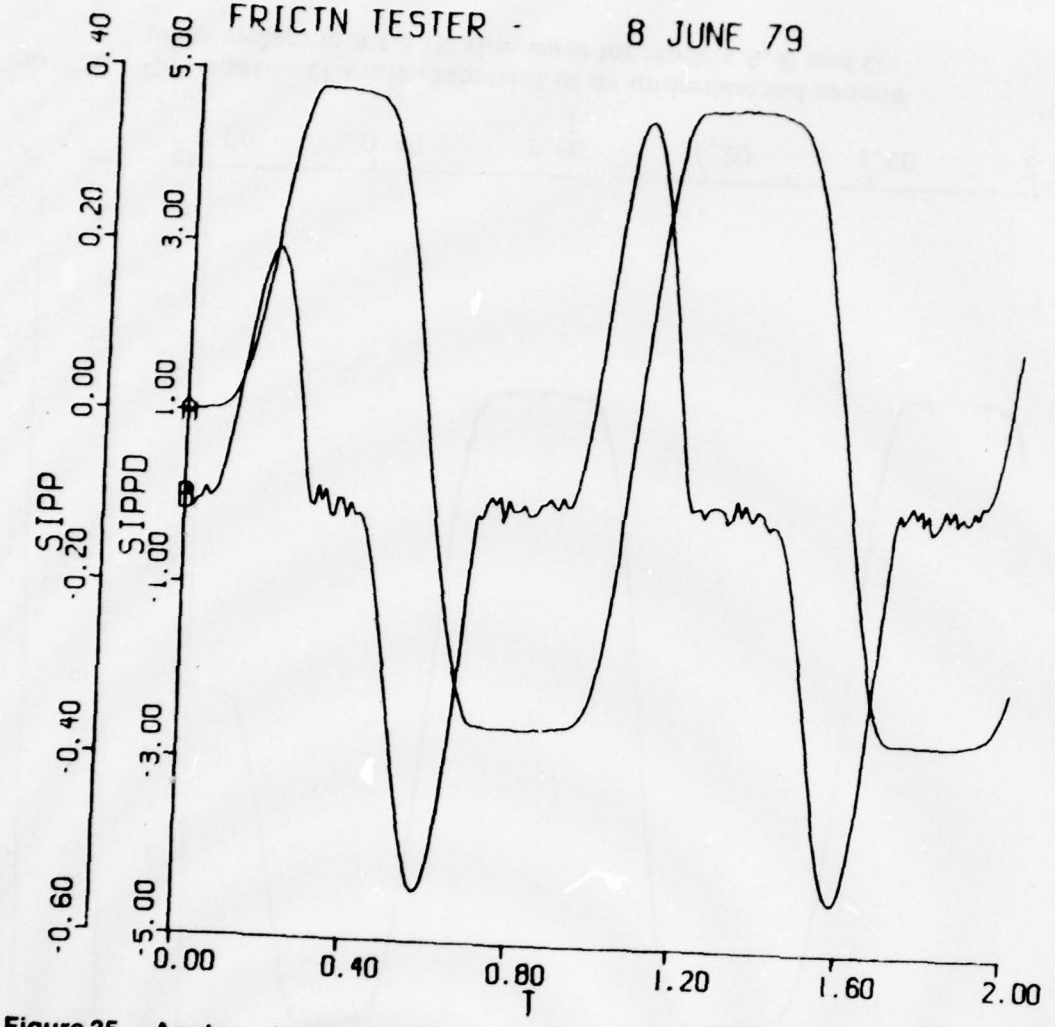

Figure 35. **Angle and rate response of an underdamped second order system to a 1.0 Hz sine wave — model A.**

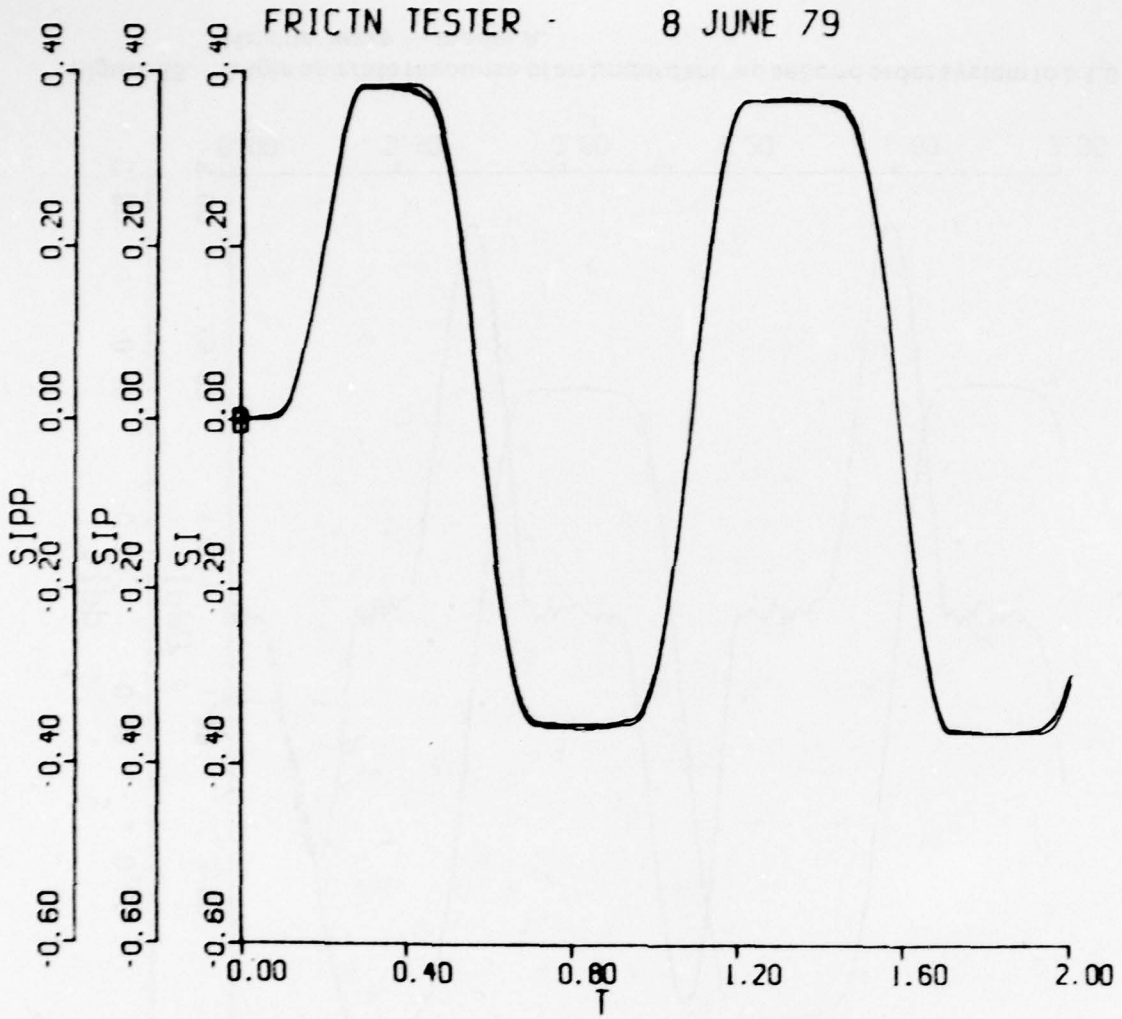

Figure 36. Comparison of angle responses of an underdamped second order system to a 1.0 Hz sine wave for models A, B and C.

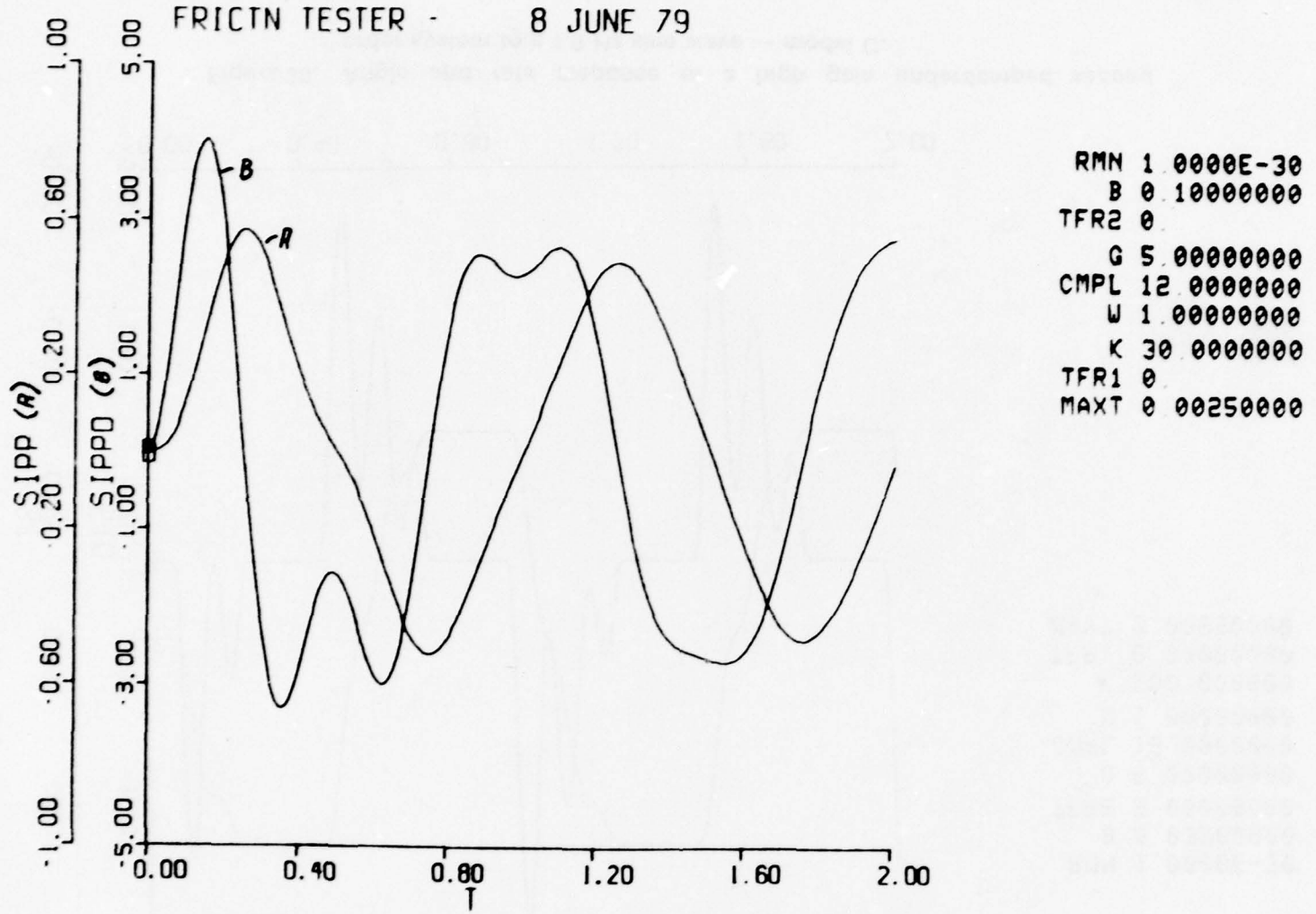

Figure 37. Angle and rate response of a frictionless underdamped second order system to a 1.0 Hz sine wave.

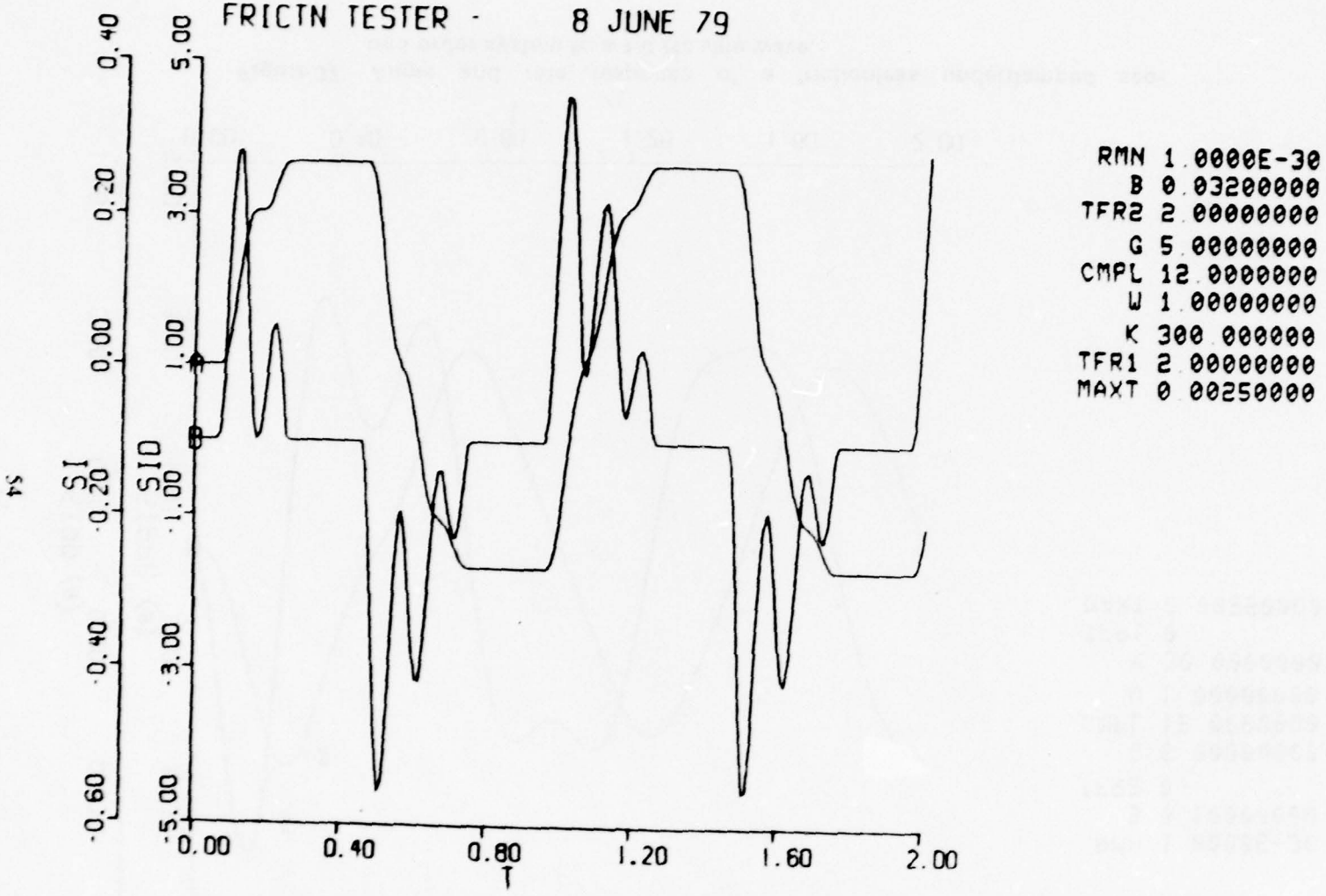

Figure 38. Angle and rate response of a high gain underdamped second order system to a 1.0 Hz sine wave — model C.

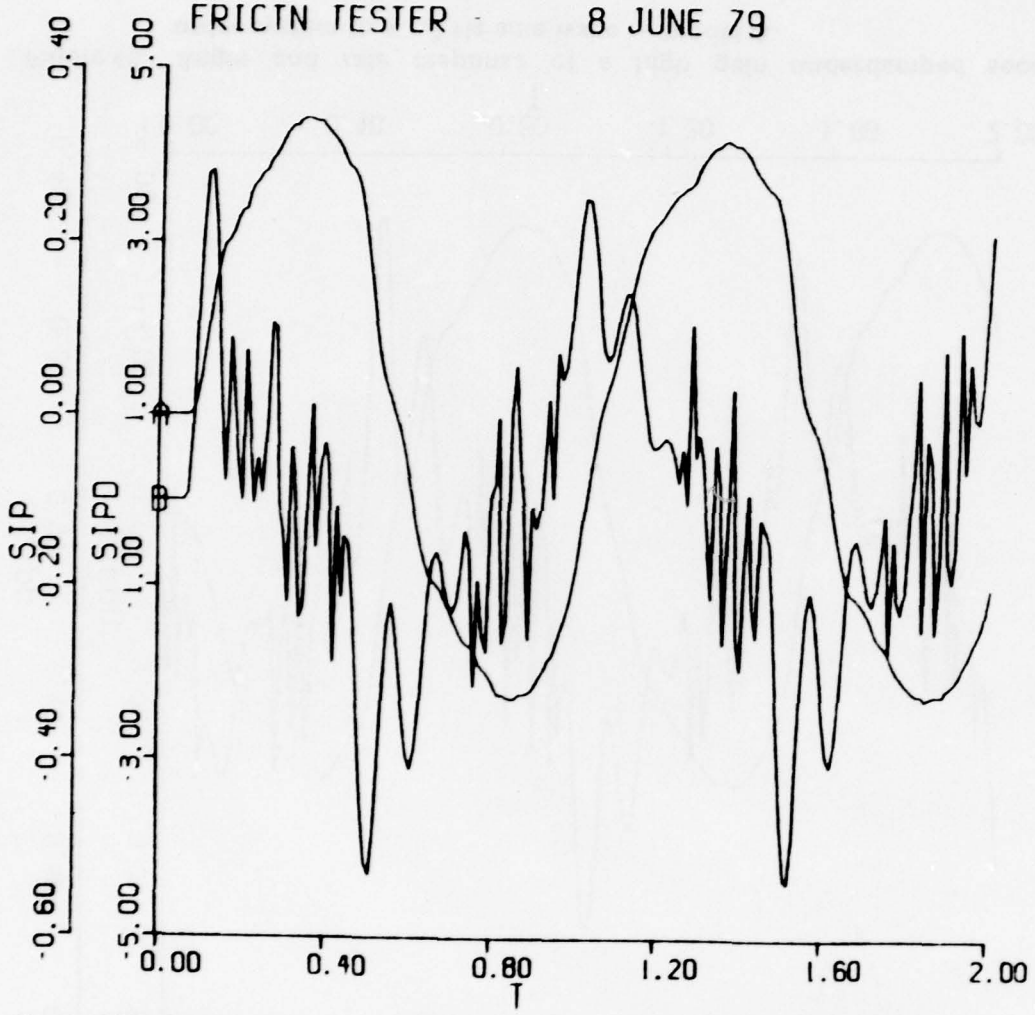

Figure 39. Angle and rate response of a high gain underdamped second order system to a 1.0 Hz sine wave — model B.

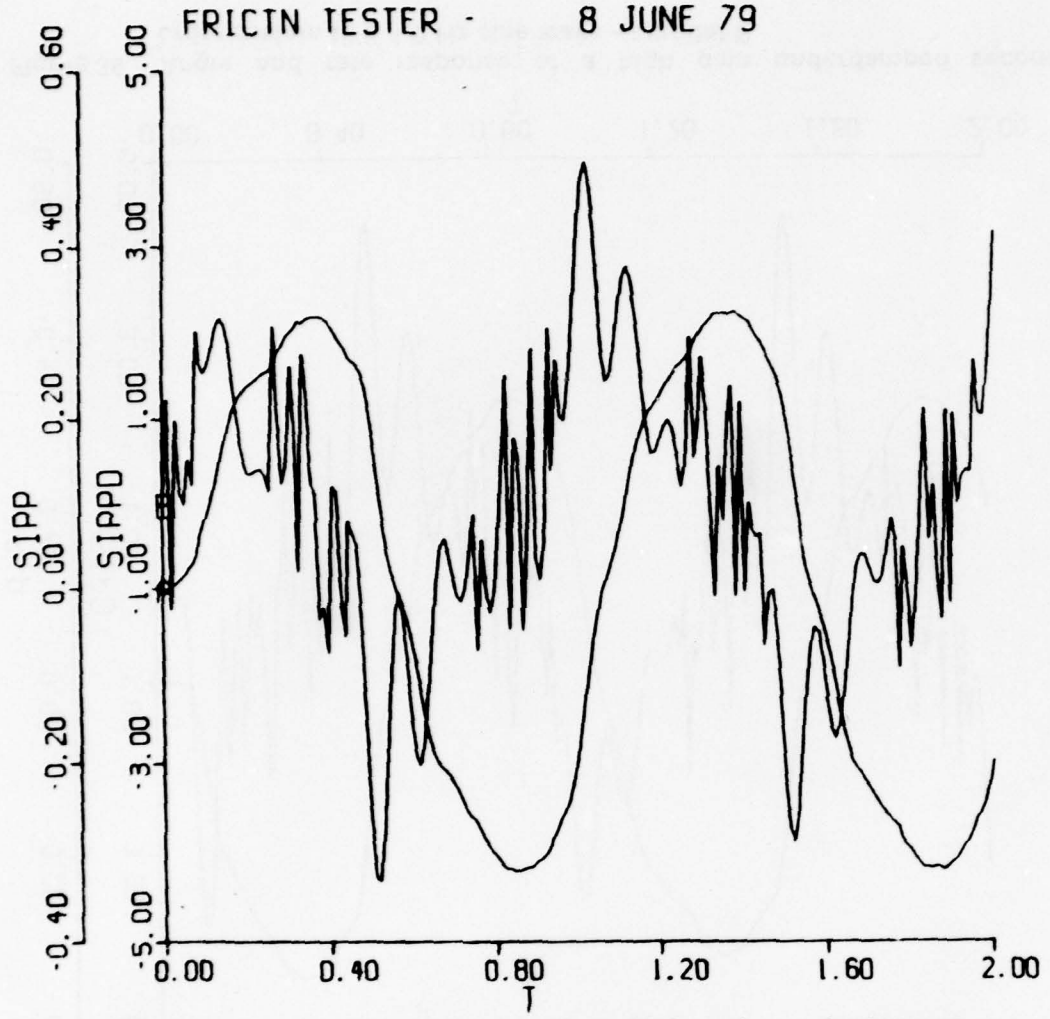

Figure 40. Angle and rate response of a high gain underdamped second order system to a 1.0 Hz sine wave — model A.

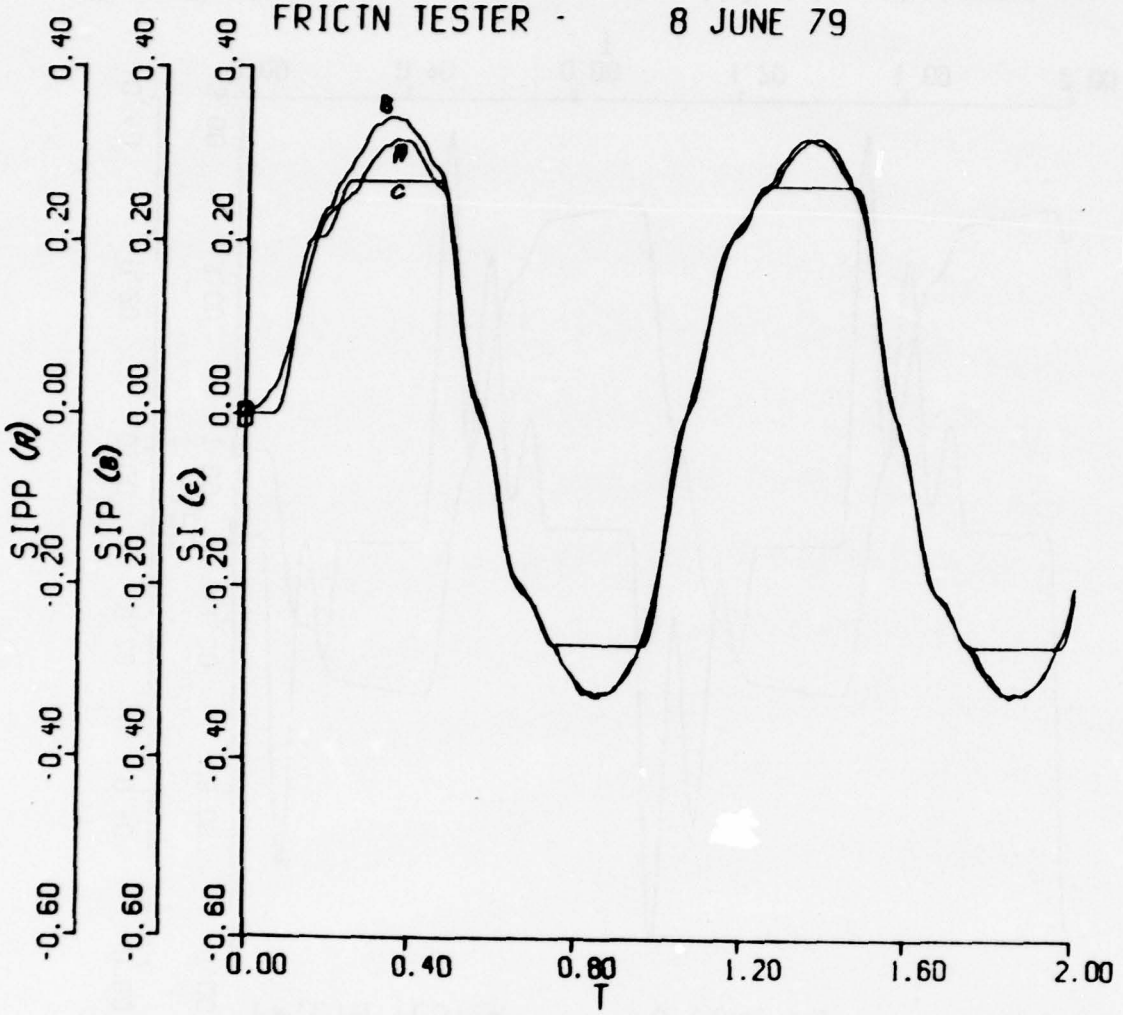

Figure 41. Comparison of angle responses of a high gain underdamped second order system to a 1.0 Hz sine wave for models A, B and C.

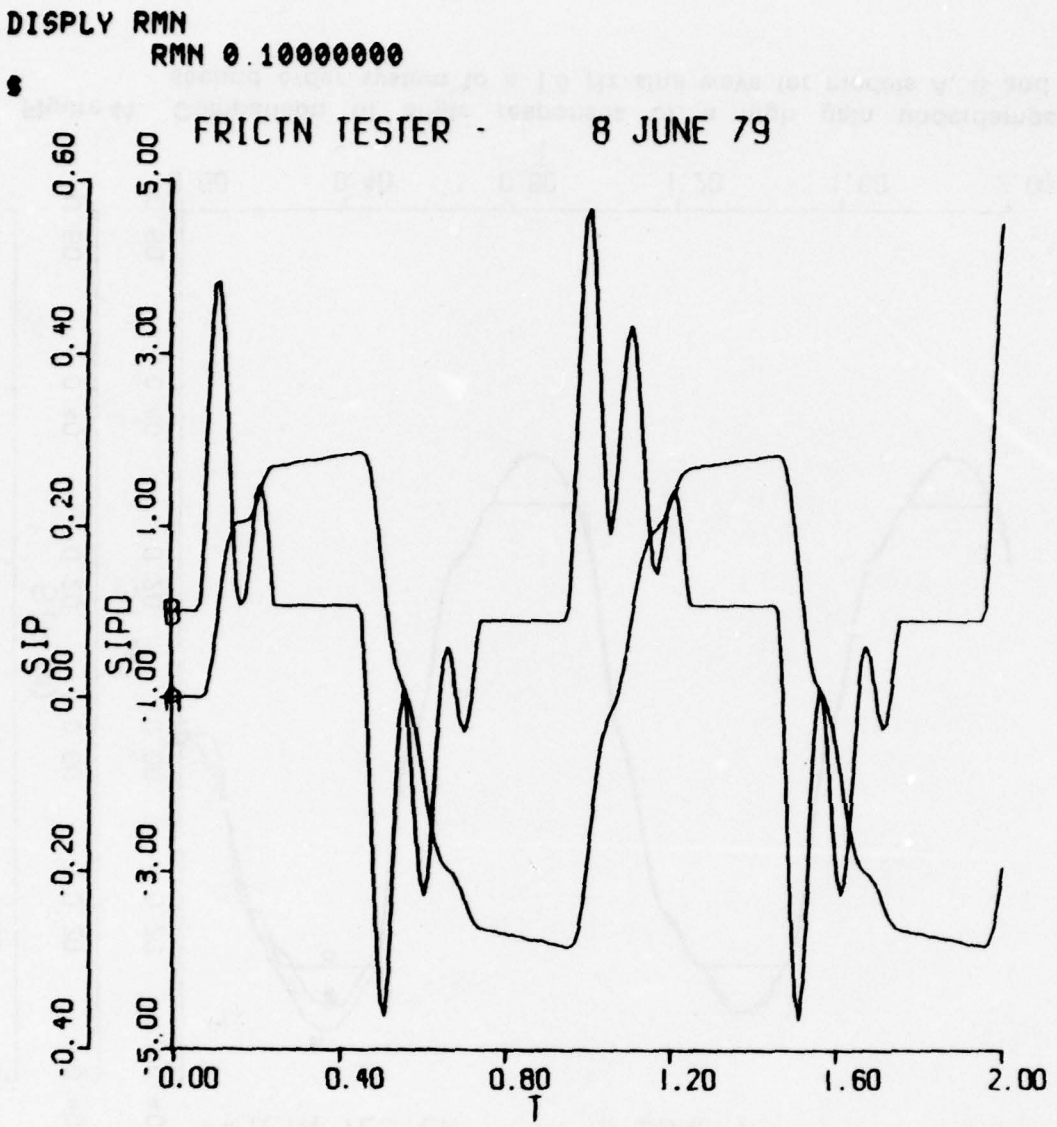

Figure 42. Angle and rate response of a high gain underdamped second order system to a 1.0 Hz sine wave for model B with RMN = 0.1.

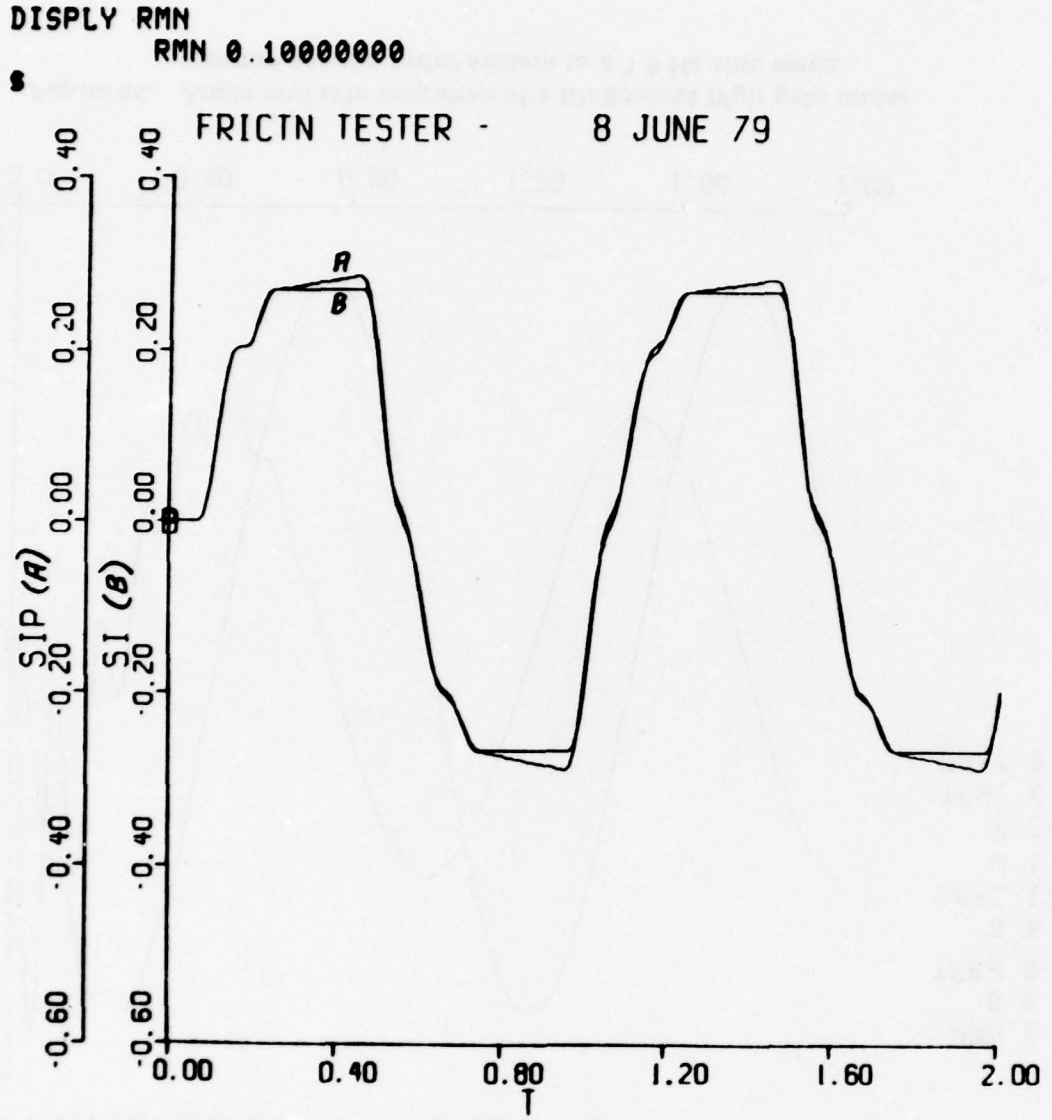

Figure 43. Comparison of angle responses of a high gain underdamped second order system to a 1.0 Hz sine wave for models B and C with RMN = 0.1.

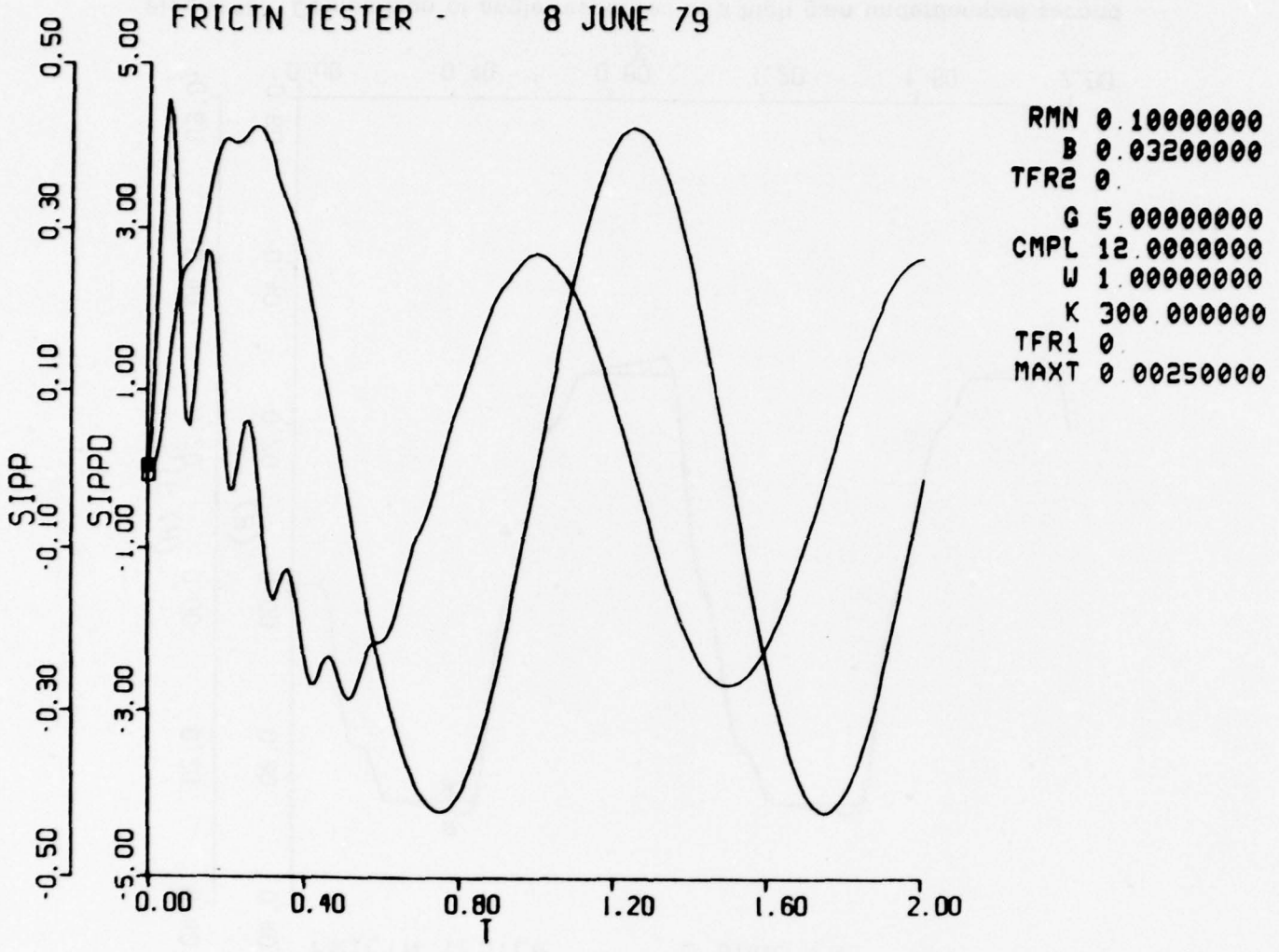

Figure 44. Angle and rate response of a frictionless high gain underdamped second order system to a 1.0 Hz sine wave.

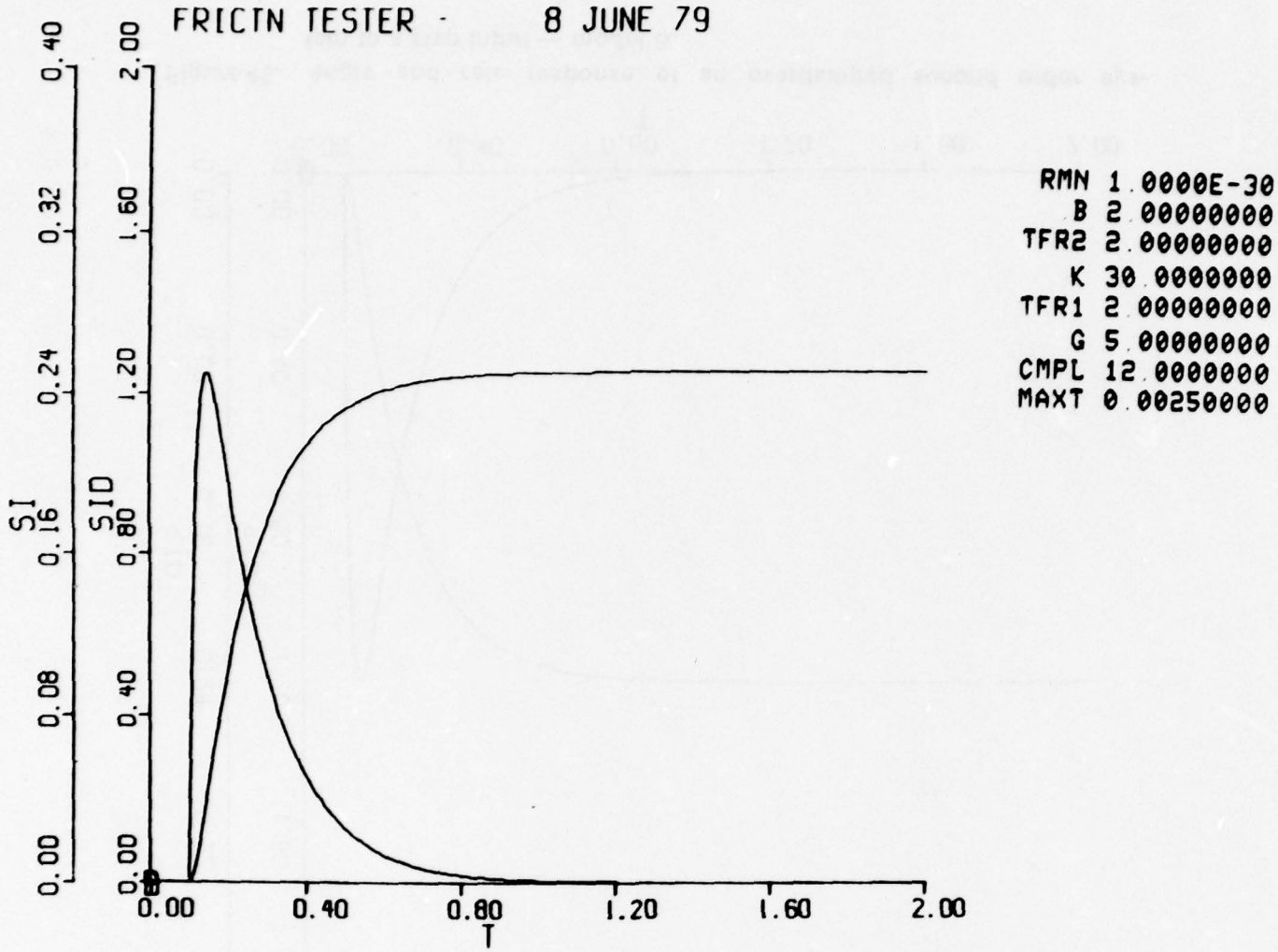

Figure 45. Angle and rate response of an overdamped second order system to a step input — model C.

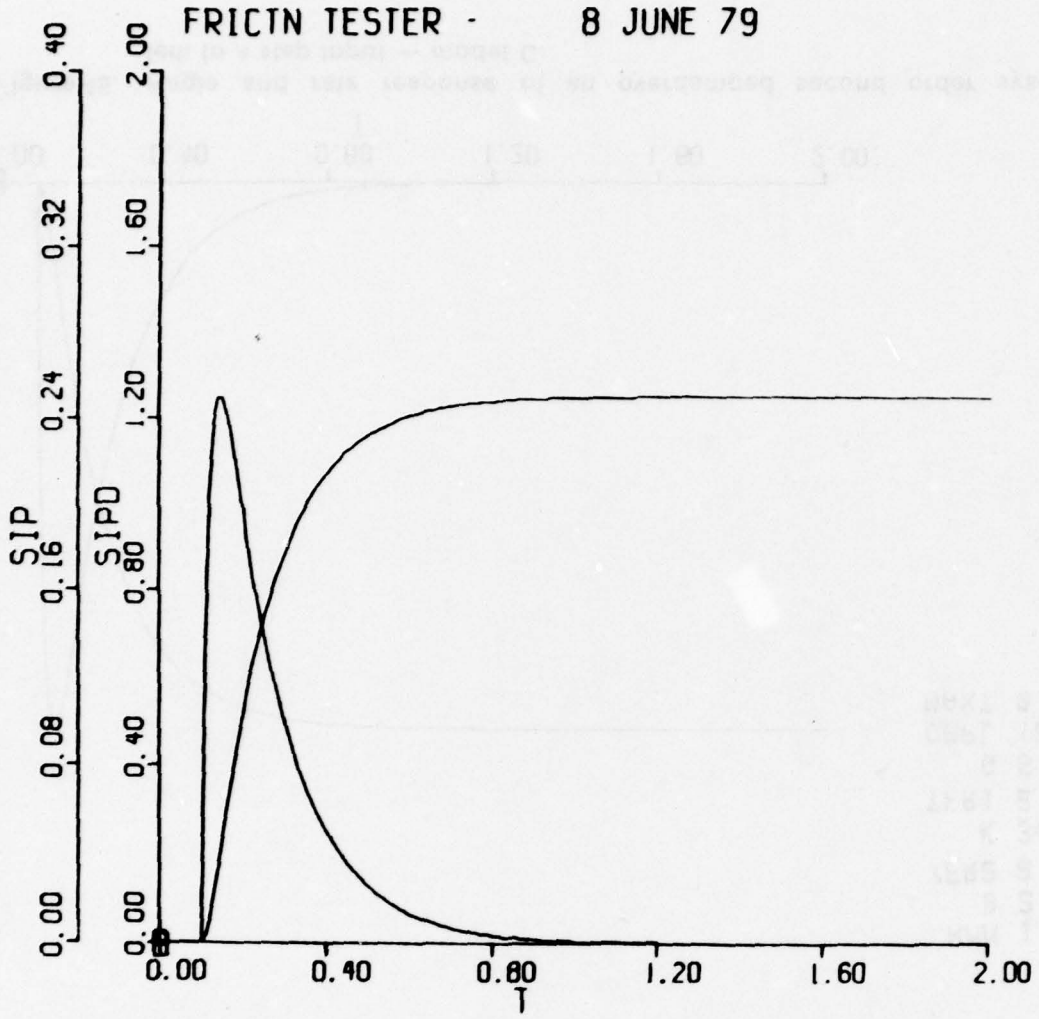

Figure 46. Angle and rate response of an overdamped second order system to a step input — model B.

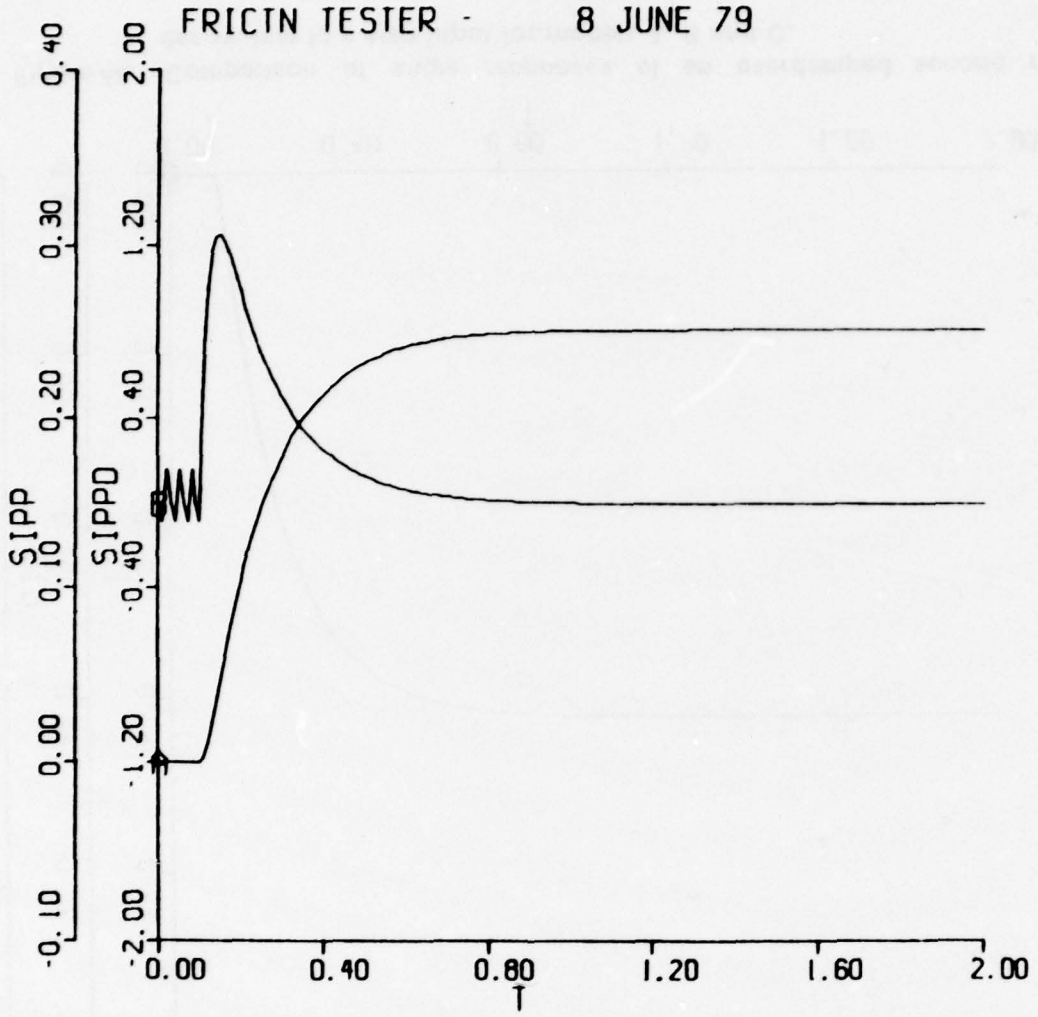

Figure 47. Angle and rate response of an overdamped second order system to a step input — model A.

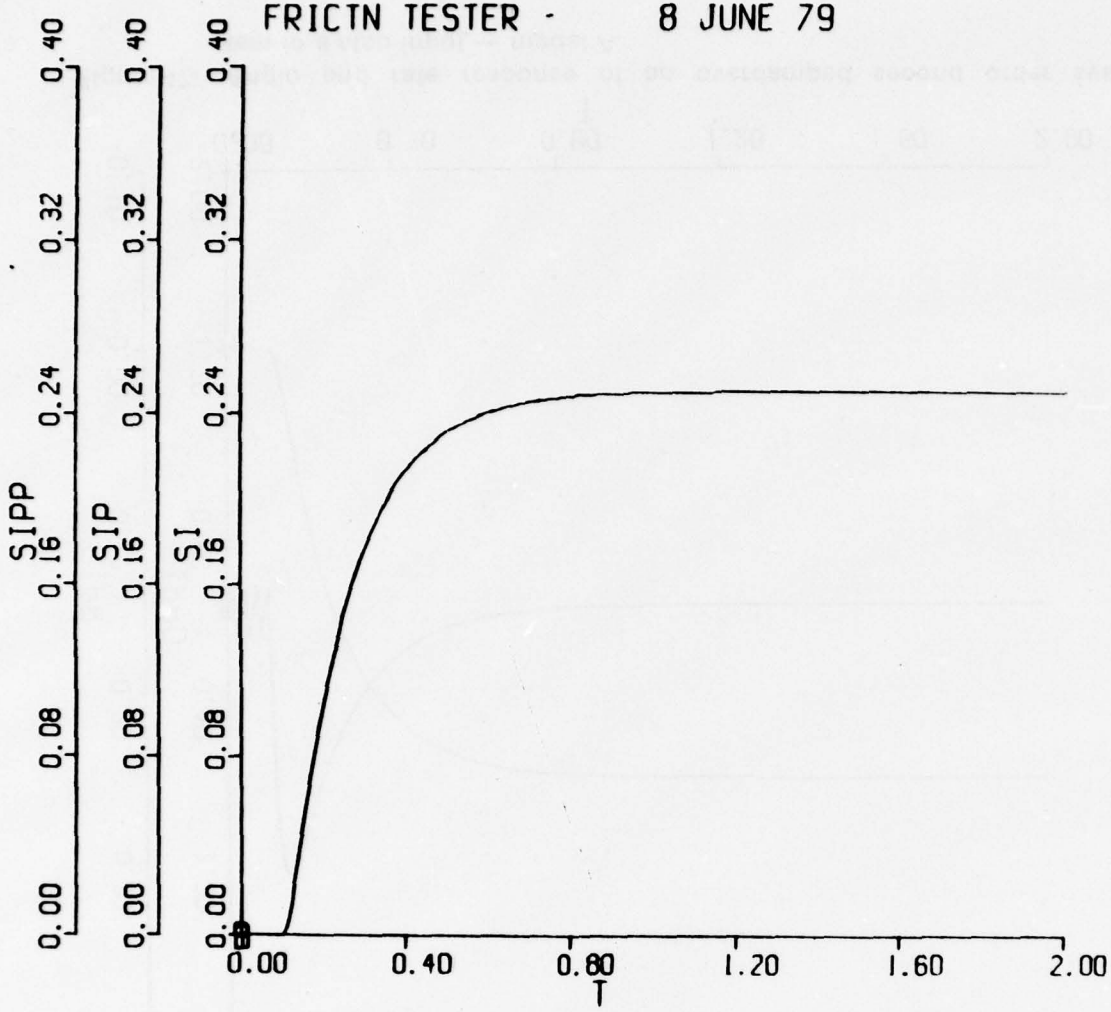

Figure 48. Comparison of angle responses of an overdamped second order system to a step input for models A, B and C.

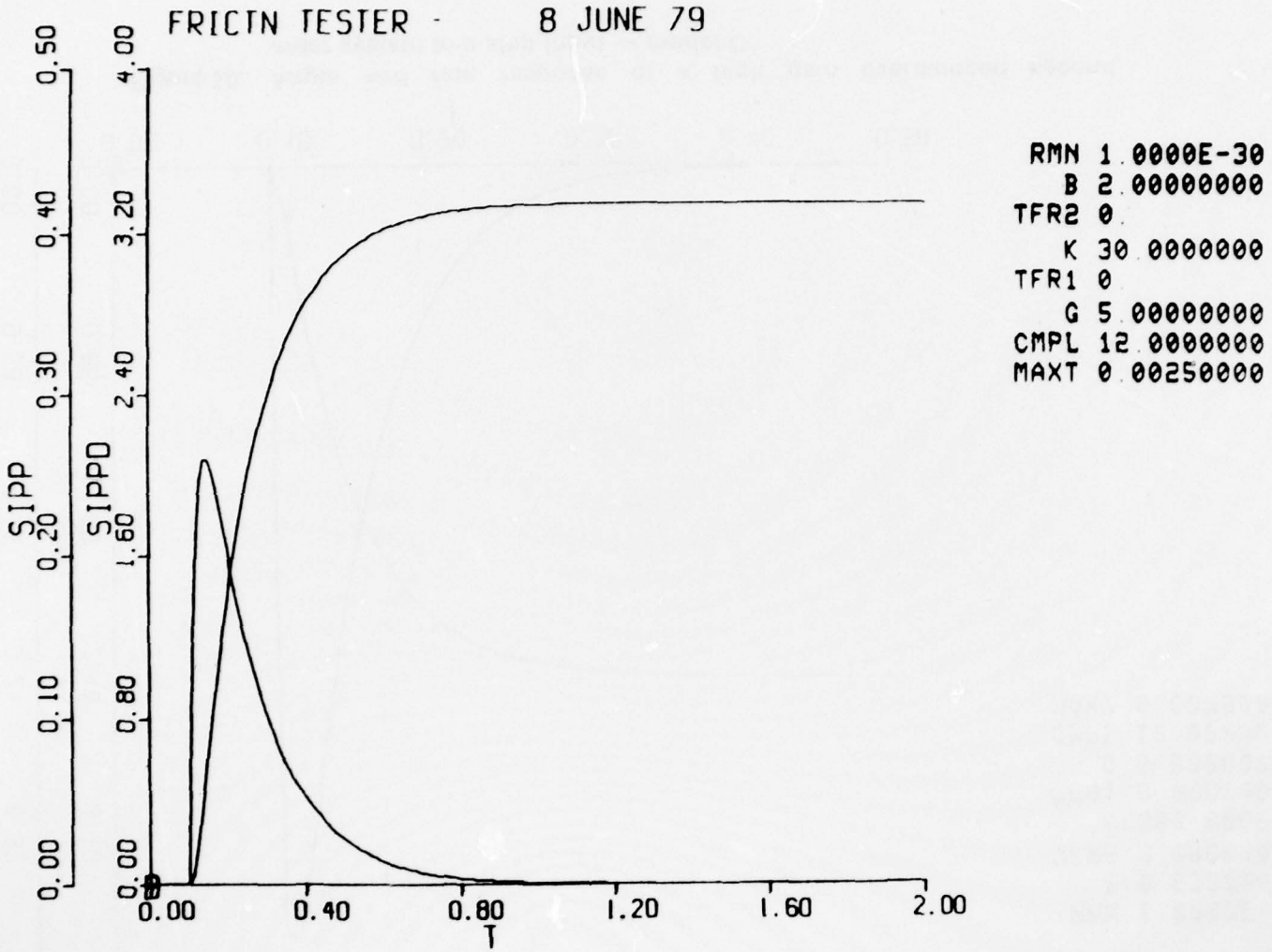

Figure 49. Angle and rate response of a frictionless overdamped second order system to a step input.

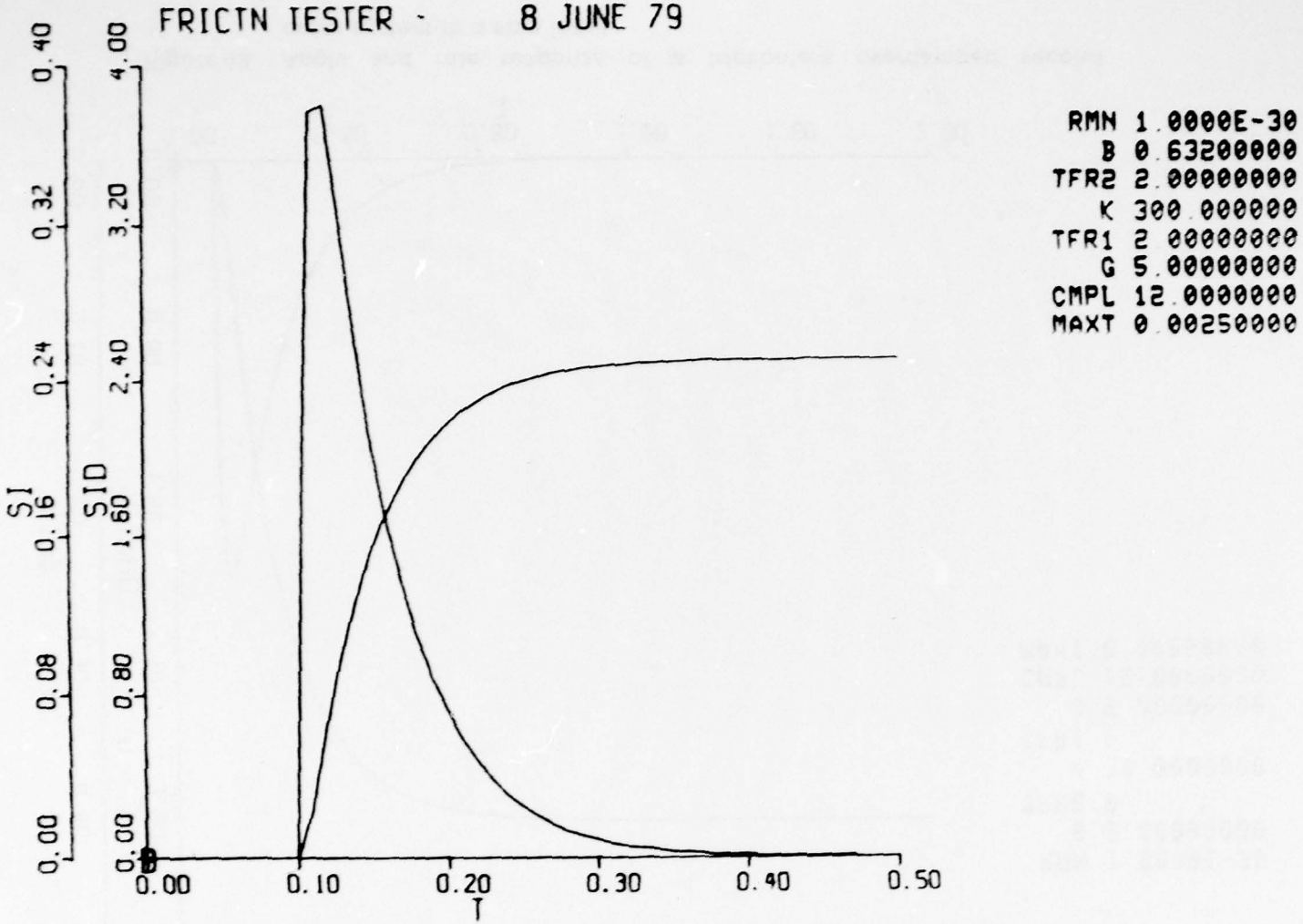

Figure 50. Angle and rate response of a high gain overdamped second order system to a step input — model C.

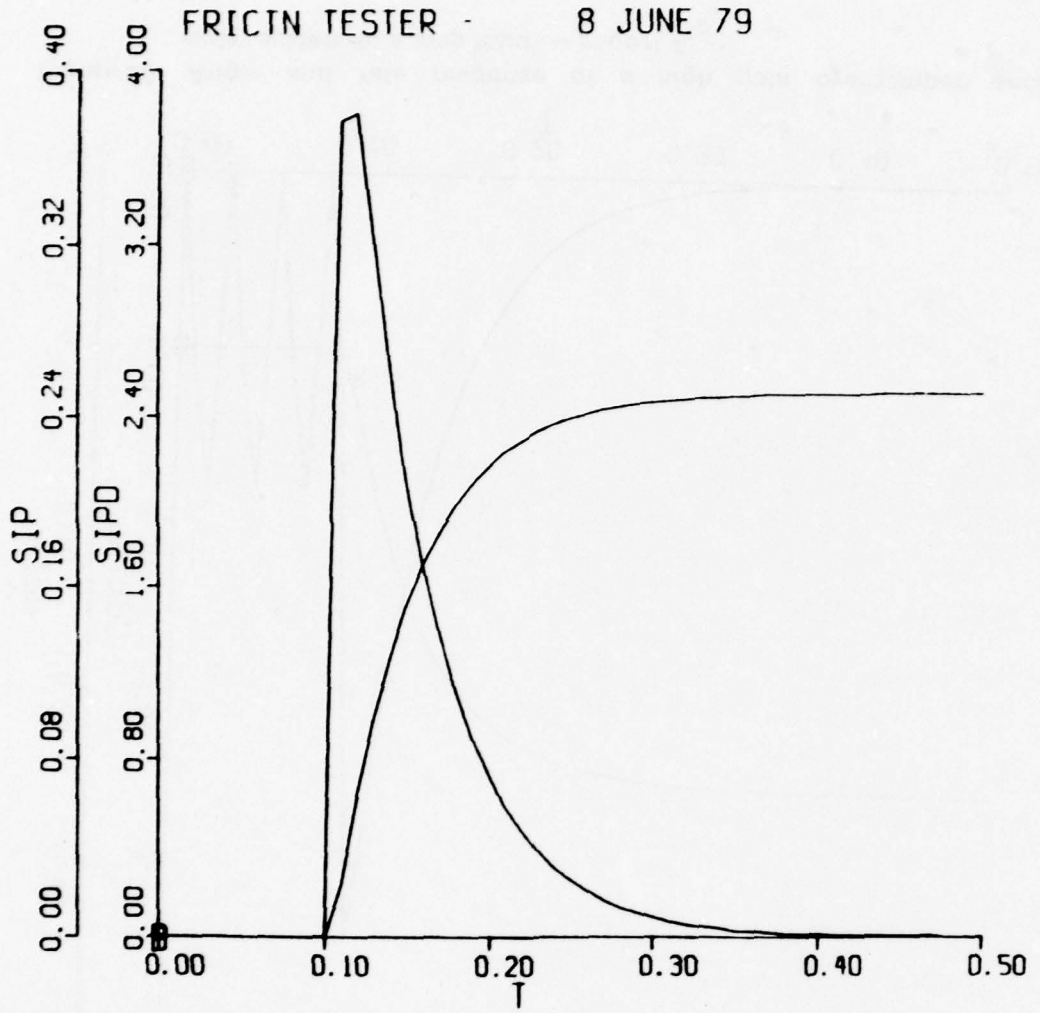

Figure 51. Angle and rate response of a high gain overdamped second order system to a step input — model B.

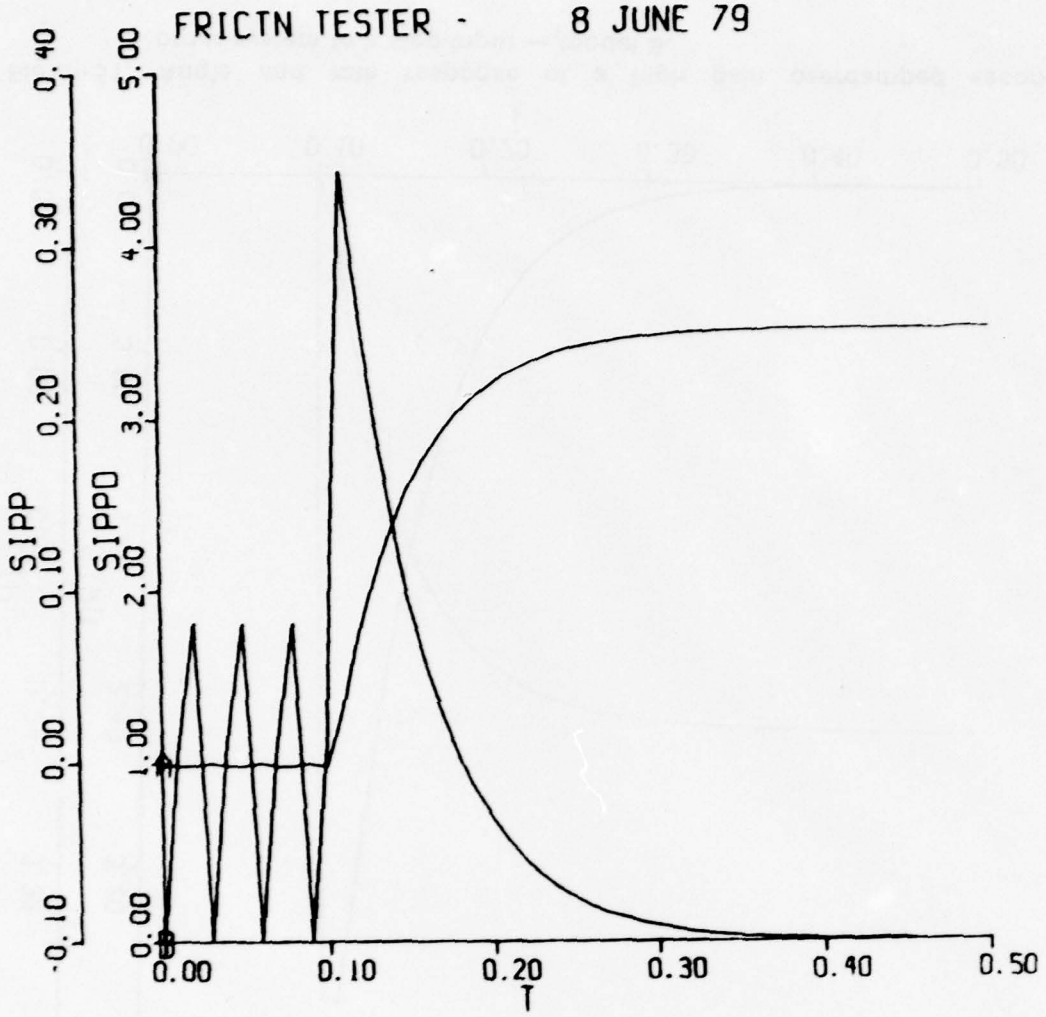

Figure 52. Angle and rate response of a high gain overdamped second order system to a step input — model A.

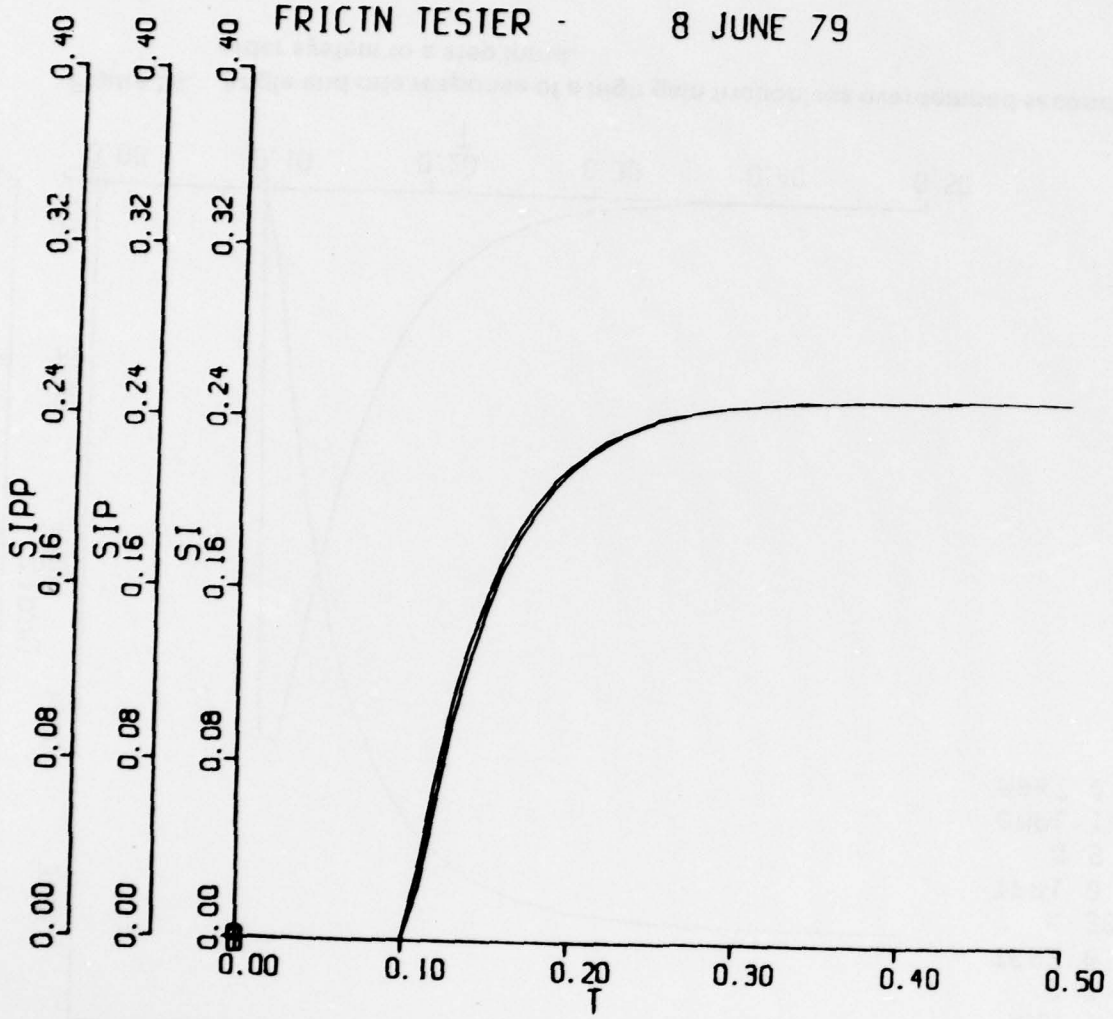

Figure 53. Comparison of angle responses of a high gain overdamped second order system to a step input for models A, B and C.

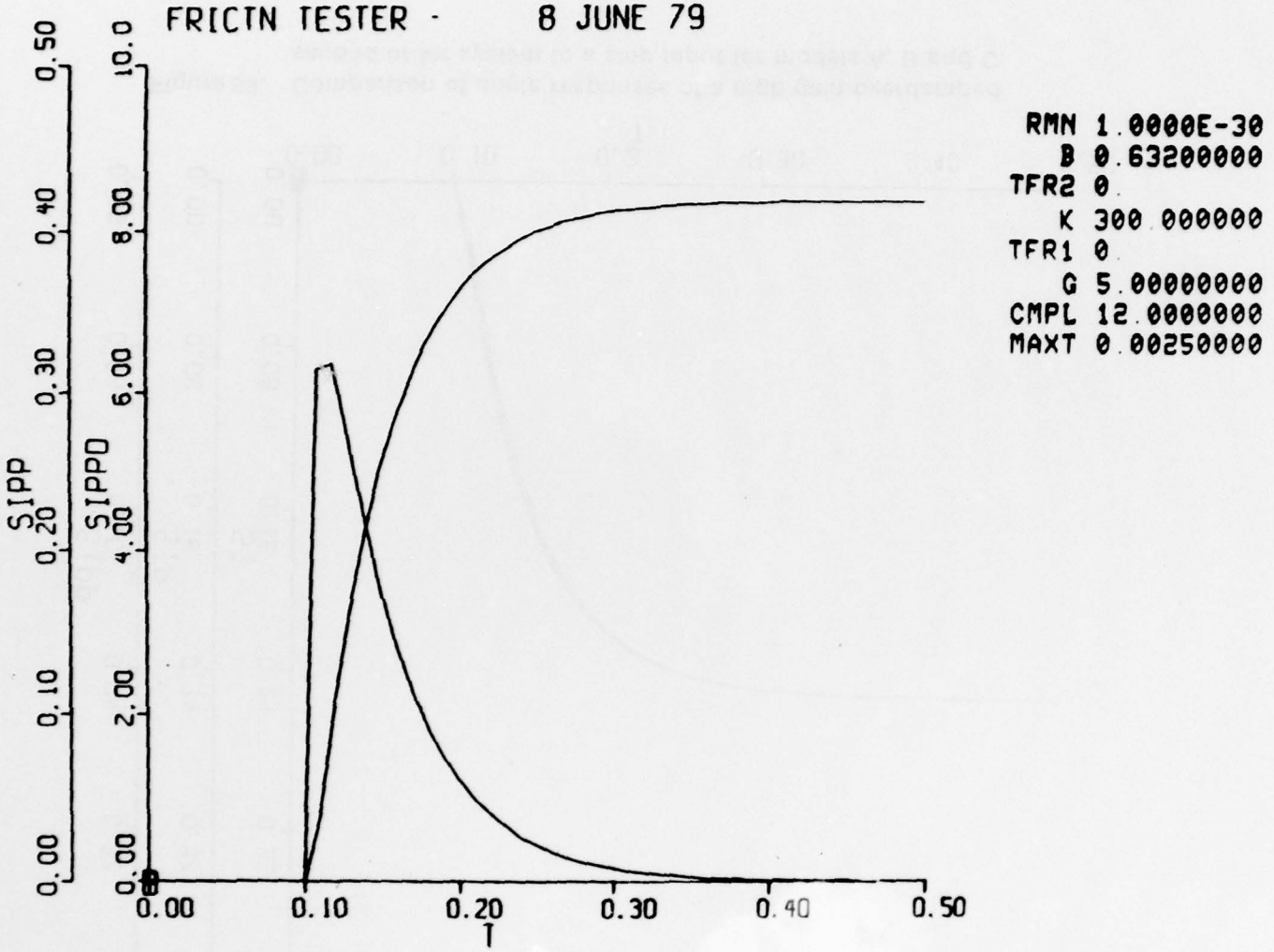

Figure 54. Angle and rate response of a high gain frictionless overdamped second order system to a step input.

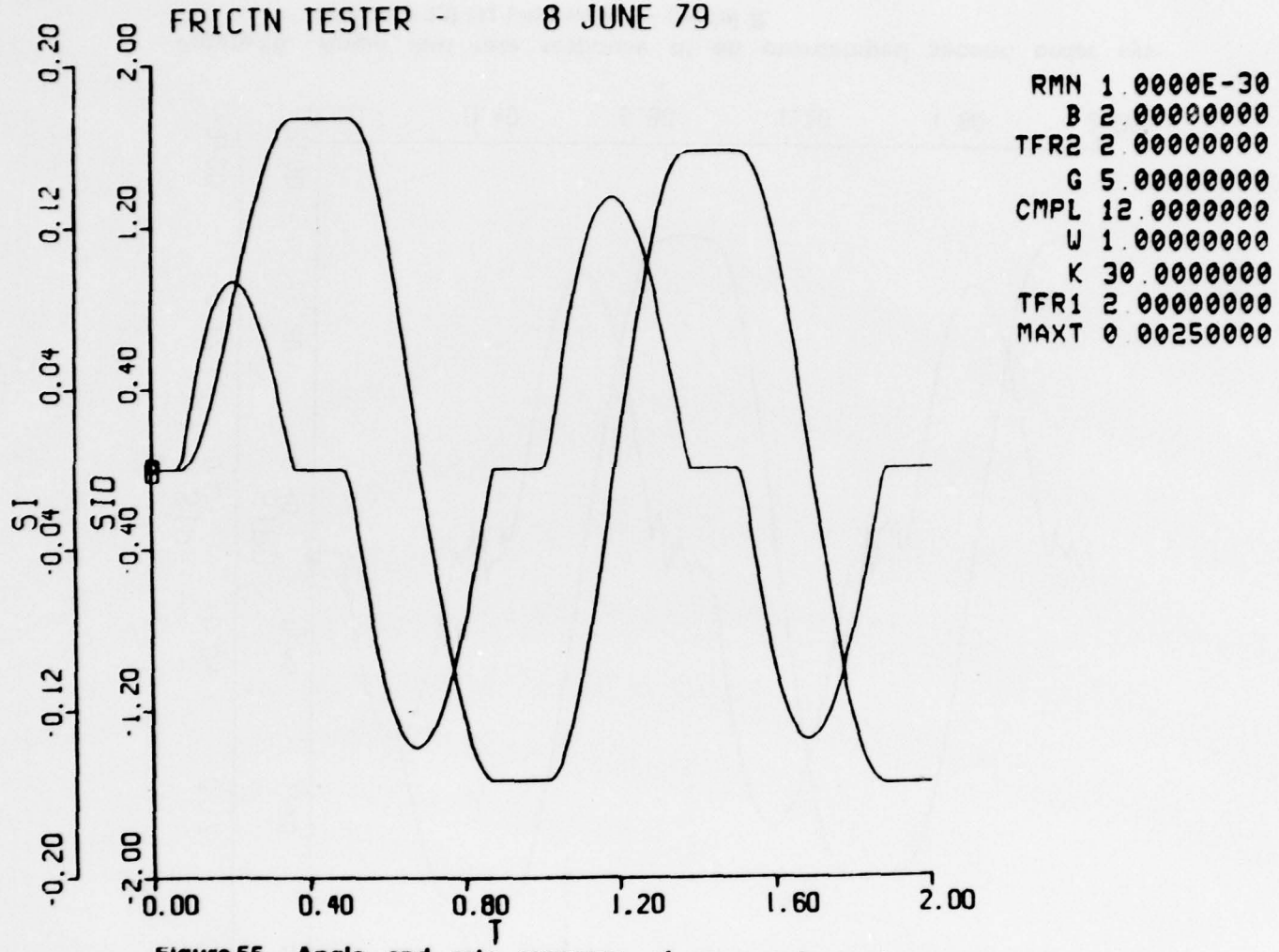

Figure 55. **Angle and rate response of an overdamped second order system to a 1.0 Hz sine wave — model C.**

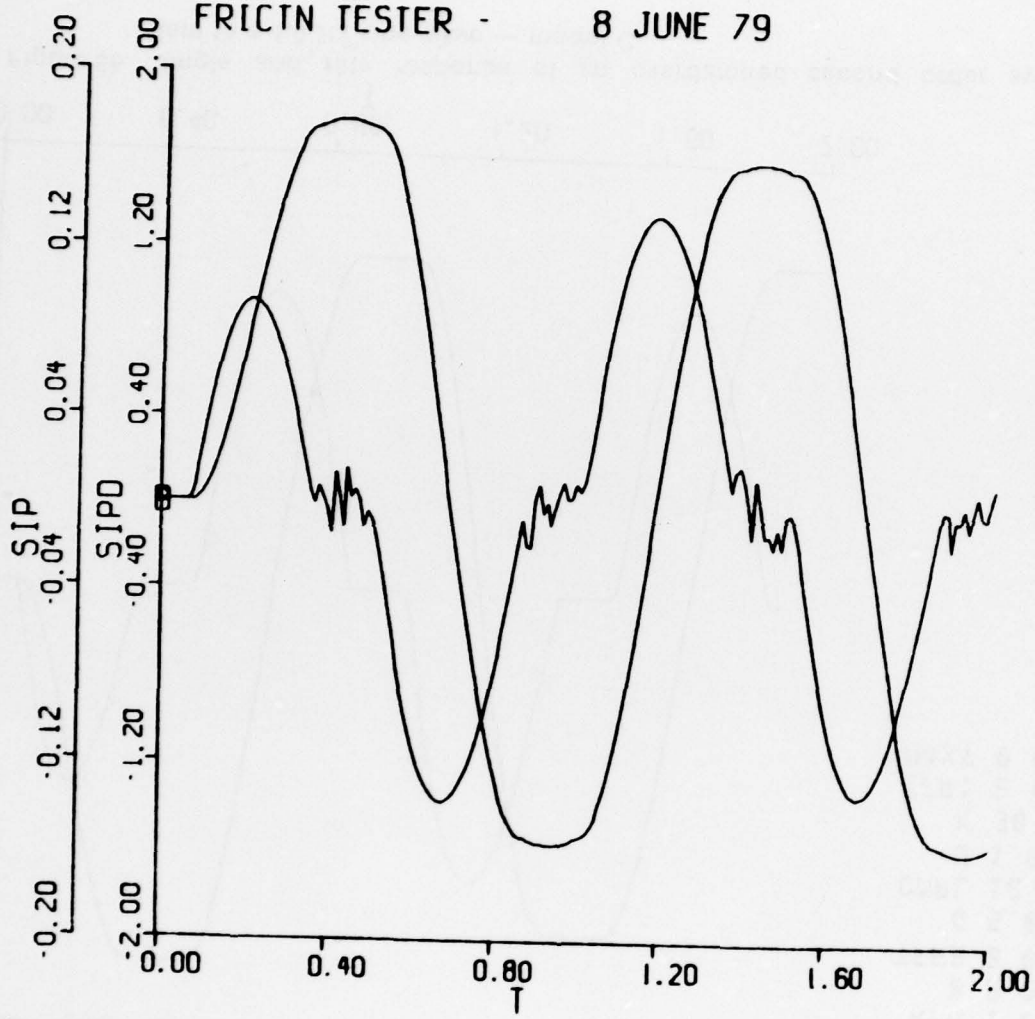

Figure 56. Angle and rate response of an overdamped second order system to a 1.0 Hz sine wave — model B.

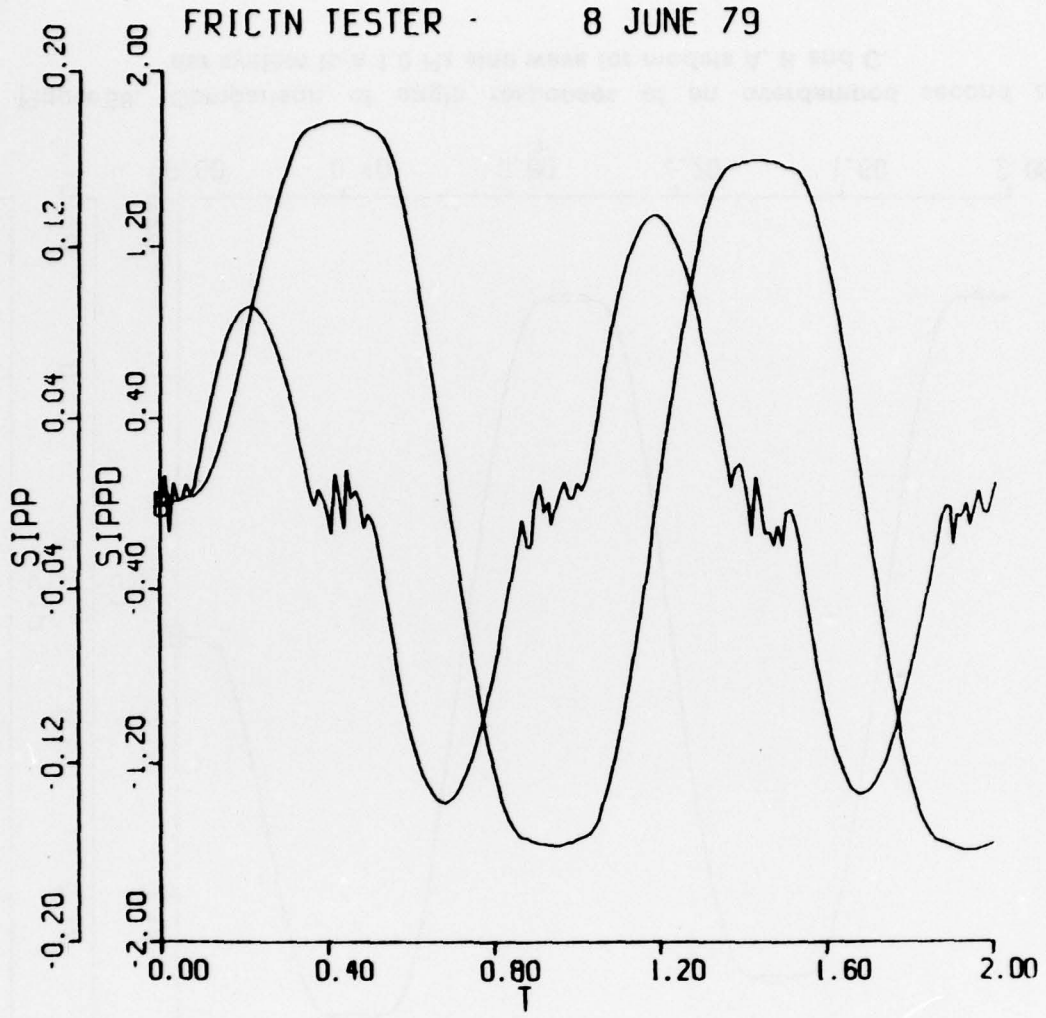

Figure 57. Angle and rate response of an overdamped second order system to a 1.0 Hz sine wave — model A.

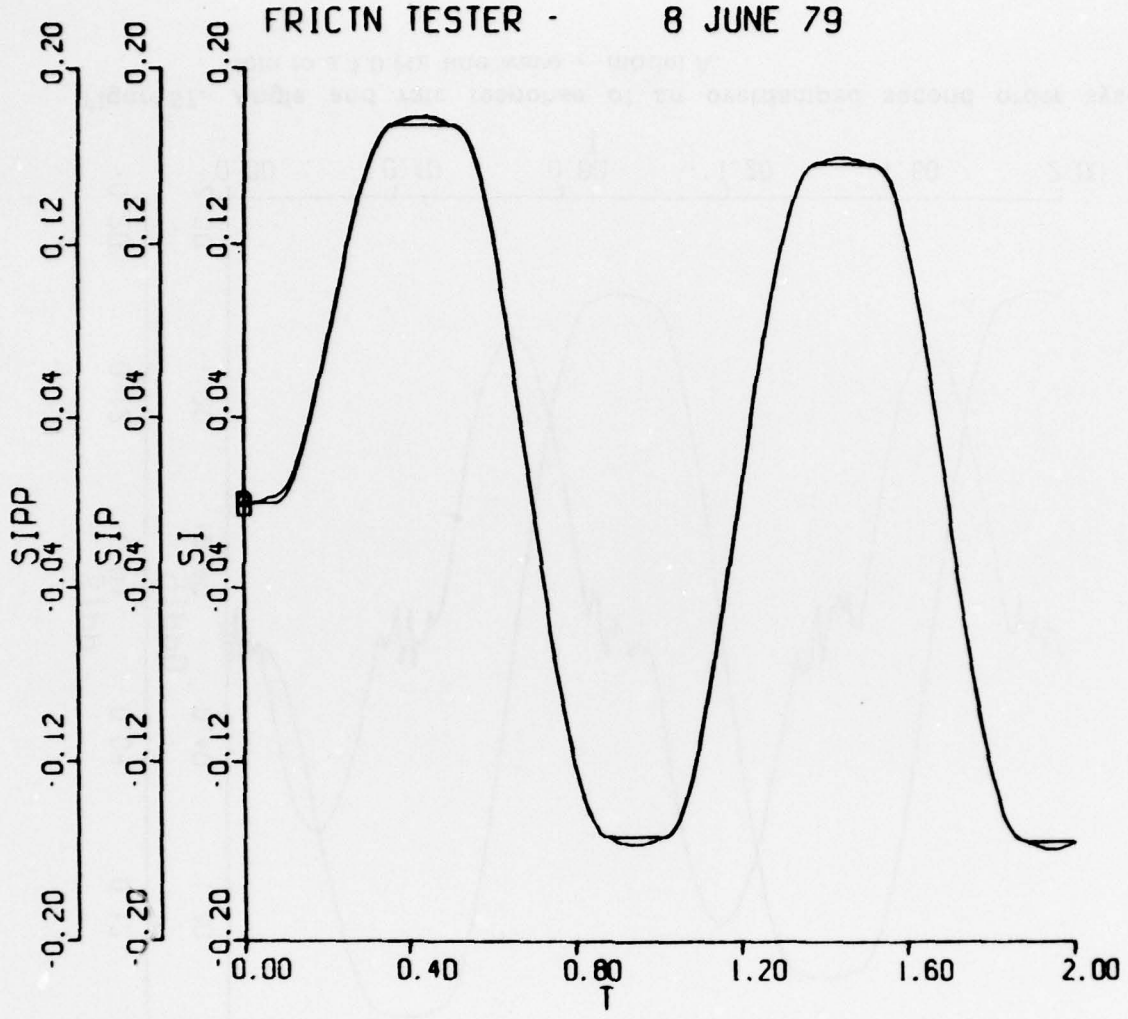

Figure 58. Comparison of angle responses of an overdamped second order system to a 1.0 Hz sine wave for models A, B and C.

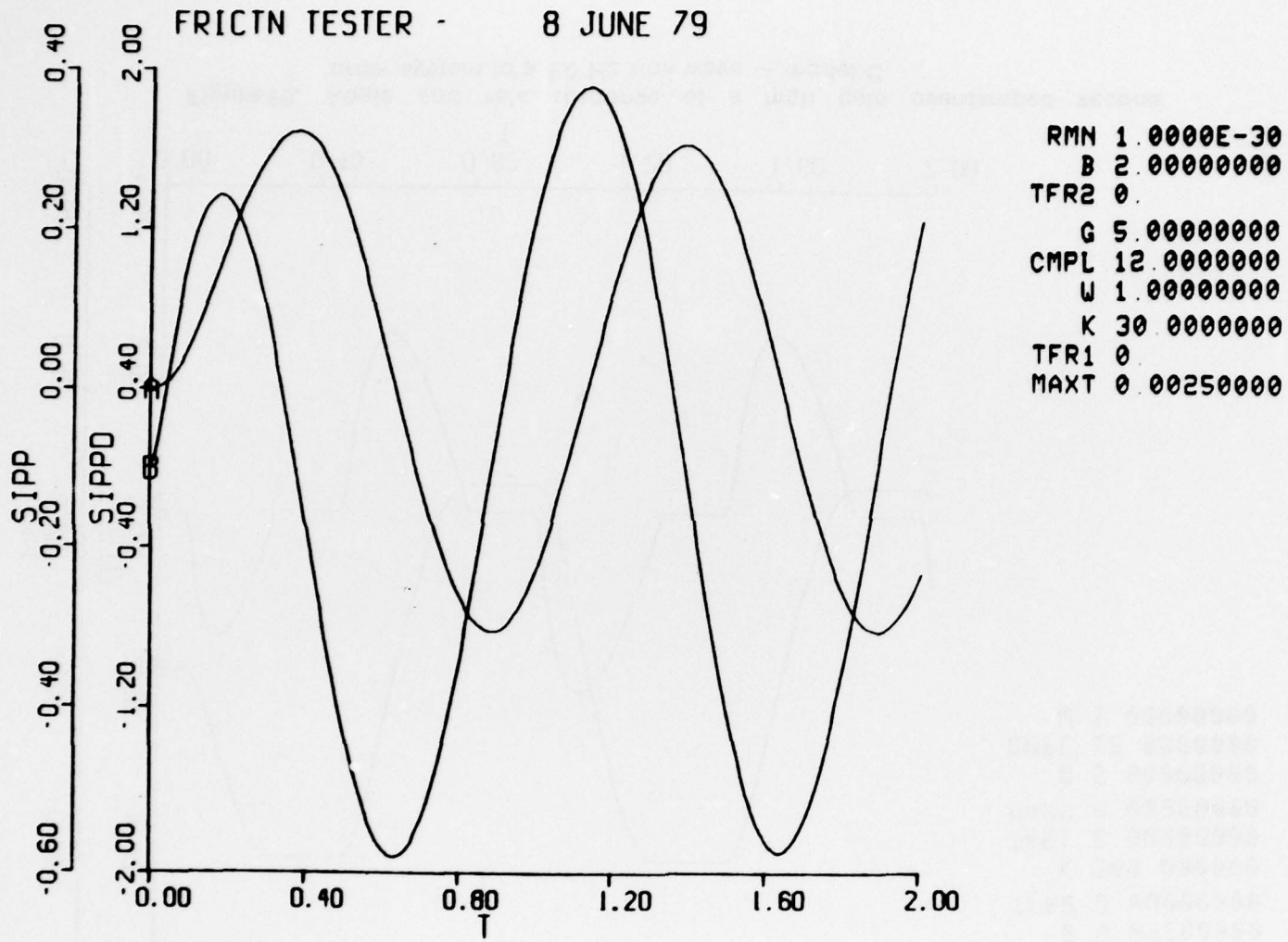

Figure 59. Angle and rate response of a frictionless overdamped second order system to a 1.0 Hz sine wave.

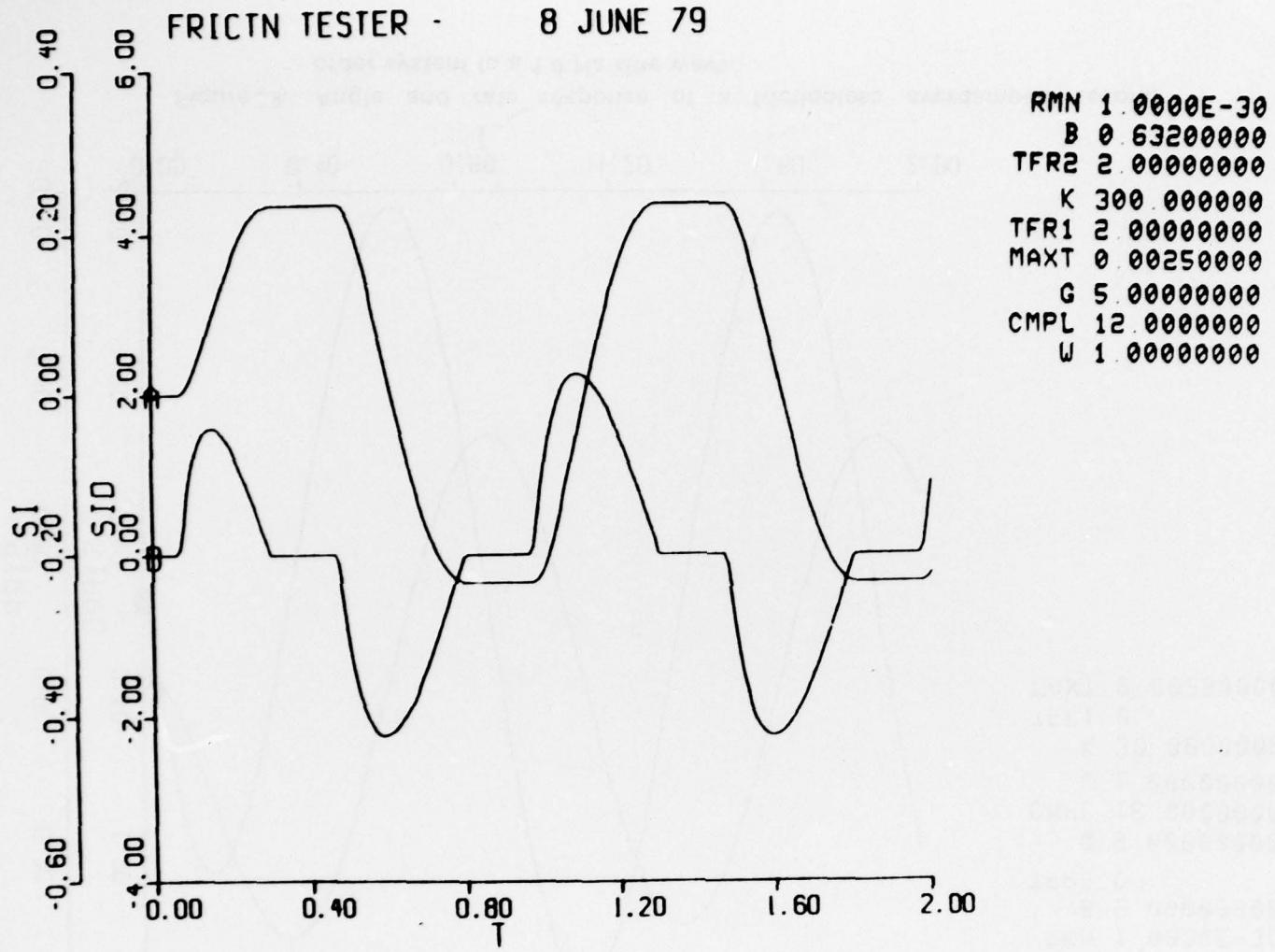

Figure 60. Angle and rate response of a high gain overdamped second order system to a 1.0 Hz sine wave — model C.

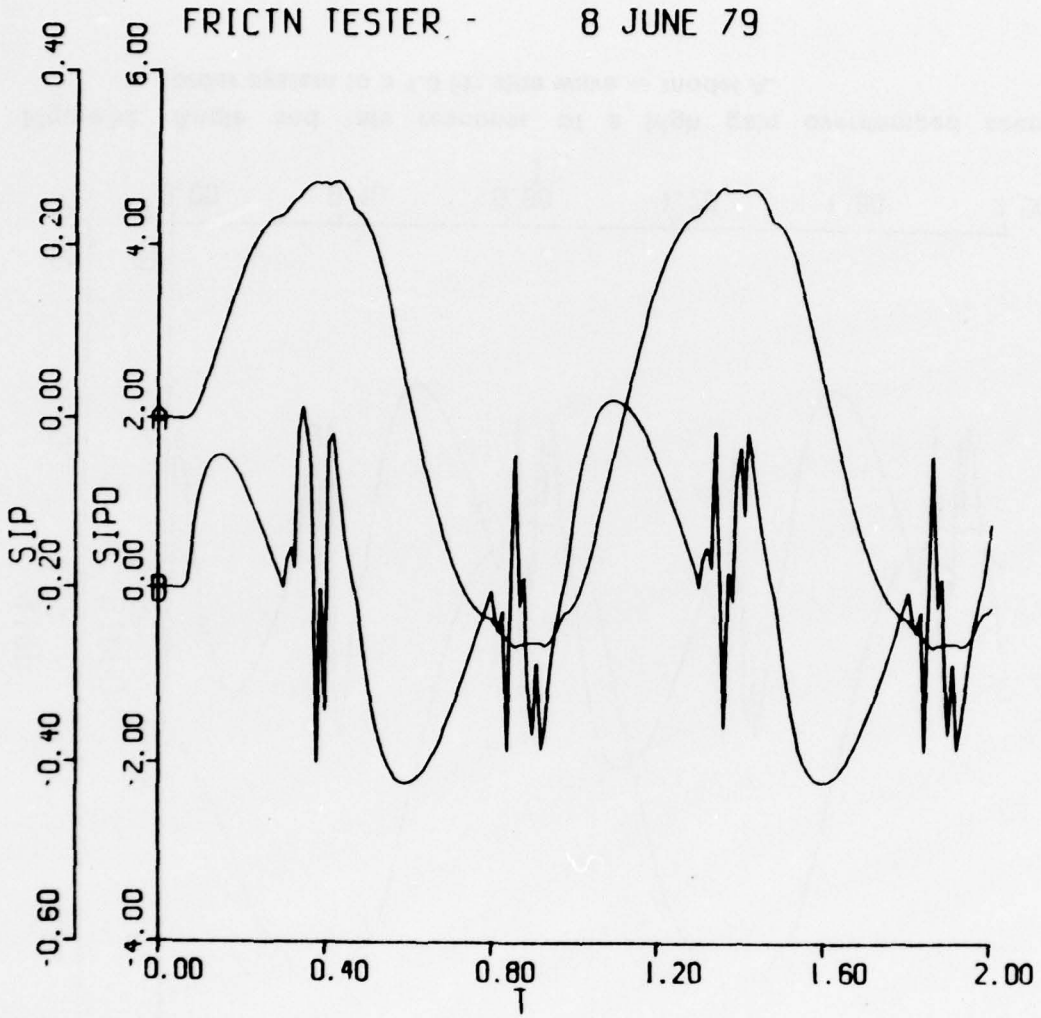

Figure 61. Angle and rate response of a high gain overdamped second order system to a 1.0 Hz sine wave — model B.

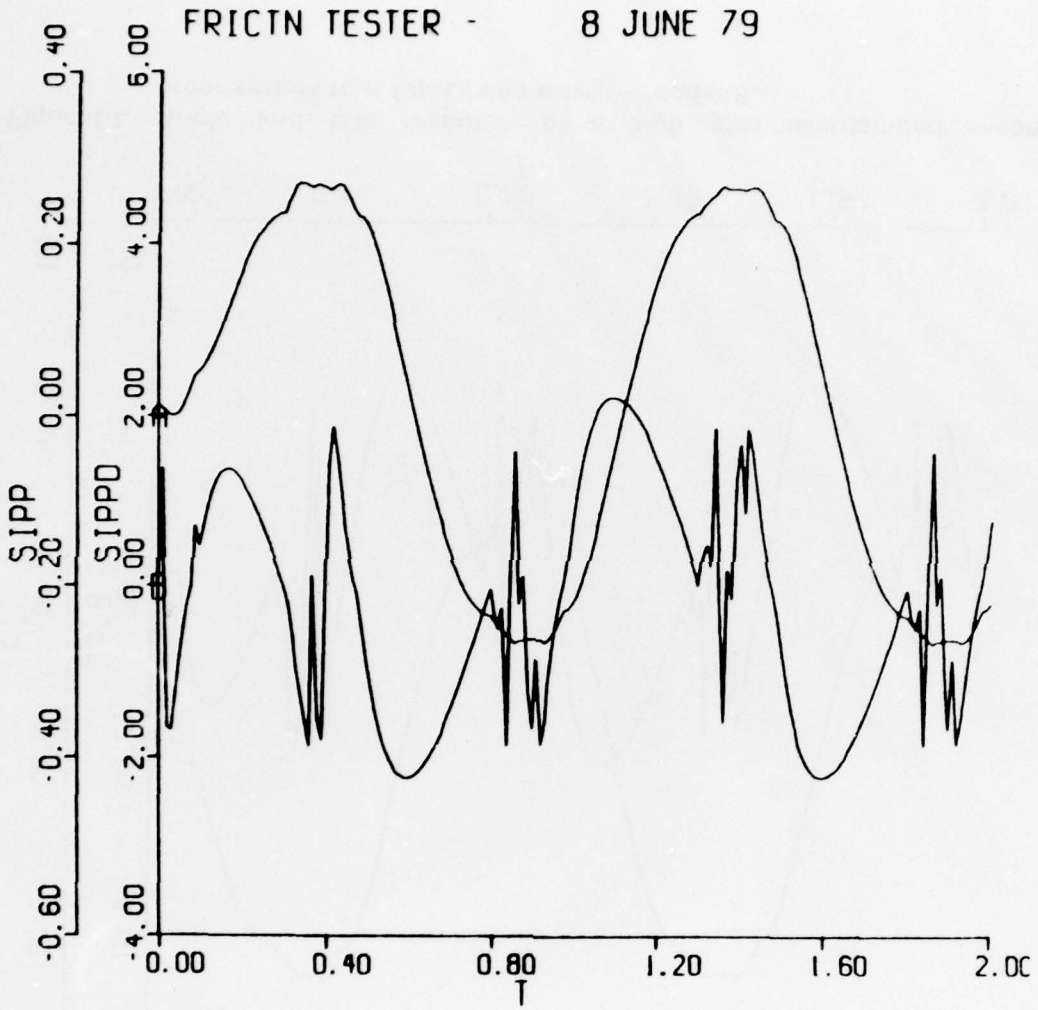

Figure 62. Angle and rate response of a high gain overdamped second order system to a 1.0 Hz sine wave — model A.

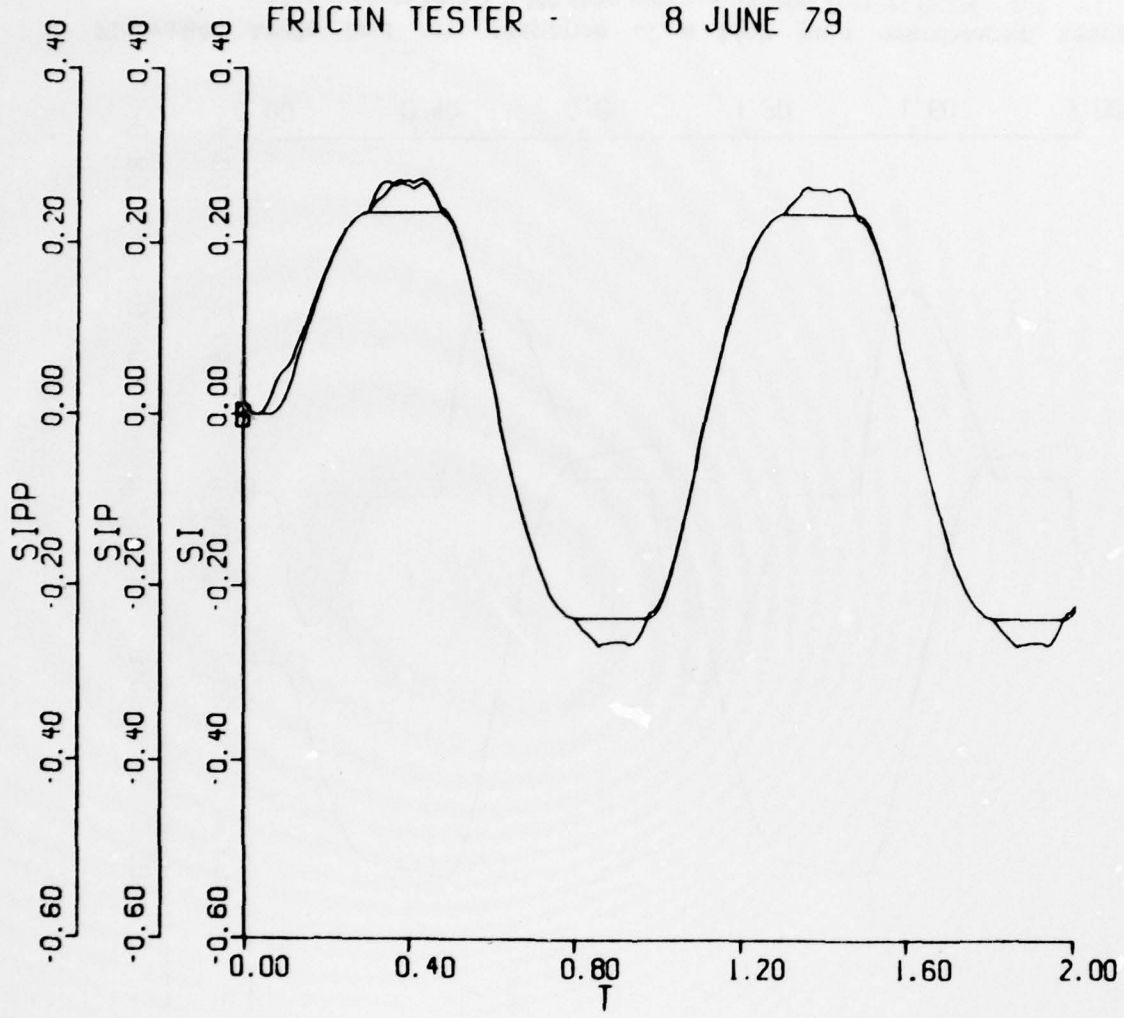

Figure 63. Comparison of angle responses of a high gain overdamped second order system to a 1.0 Hz sine wave for models A, B and C.

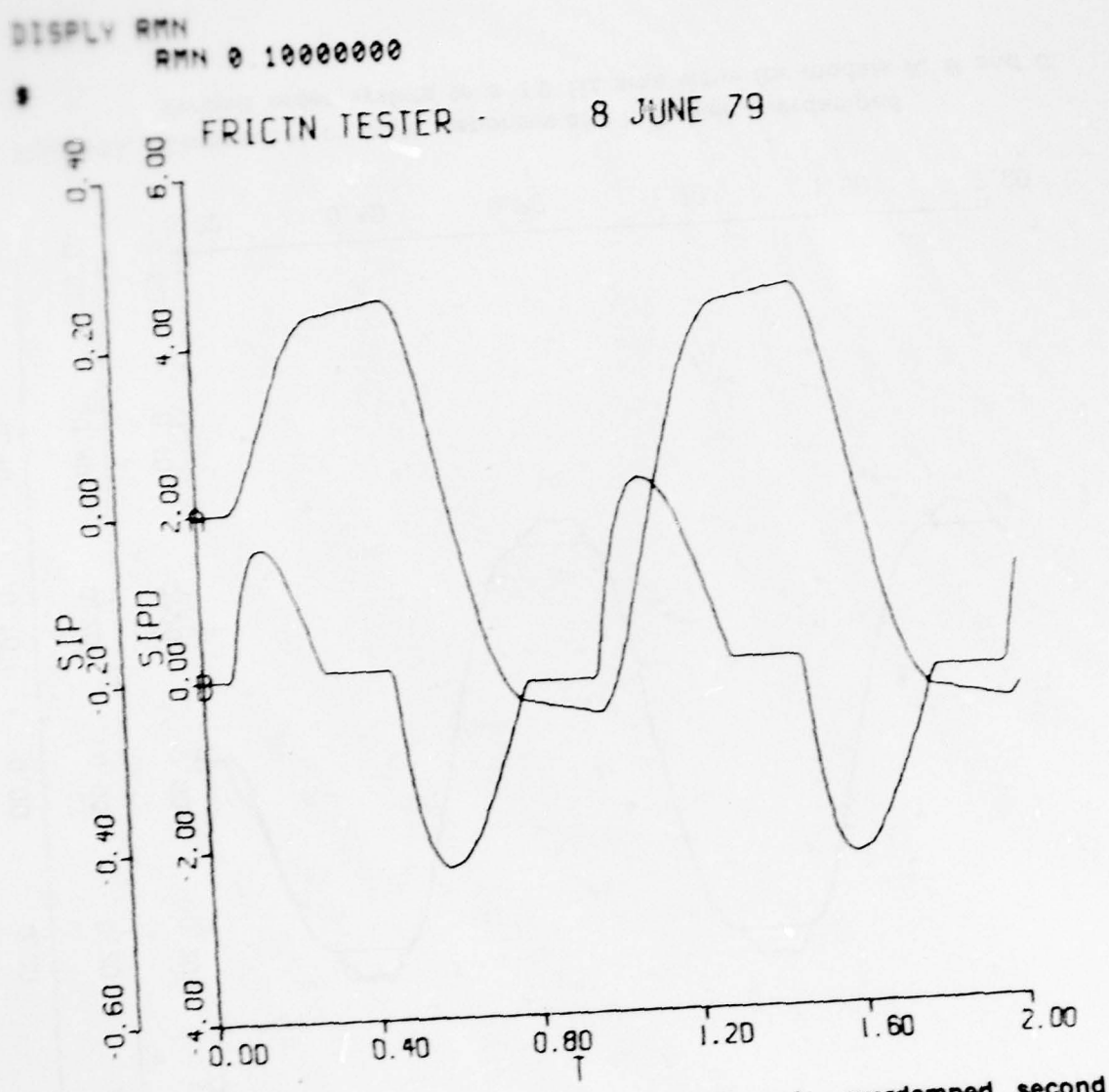

Figure 64. Angle and rate response of a high gain overdamped second order system to a 1.0 Hz sine wave — model B with RMN = 0.1.

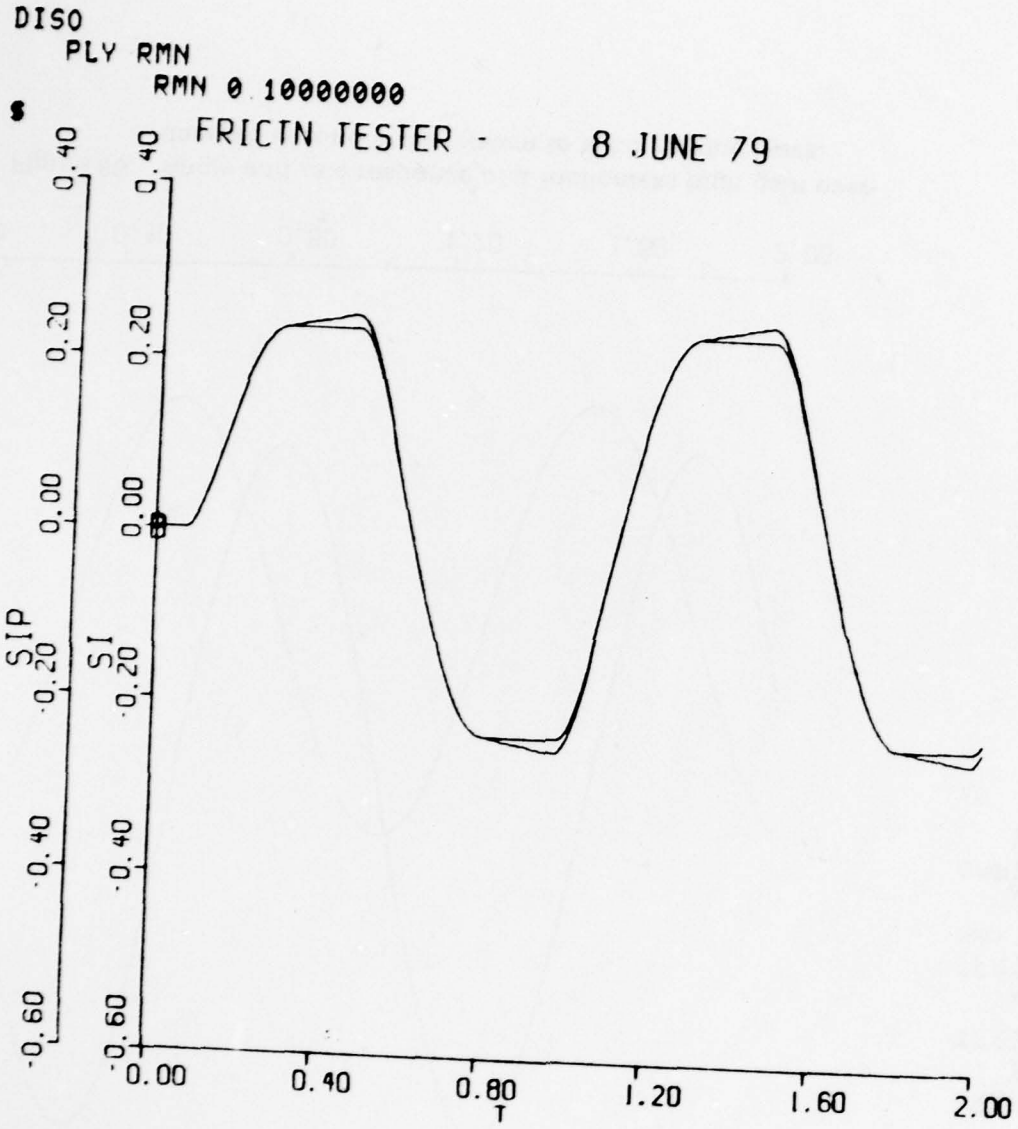

Figure 65. Comparison of angle responses of a high gain overdamped second order system to a 1.0 Hz sine wave for models B and C with RMN = 0.1.

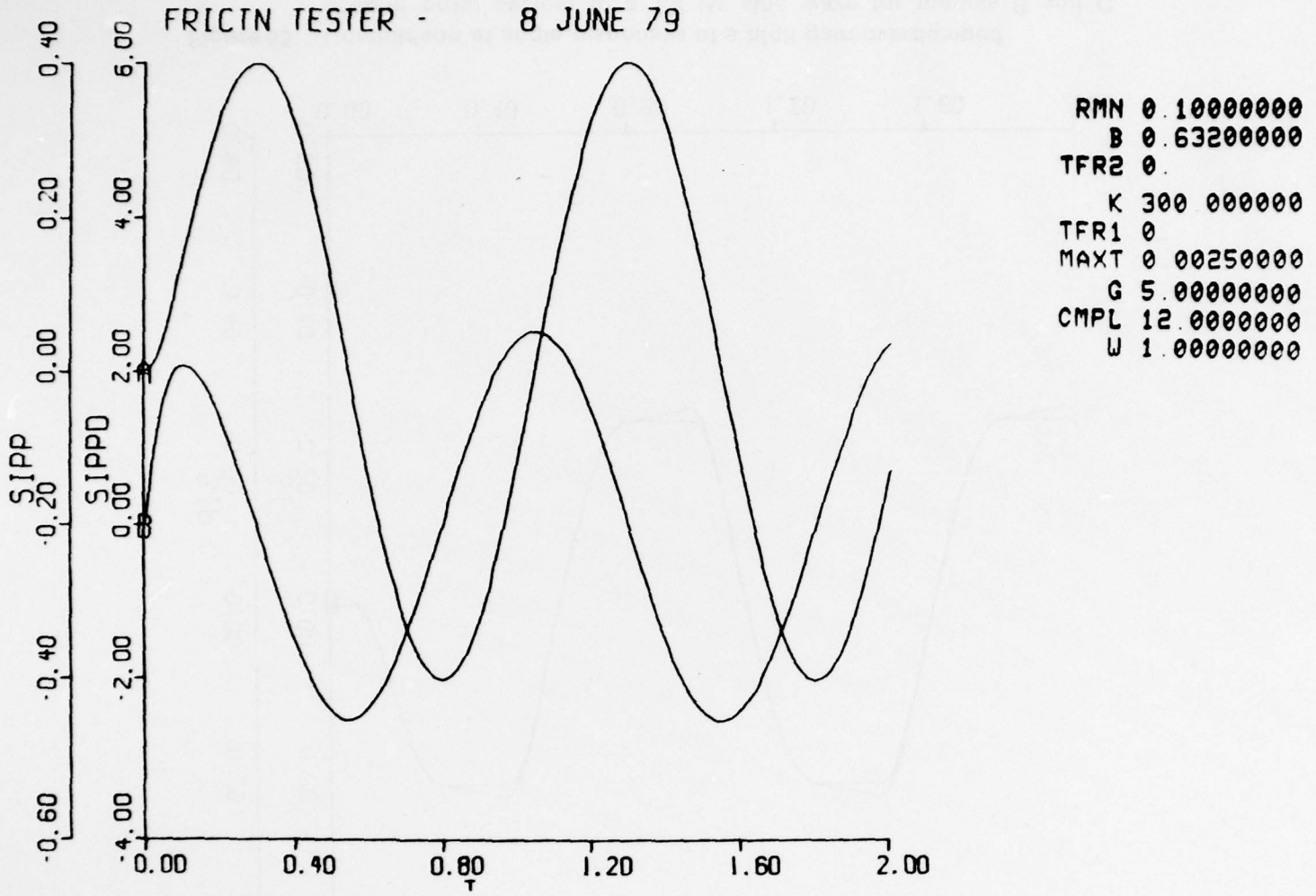

Figure 66. Angle and rate response of a frictionless high gain overdamped second order system to a 1.0 Hz sine wave.

DISTRIBUTION

	No. of Copies
Defense Documentation Center Cameron Station Alexandria, Virginia 22314	12
IIT Research Institute ATTN: GACIAC 10 West 35th Street Chicago, Illinois 60616	1
DRSMI-LP, Mr. Voigt	1
DRDMI-T, Dr. Kobler	1
DRDMI-TBD	3
DRDMI-TI (Reference Copy)	1
DRDMI-TI (Record Set)	1
DRDMI-TDD D.B. Merriman	25
DRDMI-TD Dr. McCorkle	1
DRDMI-TD Dr. Grider	1
DRDMI-TDD R. Powell	1